EFFECTIVENESS OF ENERGY WHEELS FROM TRANSIENT MEASUREMENTS

A Thesis Submitted to the College of

Graduate Studies and Research

in Partial Fulfillment of the Requirements

for the Degree of Master of Science

in the Department of Mechanical Engineering

University of Saskatchewan

Saskatoon, Canada

By

Oyetope Omobayode Abe

PERMISSION TO USE

The author has agreed that the Library, University of Saskatchewan, may make this thesis freely available for inspection. Moreover, the author has agreed that permission for extensive copying of this thesis for scholarly purposes may be granted by the professor or professors who supervised the thesis work recorded herein or, in their absence by Head of the Department or Dean of the College in which the thesis work was done. It is understood that due recognition will be given to the author of this thesis and to the University of Saskatchewan in any use of the material in this thesis. Copying for publication or any other use of this thesis for financial gain without approval by the University of Saskatchewan and the author's written permission is prohibited.

Request for permission to copy or make any other use of the material in this thesis in whole or in part should be addressed to:

Head of the Department of Mechanical Engineering

University of Saskatchewan

57 Campus Drive

Saskatoon, Saskatchewan

Canada S7N 5A9

ABSTRACT

Certification of energy wheel effectiveness by a selected international laboratory for many types and sizes of wheel produced by each manufacturer has proven to be very expensive and has been prone to large uncertainties. This research uses a new, low-cost, transient method to predict the effectiveness using only data obtained from transient measurements.

In this thesis, an analytical model is presented for predicting the effectiveness of rotating energy wheels using only the characteristics measured on the same non-rotating wheels exposed to a step change in temperature and humidity. A relationship between the step response and the periodic response of an energy wheel is developed using first order linear system design theory. This allows the effectiveness of an energy wheel to be predicted when the characteristics of a step response are known. The effectiveness correlations and uncertainty bounds for sensible and latent effectiveness of energy wheels determined from transient measurements are thus presented.

The experimental transient testing method and experimental verification of the effectiveness model for several different wheels are also presented in this thesis. The results obtained from the new effectiveness model are shown to agree, within uncertainty bounds, with the results obtained from the standard steady state experimental testing method and numerical simulations.

ACKNOWLEDGEMENTS

Thanks be to God who has made all things beautiful in His time. I am thankful to God for making it possible for me to start and finish this program.

My sincere and profound gratitude goes to my indefatigable supervisors: Professor R.W. Besant and Professor C.J. Simonson. Your thoughtful pieces of advice, support and wealth of experience have made this work a great success. Your insight and guidance will forever be invaluable to me.

I want to thank Messrs. Chris James and Dave Deutscher for their assistance at the laboratory. I also want to thank Dr. Wei Shang and Mr. Yiheng Wang for their contributions to this work.

Lastly but not the least, I wish to express my appreciation to the National Science and Engineering Research Council (NSERC) and VenmarCES, Saskatoon for funding this research work.

DEDICATION

This thesis is dedicated to:

my parents: Professor and Mrs. G.O. Abe,

my siblings: Yemi, Dele, Kemi and Gboyega

and

my fiancée, Bola,

for their love, care and support.

TABLE OF CONTENTS

LIST OF FIGURES

LIST OF TABLES

LIST OF SYMBOLS

a	characteristic of the system, inverse of the time constant, τ (1/s)
a_n	constant in Fourier series
A	area of solid (m^2)
A'	represents the output and input amplitude energy ratio averaged over one half cycle (energy transfer)
A_s	heat and mass transfer surface area on the supply or exhaust side (m^2)
ARI	American Refrigeration Institute
ASHRAE	American Society of Heating, Refrigerating and Air Conditioning Engineers Inc.
ASME	American Society of Mechanical Engineers
b	constant forcing or input function (°C or kg/m^3) or constant in Fourier series
B	Bias error
c	constant of integration
Cp	specific heat capacity (J/(kg·K))
Cr	ratio of the minimum to maximum heat capacity rate of the air streams
Cr^*	matrix heat (or moisture) capacity ratio on the supply or exhaust side
d	constant used in correlation equation (3.42)
D	diameter (m) or desiccant
D_h	hydraulic diameter (m)
e	constant used in correlation equation (3.42)
EATR	exhaust air transfer ratio
f	function of

$f(t)$	forcing function or external input (°C or kg/m^3)
$af(t)$	experimental forcing function or external input (°C/s or kg/(m^3·s))
F(t)	response of wheel alone
h	convective heat transfer coefficient (W/(m^2·K))
h_m	convective mass transfer coefficient (m/s)
HVAC	heating, ventilating and air-conditioning
j	number of samples
k	number of samples or function of the two time constants of the sensors
k_{air}	thermal conductivity of air (W/(m·K))
L	thickness of wheel (m)
M	total mass of wheel (kg)
$\dot{m}$	mass flow rate of dry air on the supply or exhaust side (kg/s)
MS-100	a 100 mm thick energy wheel coated with a molecular sieve desiccant
MS-200	a 200 mm thick energy wheel coated with a molecular sieve desiccant
N	angular speed of the wheel (cycle/s)
n	integer constant in Fourier series or number of samples
NTU	number of transfer units
OACF	outside air correction factor
p	period of exposure per cycle for the supply or exhaust gas (s/cycle)
P	pressure (Pa)
PVC	poly-vinyl chloride
Q	volume flow rate of air on the supply or exhaust side (m^3/s)
r	a dependent variable or function r^2 which describes the goodness of the curve fit

r_i	inner radius of tube (m)
r_o	outer radius of tube (m)
RH	relative humidity
RTD	resistance temperature device
rpm	revolutions per minute
S	precision error index
SG-150	a 150 mm thick energy wheel coated with silica gel desiccant
t	time (s) or Student's multiplier for 95% confidence
t^*	dimensionless time $\left(\frac{1}{p}\left(t-\frac{z}{\overline{U}}\right)\right)$
t_1	first time constant, sensor or thermocouple alone (s)
t_2	second time constant, sensor or thermocouple alone (s)
T	bulk temperature (°C or K)
T_1	first time constant, wheel plus humidity sensor or wheel plus thermocouple (s)
T_2	second time constant, wheel plus humidity sensor or wheel plus thermocouple (s)
TC	measured temperature of thermocouple (°C)
u	mass fraction of water in the desiccant (kg_w/kg_d)
$\overline{U}$	mean air flow velocity in an exchanger flow channel (m/s)
U	uncertainty
V_{air}	air face velocity (m/s)
V	volume (m^3)
w	angular frequency of the forcing function (rad/s)

x	output or response of the system, the same as $x(t)$
x_1	first weighting factor, sensor alone
x_2	second weighting factor, sensor alone
X_1	first weighting factor, wheel plus humidity sensor
X_2	second weighting factor, wheel plus humidity sensor
y_1	first weighting factor, thermocouple alone
y_2	second weighting factor, thermocouple alone
Y_1	first weighting factor, wheel plus thermocouple
Y_2	second weighting factor, wheel plus thermocouple
z	axial coordinate (m)
z^*	dimensionless axial coordinate $\left(z/L\right)$

Greek letters

α	phase shift angle (rad)
β_1	first weighting factor, energy wheel alone (temperature)
β_2	second weighting factor, energy wheel alone (temperature)
γ	temperature, thermocouple alone (°C)
Δ	difference
ε	effectiveness
$\bar{\varepsilon}$	weighted or average effectiveness
θ	angle (rad) or sensitivity of dependent variable r
Θ	temperature, wheel plus thermocouple alone (°C)
η	independent variable used in Appendix B

ρ	density (kg/m^3)
σ	constant used in equation (5.1)
τ	time constant (s)
τ_1	first time constant, wheel alone (s)
τ_2	second time constant, wheel alone (s)
φ	relative humidity, wheel alone
ϕ	relative humidity, sensor alone
Φ	relative humidity, wheel plus sensor
χ_1	first weighting factor, energy wheel alone (relative humidity)
χ_2	second weighting factor, energy wheel alone (relative humidity)
ψ	dependent variable (temperature, humidity ratio or enthalpy) used in equation (1.1)
$\aleph$	constant used in equation (3.30)
Ω	temperature, wheel alone (°C)
∞	infinity

Subscripts

a	air
ads	adsorption
al	aluminium
B	bias
CF	counterflow
d	desiccant
des	desorption

e	exhaust
f	final condition
g	total gas phase (air and water vapour)
i	inlet
j	initial
l	latent
m	matrix (including support material, desiccant and moisture)
min	minimum
mt	dimensionless moisture transfer group for energy wheels
o	outlet
P	precision
PF	parallel flow
s	supply or sensible
t	total
v	water vapour

Superscripts

rec	recuperator

CHAPTER 1

INTRODUCTION

Buildings are exposed to a wide range of weather conditions; however, two weather conditions are of major importance in heating, ventilating and air conditioning (HVAC) applications (hot and humid and cold and dry) because they imply a large rate of energy use to keep a building comfortable for the occupants. Large variations in the ambient air conditions over the year often occur in many climatic regions. This is why HVAC engineers are always concerned with optimization of their design to improve indoor air quality, productivity and at the same time reduce HVAC capital and operating costs. To achieve some design optimization, engineers use various energy recovery systems. Fixed plate, regenerative heat wheel, heat pipe, run-around coil loop, thermosiphon and twin-tower heat exchangers had been developed to exchange heat and, for some, moisture between the ventilation supply and the exhaust air flows (ASHRAE, 1996). The use of these heat recovery devices has shown large benefits over the past decades by lowering operating costs and providing good indoor air quality (Dhital et al., 1995). Researchers have also shown that air-to-air energy recovery equipment for heat and moisture exchange show good performance, larger energy and cost savings, and excellent maintenance and reliability characteristics.

Although, several years are often required to pay back the initial investment for retrofit applications, energy recovery is often the least cost alternative for new buidings (Asiedu et al., 2004). During cold weather, they are used when the ambient air temperatures drop below the supply air set point (e.g., 15°C). During warm ambient air conditions, they are used when the ambient air temperatures rise above the indoor air conditions (e.g., 24°C) (Besant and Simonson, 2000).

A common air-to-air energy exchanger is the energy wheel (Figure 1.1). In the literature, energy wheels are also called enthalpy wheels or wheels with a matrix that is coated with desiccant or rotary regenerative heat and moisture exchangers or air-to-air energy exchangers. Energy wheels are often constructed by winding desiccant-coated corrugated material, such as very thin aluminium sheet, around a core. The desiccant coated aluminium sheet makes up the matrix or medium through which air flows. Energy wheels transfer both heat and moisture between the supply and exhaust airstreams for the ventilation air heating and cooling processes. These devices are often the most cost effective HVAC design alternative (Asiedu et al., 2004 and Asiedu et al., 2005). During warm humid summer weather, heat and moisture energies are stored in the supply section of the wheel matrix and as the wheel rotates, the stored energies are transferred from the supply inlet air to the exhaust air streams and this results in a cooler dryer outlet air. During cold dry winter weather, heat and moisture are transferred from the exhaust air of buildings and transferred to the supply air stream. Therefore, with the use of an energy wheel, the same device and airflow configuration can be used for both cold and warm ambient air temperatures.

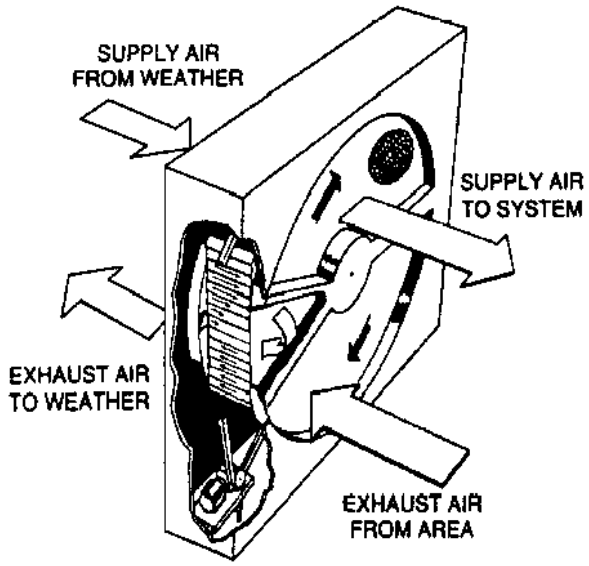

Figure 1.1. *A schematic diagram of a rotary regenerative air-to-air energy exchanger (energy wheel) showing the counter-flow configuration with purge section (ASHRAE Systems and Equipment Handbook, 1996, pp. 42.11).*

1.1 Characterization of energy wheels

The characteristics of each air-to-air energy recovery device are different, especially their ability to transfer different forms of energy. Energy wheels transfer both sensible and latent energy between the air streams due to the desiccant attached to the aluminium substrate of the wheel matrix. Sensible energy transfer is caused by the temperature differences between the two airstreams and latent energy transfer is caused by the water vapour pressure differences between the two airstreams. The total energy transfer rate in energy wheels is the sum of both sensible and latent energy transfer rates.

Testing of energy recovery devices is very important to predict the energy transfer in HVAC design applications. However, this testing exercise under certification operating conditions for summer and winter has proven to be very expensive. Testing of energy wheels is more difficult than air-to-air heat exchangers because of the inherent coupled heat and mass transfer associated with energy wheels and the need to maintain steady state balances of air flow, water vapour flow and energy. There are many performance factors that should be considered to fully test or characterize the performance of an energy wheel when the operating conditions are steady state and known (ARI Standard 1060, 2003). These factors include: the sensible (ε_s), latent (ε_l) and total (ε_t) effectiveness, the outside air correction factor (OACF) for the supply air delivered, the exhaust air transfer ratio (EATR), and the air pressure drop across the wheel (ΔP) for both the supply and exhaust airflows through the wheel. In this vein, testing of energy wheels has been very time consuming and it has been difficult to maintain small uncertainties for all the parameters.

However, effectiveness has the greatest impact on the economic viability of the exchanger in a given HVAC application. Since the inlet operating conditions (temperature, humidity, and air flow rate) usually change quite slowly in typical HVAC applications, the effectiveness determined at steady state test conditions can be used to characterize the performance of energy exchangers in most HVAC application. ASHRAE Standard 84-1991 test standard uses equation (1.1) to define the effectiveness of an energy recovery device as:

$$\varepsilon = \frac{\dot{m}_s (\psi_i - \psi_o)|_s}{\dot{m}_{\min} (\psi_{s,i} - \psi_{e,i})} \tag{1.1}$$

where

$$\dot{m}_s (\psi_i - \psi_o)|_s = \dot{m}_e (\psi_o - \psi_i)|_e \tag{1.2}$$

for steady state energy balance and $\dot{m}$ is the mass flow rate of dry air and ψ represents temperature, humidity ratio and enthalpy for sensible, latent and total effectiveness respectively. $\dot{m}_{\min}$ is the minimum value of either $\dot{m}_s$ or $\dot{m}_e$. Subscripts i, o, s and e represent the inlet, outlet, supply and exhaust sides of the heat exchanger. Certification tests for effectiveness are done only for $\dot{m}_s = \dot{m}_e$.

Figure 1.2 shows a schematic of the test facility for determining the performance of an energy wheel at steady state operating conditions using the ASHRAE Standard 84-1991 test standard and ARI Standard 1060-2003 test conditions presented in Table 1.1.

Table 1.1. ARI (American Refrigeration Institute) summer and winter test conditions

Item	Conditions	
	Summer	Winter
Supply inlet air	35°C 47.5% RH	1.7°C 82.1% RH
Exhaust inlet air	23.9°C 51.5% RH	21.1 °C 48.1 % RH

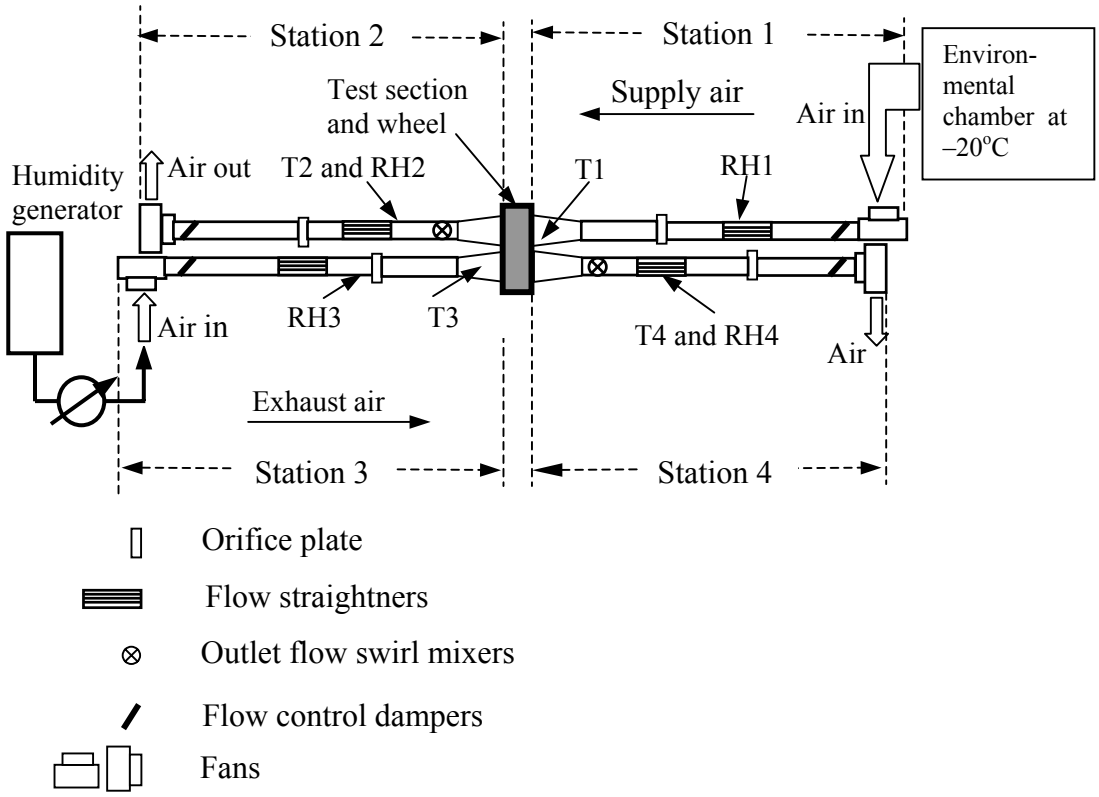

Figure 1.2. *A schematic diagram showing the apparatus for testing air-to-air heat exchangers (Shang, 2002).*

In Figure 1.2, the test facility is completely sealed and well insulated to ensure negligible air leaks and very small heat gains or losses during steady state operations. For the steady state experiments, the inlet air properties are uniform and steady for at least 30 minutes through the inlet flow ducts at stations 1 and 3. When the wheel rotates, the airflow properties at the outlet face of the wheel will not be uniform. Thus, these outlet flow properties are measured downstream of flow swirl mixers shown in Figure 1.2. The test standard requires that the bulk properties of the air at the outlet tubes 2 and 4 be uniform and steady for at least 30 minutes. The experimental apparatus set up for the steady state experiments can cost millions of dollars and each test, which

costs about $5000 when done in a certified laboratory, will require about 3 hours of operation to get 30 minutes of accurate test data for each test condition.

1.2 Research motivation

There have been several research papers on the determination of the effectiveness of heat exchangers under steady state operating conditions (Gawley and Fisher, 1975, Klein et al., 1990, Ciepliski et al., 1998, Simonson et al., 1999a and b, Simonson and Besant, 1999a and b). However, there are no research papers on the determination of effectiveness of exchangers using measured data from non-steady state (or transient) operating conditions. During normal operation for testing and in HVAC systems, the matrix of energy wheels undergoes a periodic step change in input conditions as the wheel rotates between the cold and warm airflows. It is hypothesized that it will be possible to predict the effectiveness of an energy wheel using only data obtained during a single step response.

In addition, characterization of energy wheel effectiveness by the laboratory selected by the American Refrigeration Institute (ARI) to certify the effectiveness of many types and sizes of wheels produced by each manufacturer has proven to be very expensive and has been prone to large uncertainties. These facts have motivated this research. A new transient test method is therefore proposed (herein called the *transient test method*), which requires a small, inexpensive, and simple-to-use experimental apparatus.

1.3 Literature review

This section presents previous research on energy wheel steady state effectiveness measurements and correlations. It also presents previous research on humidity and temperature transient response of heat and moisture exchangers.

1.3.1 Steady state effectiveness

Many research investigations have been published on the effectiveness of desiccant coated energy wheels under steady state conditions. These include numerical simulations and experimental investigations on the latent, sensible, and total effectiveness of desiccant coated energy wheels.

Kays and London (1984) presented an "Effectiveness-NTU" (***ε****-NTU)* method for predicting the effectiveness of a sensible recuperative and rotary (regenerative) heat exchangers as a function of dimensionless numbers. Recuperators are heat exchangers which allow fluids to pass simultaneously and continuously through partitions of the exchanger. Regenerators are heat exchangers containing a heat storing mass and they allow two fluids to flow alternately at a fixed regular time interval through the same cross section of the exchanger. For example, a car radiator is a recuperator and an energy wheel is a regenerator. Kays and London (1984) showed that the effectiveness depends on two dimensionless numbers for sensible recuperative heat exchangers (*NTU* and *Cr*) and four dimensionless numbers for rotary heat exchangers (*NTU, Cr, Cr** and $(hA_s)_s \big/ (hA_s)_e$) (Kays and London, 1984, Shah, 1981 and Coppage and London, 1953).

Simonson and Besant (1997a and b) presented a one-dimensional, transient numerical model to study the coupled heat and moisture transfer in desiccant coated rotary energy exchangers. The model predicts the effectivenesses (sensible, latent, and total) of rotary energy exchangers for different wheel designs and operating conditions. They validated their numerical results by comparing with experimental data. With very few exceptions, the simulations were found to be within the experimental uncertainty bounds as reported by Simonson et al. (1999a and b). To further their investigation, Simonson and Besant (1999a and b) developed dimensionless groups and effectiveness correlations for energy wheels. These dimensionless groups, derived from the governing heat and mass transfer equations, were a function of the steady state operating conditions including the inlet air temperature and humidity into the energy wheel and sorption characteristics of the desiccant on the wheel matrix. A similar approach will be used in this thesis, where dimensionless groups and effectiveness correlations will be obtained from measurements taken during transient conditions rather than steady state conditions.

1.3.2 Humidity transient response

There has been very little research on the humidity transient response and its application to energy wheels. In a recent investigation at the University of Saskatchewan, Wang et al. (2005) developed a new experimental facility to study the transient response of sensors and equipment. They studied the transient response of a humidity sensor and used the same sensor to measure the relative humidity downstream of a non-rotating energy wheel following a step change in inlet air relative humidity.

Thus, data measured downstream of the energy wheel was a function of the characteristics of both the wheel and the sensor. Wang et al. (2005) presented an analysis to determine only the wheel response from the measured step response of the humidity sensor alone and the step response of the wheel as measured by the same sensor downstream of the wheel. They found that the transient response of an energy wheel under a step change in humidity at room temperature conditions followed an exponential correlation curve with two time constants, a small and a large one. The first time constant is thought to be mostly due to diffusion of water vapour to or from the surface of the wheel matrix and adsorption or desorption on this outer surface of the desiccant particles in the wheel matrix coating. The larger second time constant is thought to be mostly a consequence of the slow diffusion process of water molecules into the inner regions of the desiccant particles in the coating of the wheel matrix and the sensor material as the wheel and sensor approach equilibrium. Wang's sensor response was similar to the humidity sensor response obtained by Kuse and Takahashi (2000) who investigated the transient behaviour of a tin oxide semiconductor under a step-like humidity change. In this thesis, the method and analysis presented by Wang et al. (2005) will be used to determine the humidity transient response of energy wheels to predict the latent effectiveness. One of the key conclusions of Wang (2005) was that the transient humidity and temperature response of wheels and sensors should be conducted separately. Therefore in this thesis, the humidity response will be measured and analysed separately from the temperature response.

1.3.3 Temperature transient response

Many researchers have presented analytical and numerical models to predict the temperature response of sensors exposed to a step change in a single-phase fluid passing through different flow configurations. These responses were determined when a fluid with constant temperature is subjected to a step change in temperature (Rizika, 1954, Romie, 1984, Romie, 1985, Roetzel and Xuan, 1992, Tan and Spinner, 1991, Yin and Jensen, 2003) or a simultaneous step change in mass flow rate and temperature (Lachi et al., 1997, Romie, 1999) by solving the continuity, flow and energy equations. In some analytical models, the outlet fluid temperature response was determined and verified with experimental data (Clark, Arpaci and Treadwell, 1958, Arpaci and Clark, 1958). Abdelghani-Idrissi et al. (2003) predicted the transient temperature response of a counter-flow heat exchanger with two single-phase fluids by a first-order response with a time constant when mass flow rate was subjected to a sudden change. However, in this thesis, the transient response of an energy wheel is obtained by a step change in one of the two inlet air temperatures alone. Although all the researchers mentioned above obtained the transient response of various exchangers, they did not use their measurements to determine the effectiveness of these exchangers. Therefore, the main focus of this thesis will be to use the transient measurements obtained from energy wheels to predict their effectiveness.

Han et al. (2005) presented an experimentally validated numerical model to predict the transient characteristics of the sensor tube of a thermal mass flow meter. They presented a correlation for predicting the response time of the sensor tube. Their

work is similar to that of Wang (2005) that presented correlation equations to predict the transient characteristics of the temperature sensor in a humidity/temperature transmitter; however, Wang's investigation is more relevant to the work in this thesis. Wang (2005) carried out some work on the temperature transient response of energy wheels using the same approach described in section 1.3.2, but using a temperature sensor and a step change in temperature. It was found that when the wheel was subjected to a step change in temperature, the outlet temperature followed an exponential function with two time constants. In this thesis, the method presented by Wang (2005) will be used to determine the temperature transient response of energy wheels to predict the sensible effectiveness.

1.4 Objectives

The primary purpose of this research is to use the newly developed transient test facility of Wang (2005) to deduce the steady state sensible and latent effectiveness of energy wheels using only data obtained during non-steady state (i.e. transient) operating conditions. The measurements will be taken when the energy wheels are subjected to a step change in humidity or temperature. The main objectives are listed below.

1. Develop a mathematical model to predict a relationship between the transient step response of an energy wheel and the steady state periodic response.
2. Develop a model to predict the effectiveness of energy wheels and their uncertainties from the steady state periodic response in objective 1.

3. Use the transient test facility of Wang (2005) to determine the transient characteristics of several different energy wheels with known latent, sensible, and total effectiveness.
4. Determine transient characteristics of energy wheels using the numerical model of Simonson and Besant (1997a and b) and predict the corresponding effectiveness using the model developed in objective 2.
5. Compare the effectiveness of the wheels tested in objective 3 and those wheels listed in objective 4 by using the model developed in objective 2.

1.5 Scope and methodology of research

The humidity transient and temperature transient response characteristics of the wheels tested in objective 3 will be determined from independent tests. The wheels will be subjected to a step change in the relative humidity with negligible temperature differences to determine the humidity transient response characteristics and the temperature transient response characteristics of the wheels will be determined from the wheels' response to step changes in temperature alone as recommended by Wang (2005). Therefore, the effectiveness, sensible and latent, in objectives 4 and 5 will be determined independently. The total effectiveness can be determined by measuring the total enthalpy change between the two airstreams or it can be predicted using a relationship that relates the total effectiveness and the sensible and latent effectiveness (Simonson and Besant, 1999a and b).

The latent, sensible, and total effectiveness obtained from steady state experiments for the wheels listed in objective 3 were determined by another researcher (Shang, 2002).

1.6 Overview of thesis

This thesis is subdivided into six chapters. Chapter 2 describes the experimental test facility and instrumentation used. In Chapter 3, a mathematical model is developed to relate the step response of an energy wheel to its steady state periodic response. In addition, this chapter presents effectiveness correlations and the uncertainties in the effectiveness derived from the mathematical model. Transient response experiments, correlation equations and data for time constants are presented in Chapter 4 while Chapter 5 compares the model-predicted effectiveness with steady state experimental test data and steady state numerical simulations. A research summary, conclusions and recommendations for future work are presented in Chapter 6.

CHAPTER 2

TEST FACILITY AND INSTRUMENTATION

In this chapter, the experimental test facility developed by Wang (2005) and used in this thesis is presented. This test facility is used to measure the transient response characteristics of sensors alone (humidity and temperature) and energy wheels with these sensors downstream. Also discussed in this chapter is the calibration of the instruments used for these tests.

2.1 Test facility

Figure 2.1 shows a schematic of the test apparatus and instrumentation for measuring the transient response characteristics of sensors and energy wheels. The apparatus is designed in such a way that a step change in the inlet air flow properties (i.e., humidity and temperature conditions) can be achieved in less than 1 second. The step change in humidity for the humidity sensor and the step change in temperature for the thermocouple is achieved through a manual quick 180° rotation of the inlet tubes. The location of the inlet flow tubes, which are attached to a rotary switch plate, is rotated 180° with respect to the outlet flow tubes which are attached to a fixed plate.

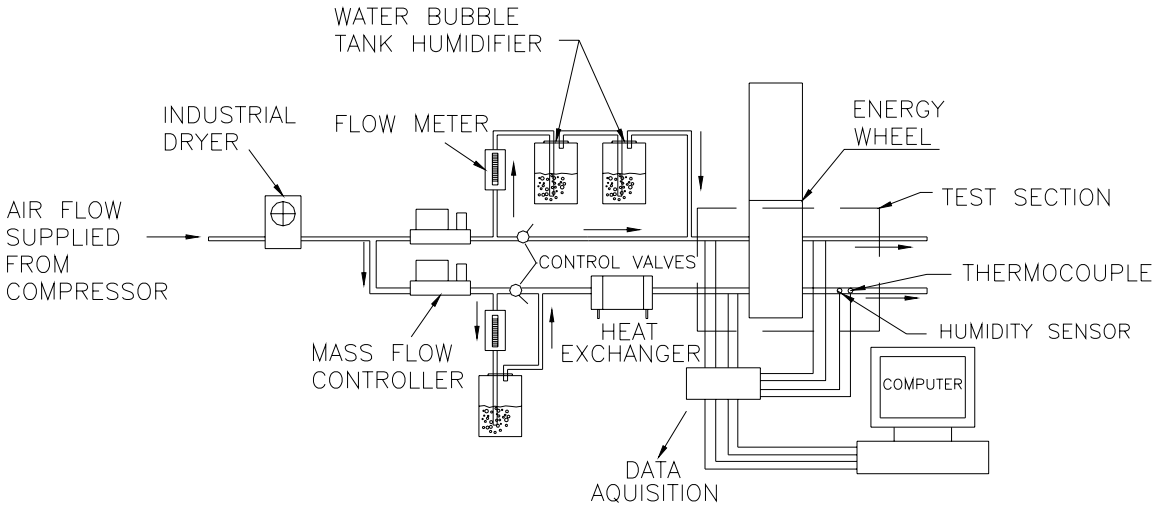

(a)

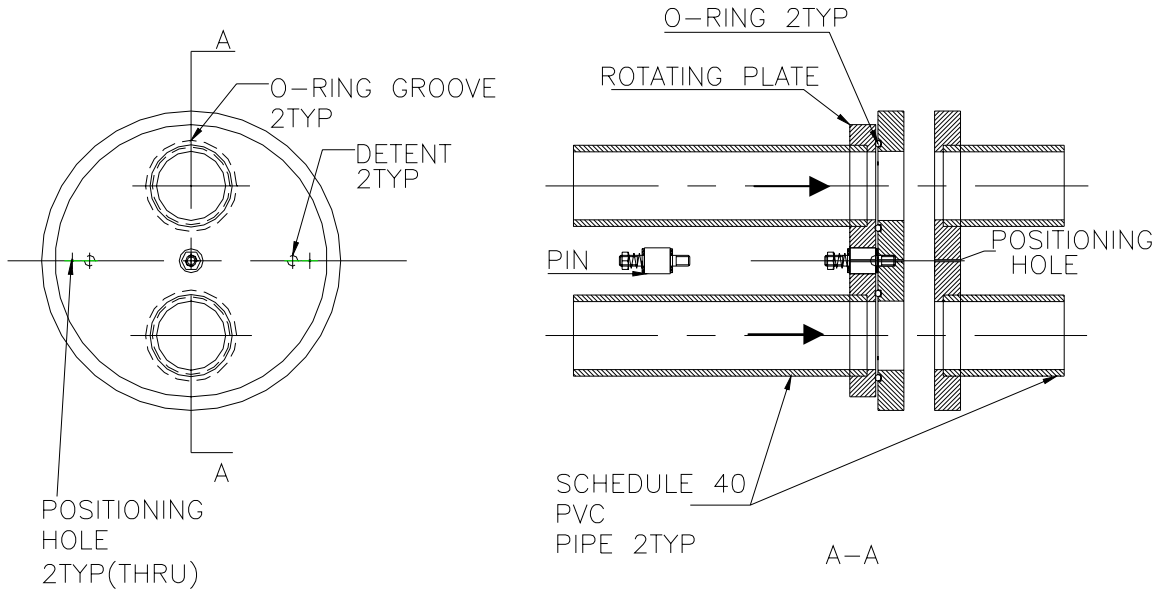

(b)

Figure 2.1. *Schematics of the test facility showing (a) the flow lines, instrumentation and test wheel and (b) the test section with its rapid tube rotation capability to interchange the two inlet flow tubes (Wang, 2005).*

Before the transient tests begin, air flow at desired operating conditions is passed through the inlet section of the apparatus with the humidity sensors and thermocouples

in place. The transient tests are commenced after the inlet and outlet temperature and relative humidity values are steady. After a step change, the test continues for about 30 minutes to allow the outlet properties to reach steady state values. During each transient test, the mass flow rate of dry air through each mass flow controller is constant.

In Figure 2.1(a), compressed air from an air compressor provides dry air for each test. Air from the compressor first passes through an industrial dryer, which reduces the inlet air relative humidity to approximately 4% RH. This supply air is then split as shown in Figure 2.1(a), before it passes through two mass flow controllers used to maintain the desired mass flow rate of air through each flow tube. The maximum flow rate capacity of each mass flow controller is 200 L/min. Each of the two inlet and outlet flow tubes shown in Figure 2.1(b) is 51 mm inside diameter. The airstreams are humidified before delivery to the test section. Three water tanks (as shown in Figure 2.1(a)) are used to generate the required inlet air relative humidity. To achieve this, the bypass control valves are used to divert a portion of the dry inlet air from the main line to the water tanks to add a desired mass of water vapour to the air. The diverted portion of the dry inlet air, which is now humidified, is recombined with the dry air from the compressor downstream of the control valves to achieve the desired air relative humidity for the airstreams passing through each inlet flow tube. To achieve the desired airstream temperatures, a tube-in-tube heat exchanger is used to heat or cool one of the airstreams using either hot water from an electrical heater or cold water directly from the tap.

Each flow tube is separated into inlet and outlet sections and is aligned in such a way that the airstreams flow directly from the inlet tube to the outlet tube (Figures 2.1(b) and 2.2). For a step change in temperature, one of the supply inlet flow tubes delivers hot or cold air which passes through insulated tubes to reduce the heat loss or gain. The other supply inlet flow tube delivers air at the ambient room temperature. The two outlet flow tubes are also insulated as seen in Figure 2.2. This insulation reduces the heat loss or gain from the ambient air, so that the properties of the air being measured at the outlet tubes are close to that from the inlet tube under steady state conditions.

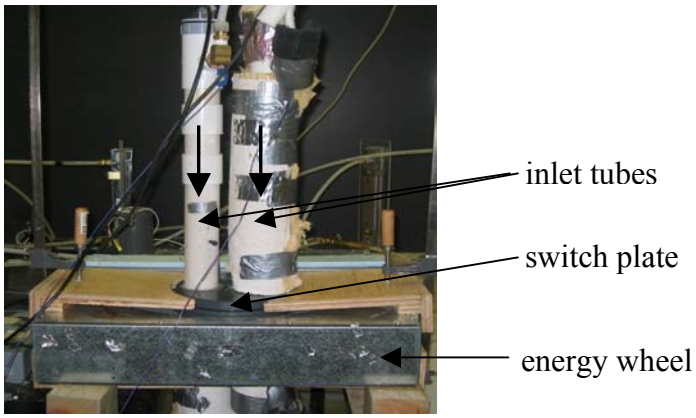

Figure 2.2. *Picture of the test section of the transient experimental test facility showing inlet airflow tubes, switch plate, and energy wheel.*

The test facility is designed so that the temperature profile of the airstreams at the outlet can be determined. As a modification to the apparatus of Wang (2005), a thermocouple holder plate made of PVC (poly-vinyl chloride) is installed inside the outlet flow tubes, so that an array of equally spaced thermocouples (TC) can be used to measure the temperature profile across one tube diameter. Figure 2.3 shows the thermocouple holder plate installed inside the outlet flow tube.

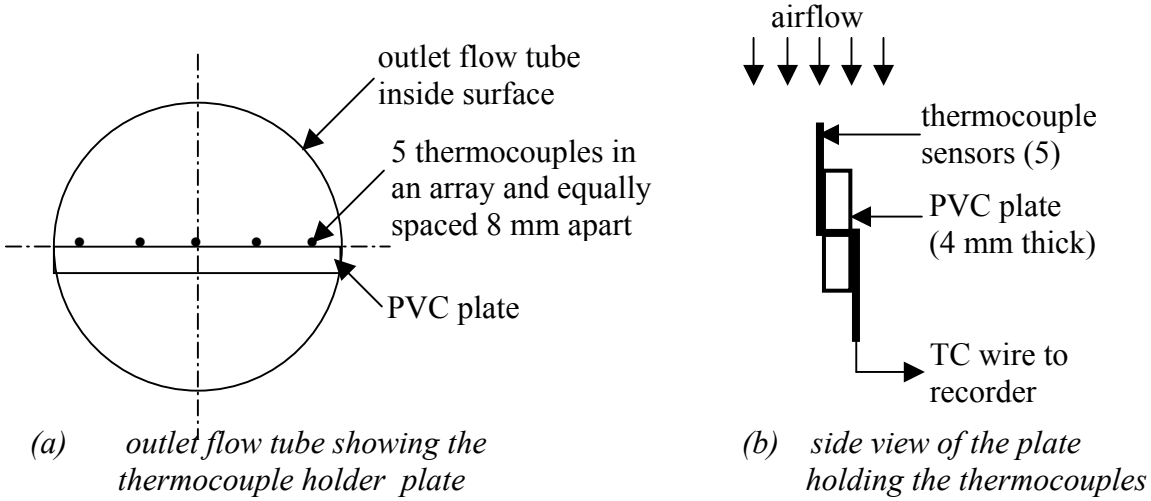

(a) outlet flow tube showing the thermocouple holder plate

(b) side view of the plate holding the thermocouples

Figure 2.3. *A schematic diagram showing the thermocouples in place at the outlet airflow section of the wheel.*

A picture of the test section clamped to a stationary energy wheel is shown in Figure 2.2. This test facility is significantly different than the standard test facilities specified in ASHRAE Standard 84-1991. This standard steady state test method uses a counter airflow configuration through rotating energy wheels (Figure 1.2), while the equipment shown in Figures 2.1 and 2.2 uses a parallel airflow configuration with both air flows in the same direction through a stationary energy wheel.

2.2 Test operating conditions

In this thesis, the humidity and temperature response of energy wheels and sensors are tested independently. Wang (2005) found that the humidity sensor response time was too slow (order of 1 minute) to be used for a transient test when temperature changes are important – so he recommended that the humidity and temperature response tests for energy wheels should be done independently. The humidity transient response experiments are performed under isothermal ($\Delta T=0$) inlet airflow conditions so that heat

transfer effects would be negligible. The temperature transient response experiments are performed under dry test conditions where there is negligible moisture transfer (i.e., $\Delta RH \approx 0$). Test conditions were chosen to represent a typical range of temperature and humidity differences between the supply and exhaust air that may occur in HVAC systems. These test conditions are given in Table 2.1 and Table 2.2.

Table 2.1. Test conditions for humidity transient response experiments ($\Delta RH \neq 0, \Delta T = 0$).

Test Conditions	Dry inlet	Wet inlet
Temperature	~23°C	~23°C
Relative humidity	~5%	~40%, 50%, 60%
Air flow rate	200 L/min, 100 L/min	200 L/min, 100 L/min
Air face velocity	1.6 m/s, 0.8 m/s	1.6 m/s, 0.8 m/s

Table 2.2. Operating conditions for the temperature transient response experiments ($\Delta RH = 0, \Delta T \neq 0$).

Test conditions	Cold inlet	Hot inlet
Temperature	~23°C	~50°C, 44°C
Relative humidity	~4%	~4%
Air flow rate	200 L/min, 100 L/min	200 L/min, 100 L/min
Air face velocity	1.6 m/s, 0.8 m/s	1.6 m/s, 0.8 m/s

2.3 Steady state calibration of instruments

2.3.1 Humidity measurement

The relative humidity is measured using a humidity sensor transmitter manufactured by Vaisala. This instrument measures the relative humidity using a capacitance based thin-film polymer sensor. Although this instrument can also measure temperature using a RTD (resistance temperature device) temperature sensor, it is not used to measure temperature in this research because this RTD sensor has a very slow

thermal response (Wang, 2005). The instrument is used to measure relative humidity under constant temperature conditions. Four humidity sensors were used for the humidity transient experiments. One sensor is located at each of the two inlet and two outlet flow tubes. According to the manufacturer, the Vaisala humidity sensor has an accuracy of ±1% RH when used within the range of 0 to 90% RH and an accuracy of ±2% RH when used within the range of 90% to 100% RH (Vaisala, 1998).

Steady state calibration of the humidity sensors are required to determine the bias error in the instrument, which is especially important for the measurements of the outlet airstreams. The humidity sensors were calibrated against a chilled mirror sensor which has a bias uncertainty of ±0.3°C in dew point and ±1% RH at 20°C. These sensors were used for humidity response experimental tests performed at room temperature (i.e., isothermal conditions). Table 2.3 shows the values for the steady state calibration of two humidity sensors used at the outlet section of the experiments (Wang et al., 2005). The bias in the calibrated humidity sensor is approximately ±1% RH at room temperature.

Table 2.3. Steady state relative humidity calibration for two outlet humidity sensors.

(Chilled Mirror) Calibrator Reading (%)	Sensor Reading (%)	
	Sensor 1	Sensor 2
10.5	10.4	10.6
21.7	20.6	20.8
32.3	31.1	31.2
41.1	41.0	41.0
52.0	52.4	52.2
62.5	62.9	63.1
71.7	72.9	73.0
83.2	83.8	84.0
94.6	94.3	95.4

2.3.2 Temperature measurement

The air temperature is measured using T-type thermocouples. The T-type thermocouples have an accuracy of ±0.1°C for temperature differences. The T-type thermocouples used for the temperature response experimental tests were calibrated at steady state against a standard Dry-Well Calibrator which has an accuracy of ±0.1°C and can be used to generate a range of temperatures. After calibration, the bias uncertainty in the T-type thermocouples was determined to be approximately ±0.2°C for the thermocouples used. The six thermocouples used across one tube diameter in the outlet tubes as shown in Figure 2.3 were calibrated in the same manner. Table 2.4 shows the values for the steady state calibration of five T-type thermocouples used at the outlet section of the experiments.

Table 2.4. Steady state temperature calibration for five outlet thermocouples.

Calibrator Reading (^{o}C)	Sensor Reading (^{o}C)				
	TC1	TC2	TC3	TC4	TC5
18.01	17.97	18.07	17.88	18.1	18.19
22	22.08	22.14	22.02	22.08	22.25
30	30.06	30.12	30.06	30.06	30.24
40	40.11	40.11	40.11	40.11	40.11
50	50.05	50.05	50.11	50.05	50.22

2.4 Data Acquisition

All the data from experiments performed in this thesis were recorded using a LabMate data acquisition and controller by Sciemetric Instruments. The LabMate data acquisition uses an analog to digital (A/D) converter of 12 bit-plus-sign to perform all analog measurements and it has a maximum sampling rate of 5 samples per second.

This data acquisition is designed in such a way that measurement signals from humidity sensors and thermocouples are sent and stored on a Compaq computer and the immediate visual recognition of stored data can be seen through the monitor. The signals that need to be collected during each experiment are: 4 humidity signals and 8 temperature signals. The thermocouples are connected directly to the data acquisition board while the humidity sensors are connected through copper paired cables.

2.5 Summary

This chapter described the experimental facility that will be used to measure the response of sensors and energy wheels to a step change in temperature or humidity conditions. The data obtained with this facility will be presented in Chapter 4. The next chapter, Chapter 3, will present a model that relates the data measured during a step change (i.e., the step response) to the periodic response of energy wheels.

CHAPTER 3

EFFECTIVENESS MODEL AND SENSITIVITY STUDIES

In this chapter, the objective is to establish a relationship between the step response and the periodic response of an energy wheel. This relationship will allow the determination of the periodic response of a regenerative heat and moisture exchange wheel from the step humidity and temperature response measured using the facility presented in Chapter 2. A first-order linear system model will be used for this purpose. In addition, effectiveness equations will be developed to predict the performance of the wheel from the calculated periodic response. In this way, the effectiveness of an energy wheel will be determined from transient step response measurements. Since it is important to quantify the uncertainty in the predicted effectiveness, an uncertainty analysis is also included which provides the 95% uncertainty bounds in the steady state effectiveness predicted from transient measurements which have known uncertainties. This chapter concludes with sensitivity studies to investigate a range of energy wheel properties and measurement uncertainties on the predicted effectiveness and its uncertainty.

3.1 Problem formulation

Often in engineering, physical problems are described and deduced from general mathematical equations of physical principles, which are solved analytically or numerically. The act of formulating these equations from physical principles for a specific engineering problem and specifying their boundary and initial conditions is referred to as modelling.

The simplified equations that govern the transfer and storage of sensible energy on the supply or exhaust side of a counter flow sensible regenerative heat wheel exchanger are presented by Shah (1981). The sensible or thermal energy balance equation on the air side describing the balance between advection heat transfer in the air and convective heat transfer between the air (g) and the wheel matrix (m) is

$$\frac{\partial T_g}{\partial z^*} = NTU(T_m - T_g)\,. \tag{3.1}$$

where T_m is the matrix temperature, T_g is the air temperature and z^* is the dimensionless axial coordinate. The equation describing the balance between thermal energy storage in the wheel matrix and convective heat transfer between the air flowing through the wheel and the matrix is

$$\frac{\partial T_m}{\partial t^*} = \frac{NTU}{Cr^*}(T_g - T_m)\,. \tag{3.2}$$

where Cr^* is the matrix heat (or moisture) capacity ratio on the supply or exhaust side. All symbols are defined in the nomenclature and the governing dimensionless groups are defined as:

$$NTU = \frac{hA_s}{(\dot{m}Cp)_g} \tag{3.3}$$

$$Cr^* = \frac{(MCp)_m N}{(\dot{m}Cp)_g} \tag{3.4}$$

where h is the convective heat transfer coefficient, A_s is the heat and mass transfer surface area on the supply or exhaust side, M is the total mass of the wheel and N is the angular speed of the wheel.

Similarly, the mass diffusion equations for water vapour transfer in a regenerative energy wheel are given by Simonson and Besant (1999a and b) as

$$\frac{\partial \rho_v}{\partial z^*} = NTU_{mt}(\rho_{v,m} - \rho_v), \tag{3.5}$$

which describes the mass balance in the air and

$$\frac{\partial \rho_{v,m}}{\partial t^*} = \frac{NTU_{mt}}{Cr^*_{mt}}(\rho_v - \rho_{v,m}), \tag{3.6}$$

which describes the mass balance in the desiccant material in the wheel matrix, where $\rho_{v,m}$ is the water vapour density of the desiccant material in the wheel matrix, ρ_v is the water vapour density of air. The dimensionless groups describing moisture transfer are:

$$NTU_{mt} = \frac{h_m A_s}{Q}, \tag{3.7}$$

which is equal to NTU if the Lewis number is unity (Simonson and Besant, 1999a and b), and

$$Cr^*_{mt} = \left(\frac{\rho_{d,dry} A_{s,d} L}{Qp}\right)\left(\frac{\partial u}{\partial \rho_{v,m}}\right) \tag{3.8}$$

where Q is the volume flow rate of air on the supply or exhaust side, L is the thickness of wheel, p is the period of exposure per cycle for the supply or exhaust gas, $\rho_{d,dry}$ is the density of dry desiccant in the wheel and u is the mass fraction of water in the desiccant.

3.2 Mathematical model

To achieve the objectives of this chapter, mathematical models of the air properties are developed as the air leaves an energy wheel when there is a step change in the inlet air humidity and temperature. Then, these models are used to predict the outlet conditions of an energy wheel when the input properties are changed in an infinite series of step changes which are periodic or steady state as occurs in rotating energy wheel matrices in HVAC applications. The energy wheel is treated as a lumped parameter system defined by input and output only and the axial coordinate z is not considered in the model.

It is noted that equations (3.2) and (3.6) are of the mathematical form of a first-order linear system having time as the independent variable. These equations can be represented by a differential equation in the form

$$\frac{dx}{dt} + ax = af(t) . \tag{3.9}$$

where t is independent variable time, a is a characteristic of the system (whose inverse is the time constant, τ), $f(t)$ is the forcing function or external input, x is the output or response of the system as a function of time. For this research, the forcing function is a

step change in temperature (K) or water vapour density (kg/m^3) of the air and the output is either the matrix temperature, T_m, or the water vapour density in the matrix $\rho_{v.m}$. The dimensionless time introduced in equations (3.2) and (3.6) is defined as

$$t^* = \left(\frac{1}{p} \left(t - \frac{z}{\overline{U}} \right) \right). \tag{3.10}$$

where $\overline{U}$ is the mean air flow velocity in an exchanger flow channel. For small dwell times or carry over ratios in the wheel, $z/\overline{U}$ is negligible and equation (3.10) becomes

$$t^* = \frac{t}{p}. \tag{3.11}$$

For this operating condition, the time response of the outlet air temperature, T_g, and vapour density, ρ_v, must have similar characteristics as that of the matrix – so by measuring the outlet air response we can get the wheel matrix response characteristics. Introducing equation (3.11) into equations (3.2) and (3.6), we have

$$\frac{\partial T_m}{\partial t} + \frac{NTU}{Cr^* p} T_m = \frac{NTU}{Cr^* p} T_g, \text{ and} \tag{3.12}$$

$$\frac{\partial \rho_{v,m}}{\partial t} + \frac{NTU_{mt}}{Cr^*_{mt} p} \rho_{v,m} = \frac{NTU_{mt}}{Cr^*_{mt} p} \rho_v. \tag{3.13}$$

Equating equations (3.12) and (3.13) with equation (3.9) implies that

$$a = \frac{1}{\tau} = \frac{NTU}{Cr^* p} \text{ and} \tag{3.14}$$

$$a = \frac{1}{\tau} = \frac{NTU_{mt}}{Cr^*_{mt} p}, \tag{3.15}$$

where τ is the time constant. This comparison also shows that the forcing function, *af(t)*, is the temperature or water vapour density in the inlet air:

$$aT_g = af(t) \tag{3.16}$$

$$a\rho_v = af(t). \tag{3.17}$$

Therefore, comparing equation (3.9) with equations (3.2), (3.6), (3.12) and (3.13), which relate the properties of the air and matrix, it is seen that the heat and mass transfer equations are coupled, first-order linear differential equations in time. Hence, a model of a linear first-order system is used in the development of the response relationship. It is important to note that, although equations (3.1) to (3.13) are for a counter flow or parallel flow exchanger, the forcing function (or boundary conditions) typically used in linear system design theory represents a parallel flow arrangement with both the supply and exhaust flow in the same direction. Therefore, the results obtained from this linear model will represent an energy wheel operating in parallel flow. Later the counter flow results will be calculated using these parallel flow results.

3.3 Response to input functions relevant to energy wheel testing

The output or response of a system to various input functions typical of energy wheels is considered in this section. These input functions are constant (or step) and rectangular periodic input functions. These are important because the response of the energy wheel to a step input function (Wang et al., 2005) will be used to estimate the steady state response which is the response to a rectangular periodic input function as the wheel matrix rotates between supply and exhaust airstreams.

3.3.1 Step input function

The step input function is defined as

$$f(t) = \begin{cases} b \text{ for } t \geq 0 \\ 0 \text{ for } t < 0 \end{cases} \tag{3.18}$$

When $f(t) = 0$, equation (3.9) is said to be homogenous and the general solution of equation (3.9) is given as

$$x(t) = ce^{-at}, \tag{3.19}$$

where $x(t)$ is the output or response of the system and c is the constant of integration. When $f(t) \neq 0$, equation (3.9) is said to be non-homogenous and the general solution in the form of equation (3.20) is applied as follows (Kaplan, 1981)

$$x(t) = e^{-at} \int_0^t e^{at} af(t)dt + ce^{-at}, \tag{3.20}$$

where c is a constant of integration. Substituting equation (3.18) into equation (3.20), gives

$$x(t) = b + ce^{-at}, \tag{3.21}$$

For the case of $x(0) = 0$, $c = -b$. Therefore $x(t) = b$ is regarded as the equilibrium or steady state solution and $-be^{-at}$ is the transient solution. Figure 3.1 shows the response of an energy wheel with various time constants to a step input function $ab = 1$. As expected, the response is quicker as the time constant decreases where 63% of the change occurs during one time constant. Two of the time constants shown in Figure 3.1 are representative of the humidity and temperature sensors used in this research (e.g τ = 4 s) and energy wheels (e.g. τ = 10 s) according to the research of Wang et al. (2005).

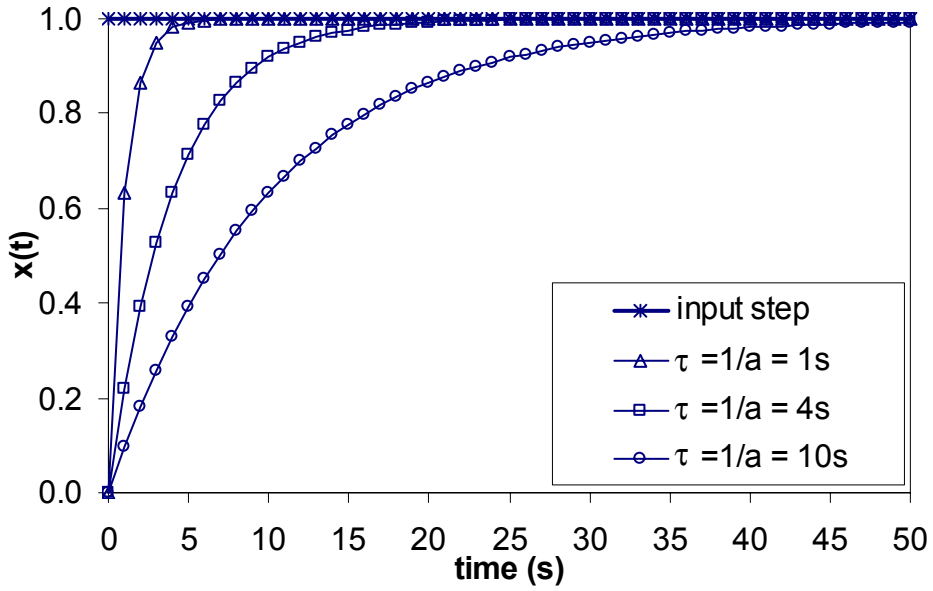

Figure 3.1. *Step response of a linear system to a unit step input.*

3.3.2 Rectangular periodic input

The dynamic operation of an energy wheel matrix rotating between two air streams with constant but different temperature and humidity conditions behaves like a linear system with a steady state rectangular periodic input forcing function. The matrix of an energy wheel rotating between hot and cold air streams will be subject to series of step changes in the inlet conditions that are periodic, steady and rectangular. The rectangular input function shown in Figure 3.2 is defined as

$$f(t) = \begin{cases} 1 & \text{for } 0 \le \theta \le \pi \\ -1 & \text{for } \pi \le \theta \le 2\pi \end{cases} \tag{3.22}$$

where θ is the angle of wheel rotation, wt , (radians) and w is the wheel speed (rad/s).

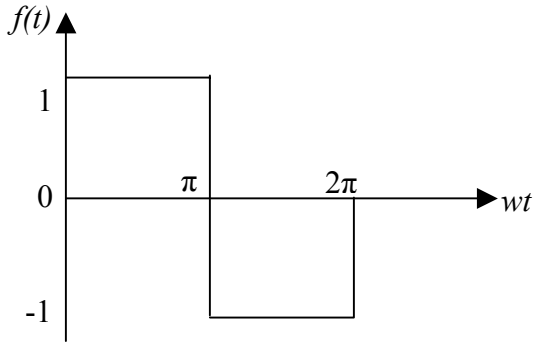

Figure 3.2. *Periodic (rectangular) unit input function of an energy wheel.*

This rectangular wave input function can be written in the form of a Fourier series,

$$f(t) = a_o + \sum_{n=1}^{\infty} \left(a_n \cos nwt + b_1 \sin nwt \right), \tag{3.23}$$

$$\text{where } a_o = \frac{1}{\pi}\int_0^{\pi/w} f(t)dt + \frac{1}{\pi}\int_{\pi}^{2\pi/w} f(t)dt = 0, \tag{3.24}$$

$$a_n = \frac{1}{\pi}\int_0^{\pi/w} f(t)\cos nwtdt + \frac{1}{\pi}\int_{\pi}^{2\pi/w} f(t)\cos nwtdt = 0 \text{ for all } n, \text{ and} \tag{3.25}$$

$$b_n = \frac{1}{\pi}\int_0^{\pi/w} f(t)\sin nwtdt + \frac{1}{\pi}\int_{\pi}^{2\pi/w} f(t)\sin nwtdt = \begin{cases} 4/(n\pi) \text{ for } n = 1,3,5,\ldots \\ \\ 0 \text{ for } n = 2,4,6,\ldots \end{cases}. \tag{3.26}$$

The periodic unit input function *f(t)* expressed as a Fourier series in equation (3.23) can now be rewritten to get the forcing function *af(t)*

$$af(t) = \frac{4a}{\pi}\sum_{n=1}^{\infty}\frac{\sin nwt}{n} \quad \text{for } n = 1, 3, 5,\ldots \tag{3.27}$$

Substituting equation (3.27) as the input forcing function into equation (3.18), the periodic output (or steady-state solution) is (Kreyszig, 1999):

$$x(t)=\sum_{1}^{\infty}\frac{4a}{\pi n\left(a^2+(nw)^2\right)}\left(a\sin nwt-wn\cos nwt\right) \quad \text{for } n = 1, 3, 5,\ldots \tag{3.28}$$

Rewriting this output response equation using a phase shift angle α, gives

$$x(t)=\sum_{1}^{\infty}\frac{4a}{\pi n\sqrt{a^2+(nw)^2}}\left[\sin(nwt-\alpha)\right] \quad \text{for } n = 1, 3, 5,\ldots \tag{3.29}$$

The amplitude energy ratio A', defined as the ratio of the output amplitude to the input amplitude averaged for one half cycle, which represents the energy transfer, is a function of only a and w and is given as:

$$A'=\sum_{n=1}^{\infty}\frac{a}{\sqrt{a^2+(nw)^2}}=\sum_{n=1}^{\infty}\aleph_n \quad \text{for } n = 1, 3, 5,\ldots \tag{3.30}$$

$$\text{where } \aleph_n=\frac{a}{\sqrt{a^2+(nw)^2}} \quad \text{for } n = 1, 3, 5,\ldots \tag{3.31}$$

and the corresponding phase shift angle is also constant when a and w are constant:

$$\alpha=\tan^{-1}\left(\frac{\left(\sum_{n=1}^{\infty}\frac{4awn}{\pi n\left(a^2+(nw)^2\right)}\right)^2}{\left(\sum_{n=1}^{\infty}\frac{4a^2}{\pi n\left(a^2+(nw)^2\right)}\right)^2}\right)=\tan^{-1}\left(\sum_{n=1}^{\infty}\frac{nw}{a}\right) \quad \text{for } n = 1, 3, 5,\ldots \tag{3.32}$$

Since the magnitude of the terms in series equation (3.28) decreases rapidly with increasing n, it is found that including $n \geq 21$ is unnecessary in the calculations for the time constants used. Therefore, terms $n \geq 21$ are neglected in this thesis. The error that results from neglecting these terms is less than 0.0001%.

Figure 3.3 shows the steady state periodic response $x(t)$ of a system for one cycle with various time constants when the rectangular periodic forcing function $af(t)$

in equation (3.27) has an angular frequency of (a) $\frac{\pi}{3}$ rad/s (10 rpm) and (b) $\frac{2\pi}{3}$ rad/s (20 rpm). Comparison of Figure 3*(a)* and 3*(b)* shows that as the wheel speed increases, the amplitude of the output is reduced. This output is the matrix temperature, which is closely coupled to the air temperature for a typical energy wheel. Therefore, the time constant of the matrix will be equal to the time constant measured in the airstream and presented in Chapter 4.

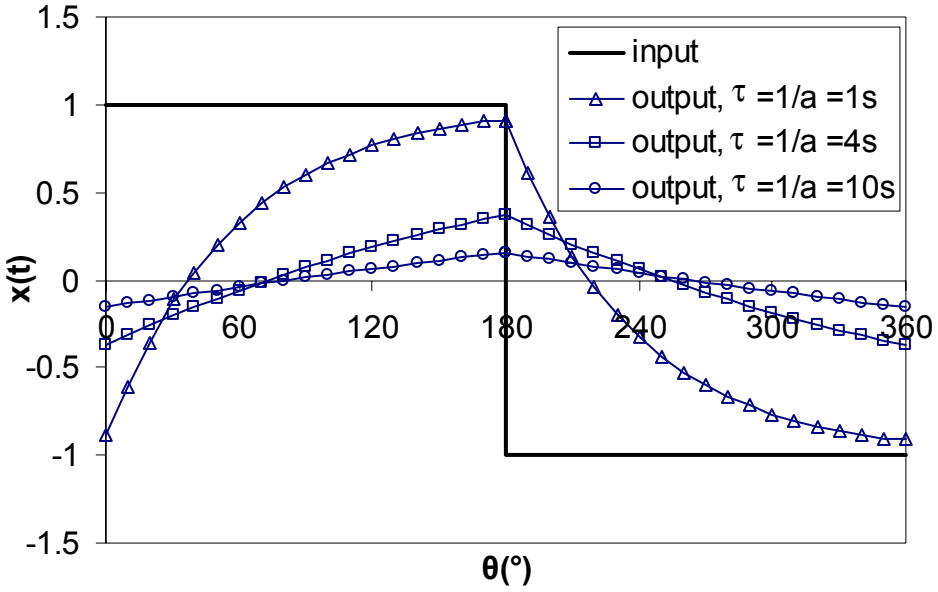

(a)

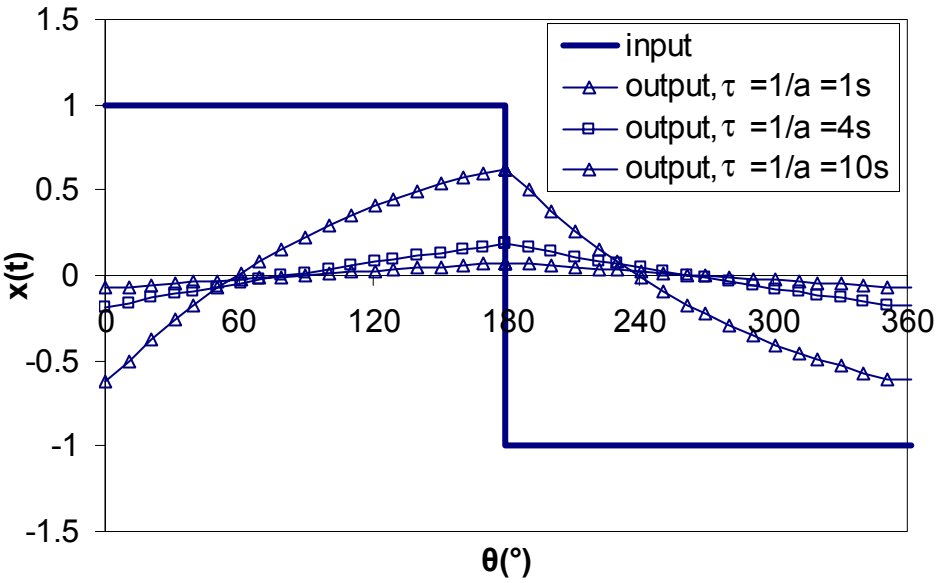

(b)

Figure 3.3. *Periodic response* $x(t)$ *of a system with various time constants to a rectangular periodic input function with (a)* $w=\frac{\pi}{3}$ *rad/s (10 rpm) and (b)* $w=\frac{2\pi}{3}$ *rad/s (20 rpm).*

Figure 3.3 shows the effects of the angular frequency and time constants on the output for a first order linear system. The output of a system with a small time constant follows the input function more closely than a system with a large time constant. In many applications, it is desirable for the output to follow the input closely, but the opposite is the case for an energy exchanger application.

To help understand this physical process, consider the results in Figure 3.3(a) and imagine that the input of 1 during the first 180° of rotation represents the inlet hot air stream dimensionless temperature and the input of –1 represents the cold air stream dimensionless temperature. For this example, the output during the first half rotation represents the dimensionless temperature of the air leaving the exchanger on the hot side and the output during the second half rotation (180° to 360°) represents the dimensionless temperature of air leaving the exchanger on the cold side. As the wheel rotates from 0° to 180°, the outlet dimensionless temperature on the hot side increases and the exchanger transfers less heat because the wheel temperature approaches that of the flowing air. Since the goal of the exchanger is to cool the hot air stream during the first 180° rotation (and heat the cold air stream an equal amount during the second 180°), it can be seen that the lower the average output during the first half cycle (and the higher the average output during the second half cycle), the better the exchanger. Therefore, the amplitude energy ratio between the output and input is related to the performance of the exchanger such that the lower the amplitude energy ratio, the higher the effectiveness of the exchanger.

The effects of the wheel speed or angular frequency (w) on the amplitude energy ratio A' (equation (3.30)) and the phase shift angle α (equation (3.32)) are shown in Figure 3.4. As $w \to \infty$, $\alpha \to 90^o$ ($\frac{\pi}{2}$ *rad*) and $A' \to 0$. At w = 0, the output is the steady state step response.

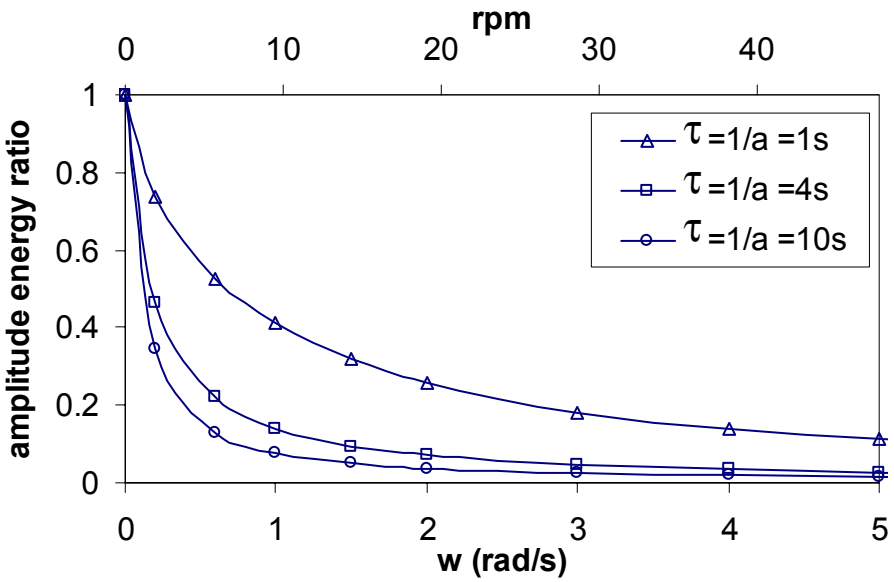

(a)

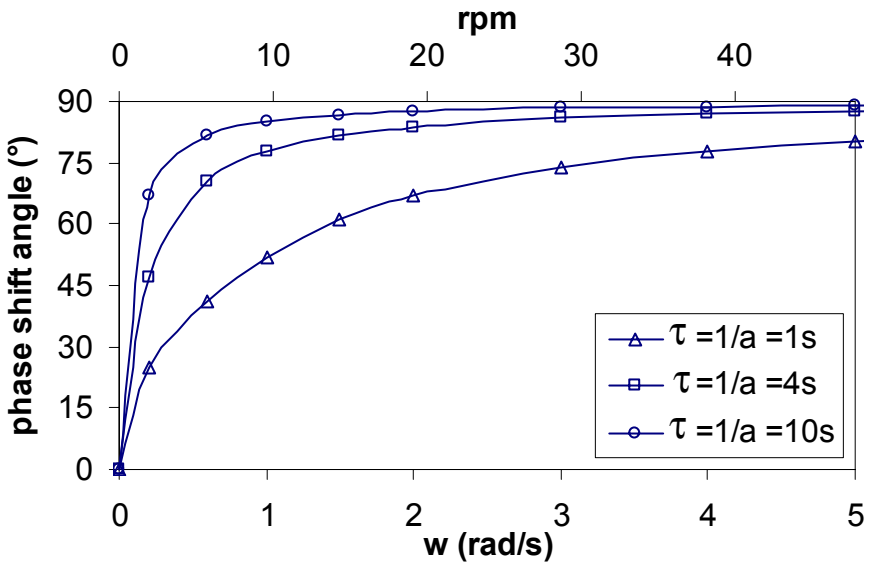

(b)

Figure 3.4. *Amplitude energy ratio (a) and phase shift angle (b) of a system with rectangular periodic input (Figure 3.2) versus wheel speed.*

Figures 3.4 shows that, as the wheel speed increases, the amplitude energy ratio decreases and the phase shift angle increases. The phase shift angle increases toward 90° as the wheel speed becomes large and time constants increase. Consider a wheel

rotating at 2 rad/s (19.1 rpm) with time constant of 4s. The amplitude energy ratio of the system is 0.07 and the phase shift angle is 83.8° while at 1 rad/s (9.55 rpm) and a time constant of 4s, the amplitude energy ratio of the system is 0.14 and the phase shift angle is 77.8°.

3.4 Effectiveness

The effectiveness of a heat exchanger is defined as the ratio of the actual heat transfer rate to the maximum possible heat transfer rate (for an infinite heat transfer surface area). This same type of definition will be used in this analysis when determining the effectiveness based on the input and output of a linear system. The effectiveness of the system can be defined using the input-output energy ratios. These energy ratios are represented by the integrated areas under the input and the output curves in Figure 3.5 and previously in Figure 3.3.

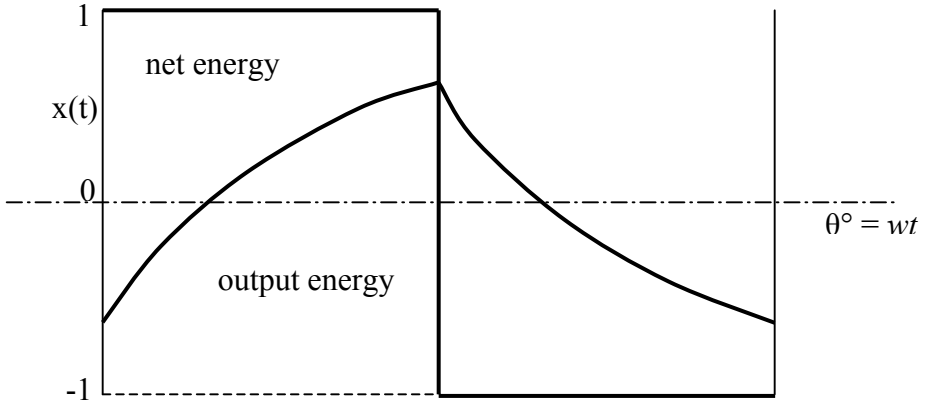

Figure 3.5. *The input and output energies of the wheel.*

Therefore, the effectiveness is defined as the ratio of the *net energy* to the *maximum possible energy*. The net energy is the difference between the maximum possible (input) area and the output area. Recalling that the model is for a parallel flow regenerator, the effectiveness of the parallel flow regenerator ε_{PF} is thus represented as:

$$\varepsilon_{PF} = \frac{\text{net energy}}{\text{maximum possible energy}} \tag{3.33}$$

Since the areas under the output and the input are both symmetrical, as shown in Figures 3.3 and 3.5, the average is taken over one-half cycle and equation (3.33) is expressed as:

$$\varepsilon_{PF} = 1 - \frac{w}{2\pi} \int_0^{\pi/w} (1 + x(t))dt \tag{3.34}$$

where $x(t)$ is given by equation (3.28). After integrating equation (3.34), the effectiveness is a function of one wheel characteristic a, which is the inverse of the time constant (to be measured experimentally), and one operating parameter, the wheel speed (w). The relation is:

$$\varepsilon_{PF} = 0.5 - \frac{1}{\pi^2} \sum_{n=1}^{\infty} \frac{4a^2}{n^2\left(a^2 + (nw)^2\right)} \quad \text{for n = 1,3,5,…} \tag{3.35}$$

A parallel flow exchanger with balanced supply and exhaust air flows will have a maximum effectiveness of 50% when the average outlet temperatures of both air streams are equal to the average temperature of the two inlet air streams (when the outlet temperatures are close to the inlet temperature, little energy will be transferred and the exchanger will have a low effectiveness). A counter flow heat exchanger has a very high effectiveness when the average outlet temperature of one air stream (say air

stream A) is close to the inlet temperature of the other air stream (say air stream B) (and consequently very far from the inlet temperature of air stream A); on the other hand, may have an effectiveness that approaches 100%. Therefore it is desired that the output does not follow the input closely.

The behaviour of the system, expressed as the amplitude energy ratio is a function of energy transferred (Cochin and Plass, 1990). Hence, the effectiveness of the system based on energy can also be defined as a function of the amplitude energy ratio of the system since the amplitude energy ratio is the ratio of the average output amplitude over the cycle to the input amplitude. It follows from Figures 3.3 and 3.4 and the previous statements, that an exchanger that operates with balanced supply and exhaust air flows or Cr =1 will have maximum effectiveness (i.e., will approach 50% for parallel flow and 100% for counter flow) as the amplitude energy ratio approaches 0 and the phase lag approaches 90°. Therefore, for an energy exchanger, a lower output amplitude results in a lower amplitude energy ratio and consequently a higher effectiveness. Substituting equations (3.30) and (3.31) into equation (3.35) provides the relationship between effectiveness ε_{PF} and the amplitude energy ratio A' - so the effectiveness of a parallel flow exchanger can also be expressed as:

$$\varepsilon_{PF} = \frac{1}{2}\left[1 - \frac{8}{\pi^2}\sum_{n=1}^{\infty}\left(\frac{\aleph_n}{n}\right)^2\right] \quad \text{for n = 1,3,5,…} \tag{3.36}$$

where $$A' = \sum_{n=1}^{\infty}\aleph_n \quad \text{for n = 1,3,5,…} \tag{3.37}$$

Figure 3.6 shows the effectiveness of a parallel flow wheel (ε_{PF}) as a function of the wheel speed for various time constants $\left(1/a = \tau\right)$.

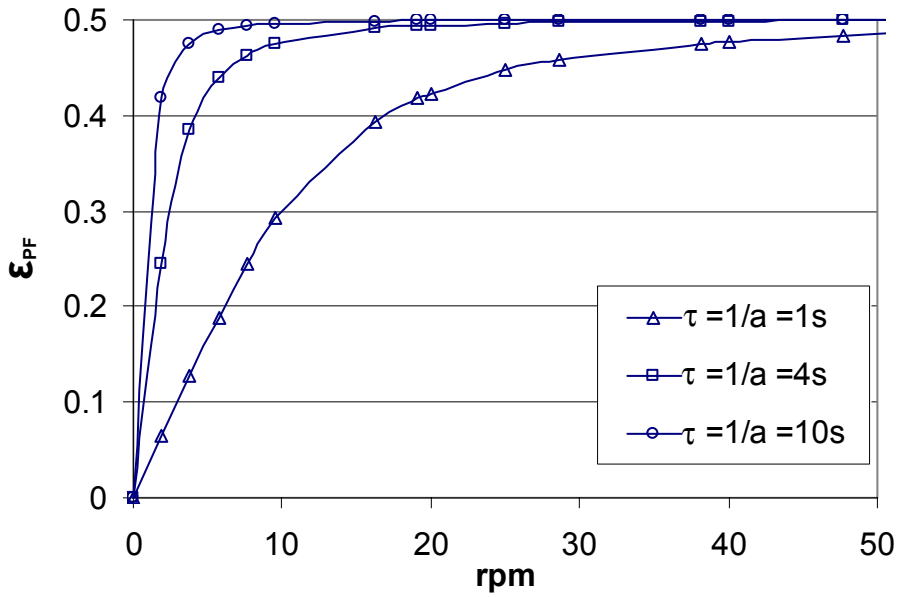

Figure 3.6. *Effectiveness of a parallel flow energy wheel as a function of the wheel speed for various time constants.*

Figure 3.6 shows that the effectiveness increases as both the time constant and wheel speed increase. It should be noted that increasing the energy wheel speed to a high value will have another less desirable consequence. It will increase the carry over of exhaust air to the supply side; so manufacturers limit the wheel speed to a practical range (e.g. 20 to 40 rpm) and the carry over is a small fraction of the total air flow rate (Simonson et al., 1999a and b). This leaves the time constant as the main parameter that needs to be examined. As the time constant increases, the output amplitude decreases thereby reducing the amplitude energy ratio shown in Figure 3.4. Equation (3.36) shows that a

reduction in the amplitude energy ratio increases the effectiveness. In Figure 3.6, the effectiveness increases from 0 to 50% as the wheel speed increases from 0 rpm to 50 rpm for time constants of 4 s and 10 s. At very large wheel speeds, the effectiveness approaches (50%) as expected for a parallel flow heat exchanger with $Cr = 1$.

To verify the effectiveness calculated from the linear system model, the results shown in Figure 3.6 are compared with analytical solutions of Romie (1992) and Hausen (1983) for a parallel flow heat regenerator. Using equations (3.4) and (3.14) to relate the key parameter in the linear system model (i.e., τ and w) with the key parameters in the analytical solution of Romie (1992) (i.e., NTU and Cr^*) allows a direct comparison between the model and the analytical solution. Figure 3.7 shows that the thermal effectiveness values calculated from the linear model (i.e., equation (3.35)) are in very close agreement with the results predicted by Romie (1992). The average and maximum differences between the effectiveness values determined with equation (3.35) and the analytical solution are 0.001 and 0.002 respectively. This demonstrates the accuracy of the linear system model applied in the thesis.

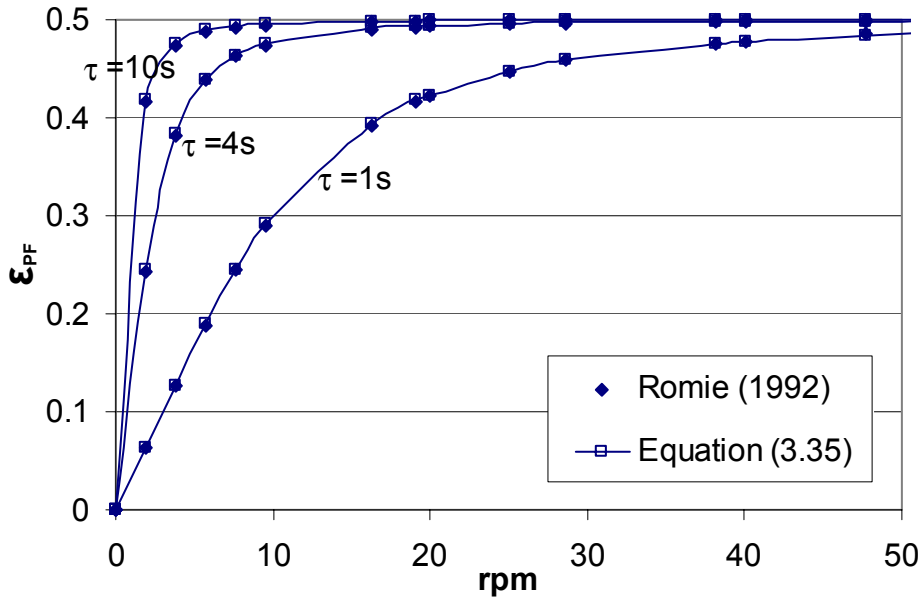

Figure 3.7. *Comparison of the effectiveness of a parallel flow regenerator calculated from equation (3.35) and Romie (1992).*

Since energy exchangers are almost always used in a counter flow and not parallel flow configuration, the effectiveness expression obtained thus far for a parallel flow regenerator (equation 3.35) needs to be modified to represent a counter flow configuration. It is known (Kays and London, 1984, and Simonson and Besant 1999a and b) that the effectiveness of a regenerator (ε) can be calculated as a product of effectiveness of a recuperator (ε^{rec}) and a function of Cr^*

$$\varepsilon = \varepsilon^{rec} f\left(Cr^*\right) \tag{3.38}$$

where Cr^* represents the matrix heat (or moisture) capacity ratio on the supply or exhaust side. Therefore, the effectiveness of a parallel flow (PF) sensible heat regenerator can be calculated as

$$\varepsilon_{PF} = \varepsilon_{PF}^{rec} f_{PF}\left(Cr^*\right) \tag{3.39}$$

where $f_{PF}\left(Cr^*\right)$ means a function of Cr^* of an exchanger operating in a parallel flow configuration and ε_{PF}^{rec} is the effectiveness of a parallel flow recuperator. In heat transfer literature, rotating heat exchangers are called regenerators and stationary heat exchangers are called recuperators. The effectiveness of a parallel flow heat exchanger (recuperator) with $Cr = 1$ is given (Incropera and Dewitt, 2002) as

$$\varepsilon_{PF}^{rec} = 0.5\left(1 - e^{-2NTU_{PF}}\right). \tag{3.40}$$

Using equations (3.35), (3.39) and (3.40), an "$NTU - a$" relationship for parallel flow heat regenerators can be established as

$$NTU_{PF} = -0.5\ln\left(1 - \frac{1}{f_{PF}\left(Cr^*\right)} + \sum_{n=1}^{\infty}\frac{8a^2}{f_{PF}\left(Cr^*\right)(\pi n)^2\left(a^2 + (\pi w)^2\right)}\right) \quad \text{for n = 1,3,5,...} \tag{3.41}$$

Note that this equation allows the calculation of NTU from a, w and $f_{PF}\left(Cr^*\right)$. Also, as a decreases (i.e., τ increases), NTU increases. To determine $f_{PF}\left(Cr^*\right)$, the results of the analytical solution presented by Romie (1992) are curve-fitted using a relationship of the same form as Kays and London (1984) and Simonson and Besant (1999a and b) used for counter flow regenerators, which is

$$\varepsilon_{PF} = \varepsilon_{PF}^{rec}\left[1 - \frac{1}{d\left(Cr^*\right)^e}\right], \tag{3.42}$$

where the values of constants d and e are adjusted to give the best fit. The value of d obtained is 330 and the value of e is 0.47. This makes the second term in equation (3.42) (i.e., the term in the square brackets) to be in the range

$$0.999 < f_{PF}\left(Cr^*\right) < 0.9998 \tag{3.43}$$

when $Cr^* \geq 5$ for typical energy wheel operation. Thus the term $f_{PF}\left(Cr^*\right)$ can be assumed equal to 1 for practical energy wheels and *NTU* can be determined knowing only the time constant and the wheel speed.

As previously stated, the aim is to relate the effectiveness of a parallel flow regenerator to a counter flow configuration. The effectiveness for a counter-flow (CF) sensible heat regenerator is presented by Kays and London (1984) as:

$$\varepsilon_{CF} = \varepsilon_{CF}^{rec}\left[1 - \frac{1}{9\left(Cr^*\right)^{1.93}}\right], \tag{3.44}$$

where

$$\varepsilon_{CF}^{rec} = f\left(NTU, Cr\right). \tag{3.45}$$

For typical energy wheels, $Cr^* \geq 5$ for wheel speeds ≥ 15 rpm, giving a practical range for the second term in equation (3.44) as

$$0.995 < f_{CF}\left(Cr^*\right) < 0.9998 \tag{3.46}$$

where $f_{CF}\left(Cr^*\right)$ means a function of Cr^* of an exchanger operating in a counter flow configuration. Thus the term $f_{CF}\left(Cr^*\right)$ can be assumed equal to 1 for practical energy wheels. Equations (3.43) and (3.46) which are approximately equal to 1 then permit relating the effectiveness of a sensible heat regenerator operating with a parallel flow configuration to one with a counter flow configuration. For the same mass flow rate of air for both cases, the *NTU* for the counter flow (CF) is equal to the *NTU* for parallel flow (PF), i.e.

$$NTU_{CF} = NTU_{PF}. \tag{3.47}$$

The statement that $NTU_{CF} = NTU_{PF}$ when the mass flow rate and inlet property conditions are the same in counter flow and parallel flow results from the fact that convection heat transfer coefficients between the air and the matrix are the same whether the air flow is arranged in counter flow or parallel flow. Therefore, the effectiveness of a counter flow heat regenerator with $Cr = 1$ and $f_{CF}\left(Cr^*\right) \approx 1$ can be approximated as:

$$\varepsilon_{CF} = \varepsilon_{CF}^{rec} = \frac{NTU_{CF}}{1 + NTU_{CF}}. \tag{3.48}$$

Substituting equations (3.41) and (3.47) into equation (3.48), the effectiveness for a counter flow regenerative heat wheel exchanger with $Cr = 1$ and $f_{CF}\left(Cr^*\right) \approx 1$ can be expressed as:

$$\varepsilon_{CF} = \frac{-0.5\ln\left[\sum_{n=1}^{\infty} \frac{8a^2}{(\pi n)^2\left(a^2 + (nw)^2\right)}\right]}{1 - 0.5\ln\left[\sum_{n=1}^{\infty} \frac{8a^2}{(\pi n)^2\left(a^2 + (nw)^2\right)}\right]} \quad \text{for n = 1,3,5,…} \tag{3.49}$$

Equation (3.49), therefore shows that the effectiveness of a regenerative exchanger (i.e. energy wheel) with a counter flow configuration can be predicted when the time constant of the wheel (which will be determined from the experimental step response) and the wheel speed are known. The predicted effectiveness of a counter flow energy wheel with various time constants using equation (3.49) is shown in Figure 3.8.

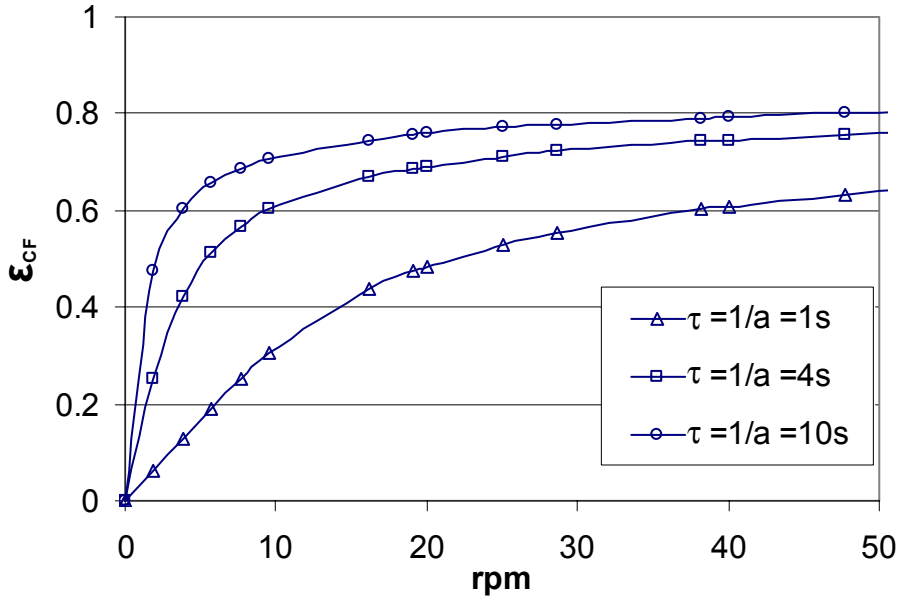

Figure 3.8. *The effectiveness of a counter flow energy wheel with various time constants calculated from equation (3.49).*

Figure 3.8 shows that as the time constant and wheel speed increase, the effectiveness increases. This is as expected because equation (3.41) shows that energy wheels that have a larger time constant will have larger values of *NTU*. The larger the NTU, the larger the heat transfer surface area and thus the higher the effectiveness.

In the research of Wang et al. (2005) and Chapter 4 of this thesis, it is found that using one time constant did not result in good correlations for the humidity or temperature step response obtained from experiments; therefore, two-time constant correlations with corresponding weighting factors are used. For combined effects of these time constants and their corresponding weighting factors (i.e., χ_1 and χ_2), NTU_{CF} is defined as

$$NTU_{CF} = \chi_1 NTU_{CF,1} + \chi_2 NTU_{CF,2} \tag{3.50}$$

where

$$\chi_1 + \chi_2 = 1\,,\ \chi_1 \geq 0\ ,\ \chi_2 \geq 0 \tag{3.51}$$

but with different values of χ_1 and χ_2 for each experiment. χ is the weighting factor of each time constant and subscripts 1 and 2 are for the properties (i.e., χ and NTU_{CF}) of the first and second time constants respectively. In Chapter 5, equation (3.50) will be used in equation (3.48) to determine the effectiveness of energy wheels whose humidity or temperature step response correlation has two time constants and two corresponding weighting factors.

3.5 Uncertainty in effectiveness

In this section, the uncertainty in the effectiveness predicted with equation (3.49) is determined using 95% confidence limits. This uncertainty in the effectiveness is calculated based on the fact that the uncertainty in the measured time constant, $\tau = 1/a$ can be determined from experiments (see Chapter 4). Knowing the uncertainty in the time constant $\left(U(\tau)/\tau = U(a)/a\right)$, the uncertainty in the effectiveness can be determined. The uncertainty in the effectiveness of an energy wheel with counterflow configuration is calculated using

$$U(\varepsilon_{CF}) = \left[\left(\frac{\partial \varepsilon_{CF}}{\partial a} U(a)\right)^2\right]^{1/2}. \tag{3.52}$$

Using equation (3.49),

$$\frac{\partial \varepsilon_{CF}}{\partial a} = \sum_{1}^{\infty}\left[\frac{-8aw^2}{\pi^2\left(a^2 + (nw)^2\right)^2\left(e^{-2NTU}\right)(1+NTU)^2}\right][1 + 2NTU] \quad \text{for n = 1,3,5,...} \tag{3.53}$$

and the uncertainty in the effectiveness of the counter flow regenerator is

$$U(\varepsilon_{CF}) = \left[\left\{ \sum_{1}^{\infty} \left[\frac{-8aw^2}{\pi^2 \left(a^2 + (nw)^2\right)^2 \left(e^{-2NTU}\right)(1+NTU)^2} \right] [1+2NTU](U(a)) \right\}^2 \right]^{1/2}$$

for n = 1,3,5,…(3.54)

3.6 Sensitivity studies

Assuming uncertainty limits for the measured time constants $\left(\frac{U(\tau)}{\tau} = \frac{U(a)}{a}\right) = \pm 10\%$ and $\pm 15\%$, the sensitivity of the uncertainty in effectiveness to the uncertainty in the measured time constant can be determined with equation (3.54). Also, the sensitivity of the uncertainty in effectiveness to measured time constants can also be determined. In addition, the sensitivity of the effectiveness and the uncertainty in effectiveness to the wheel speed is shown in this section.

In Figure 3.9, the effect of various uncertainty limits in the measured time constant on the uncertainty in the predicted effectiveness is shown. It should be noted that the typical uncertainties in the time constants measured using the newly designed transient response device for energy wheel is $\frac{U(\tau)}{\tau} = \frac{U(a)}{a} = \pm 10\%$ to $\pm 15\%$. It is seen from Figure 3.9 that as the uncertainty in the measured time constant increases, the uncertainty in effectiveness increases for all time constants. In addition, at any typical value of the uncertainty in the measured time constant, the uncertainty in effectiveness decreases as the time constant increases. Figure 3.9 shows that for an uncertainty in

time constant $U(\tau)/\tau = \pm 10\%$, the uncertainty in effectiveness $U(\varepsilon_{CF}) = \pm 5.2\%$ for a time constant of 4s whereas for an uncertainty in time constant $U(\tau)/\tau = \pm 15\%$, the uncertainty in effectiveness $U(\varepsilon_{CF}) = \pm 7.7\%$ for a time constant of 4s. This shows that the uncertainty in effectiveness is directly dependent on the uncertainty in the measured time constant.

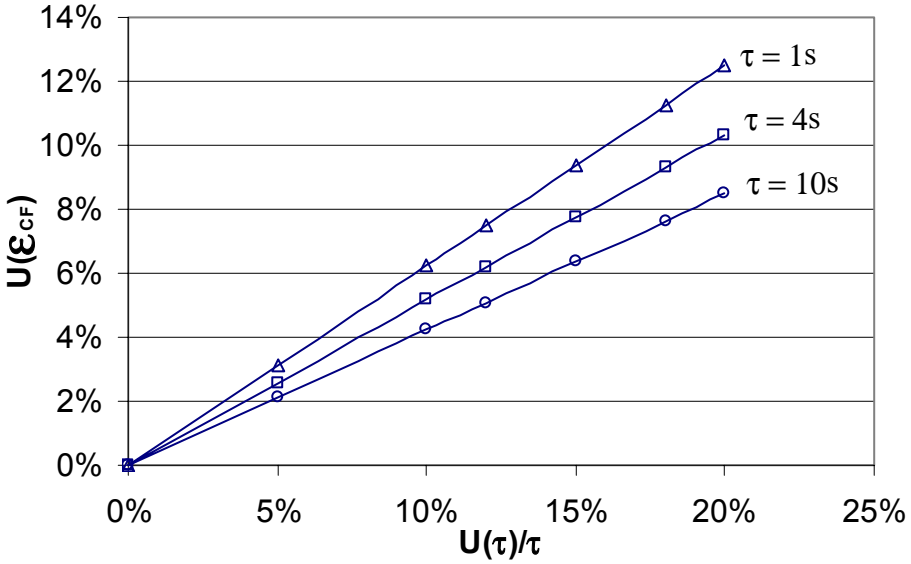

Figure 3.9. *The sensitivity of uncertainty in effectiveness to the uncertainty in the measured time constants determined at a wheel speed of 20 rpm.*

In Figure 3.10, the effect of various time constants on the uncertainty in the predicted effectiveness is shown. The figure shows the predicted uncertainty in the effectiveness of the wheel as a function of the time constant with $U(\tau)/\tau = U(a)/a = \pm 10\%$ and a wheel speed of 20 rpm. As the time constant increases, the predicted uncertainty limits in effectiveness ε_{CF} decrease. This figure shows that for an uncertainty limit of ±10% in the time constant, the uncertainty in the effectiveness

can be predicted within ±3% to ±5% for time constants of about 10s to 40s, which are expected to be the case for most commercial wheels (Wang et al., 2005 and Chapter 4 of this thesis).

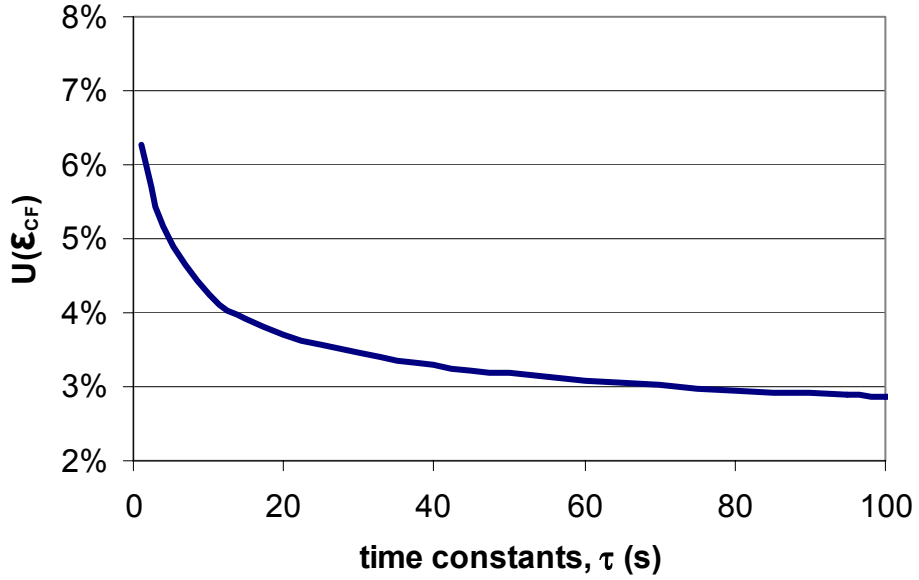

Figure 3.10. *The uncertainty limit in the effectiveness versus time constant for* $U(\tau)/\tau = \pm 10\%$*, w = 2.09 rad/s (20 rpm).*

The sensitivity of the uncertainty in effectiveness (assuming an uncertainty in the time constant $U(\tau)/\tau = \pm 10\%$) to the wheel speed is shown in Figure 3.11. The figure shows that the uncertainty in effectiveness for all time constants is zero at a wheel speed of 0 rpm. As the wheel speed increases from zero to large values, the uncertainty in effectiveness increases to about 6% and then decreases as the wheel speed becomes large.

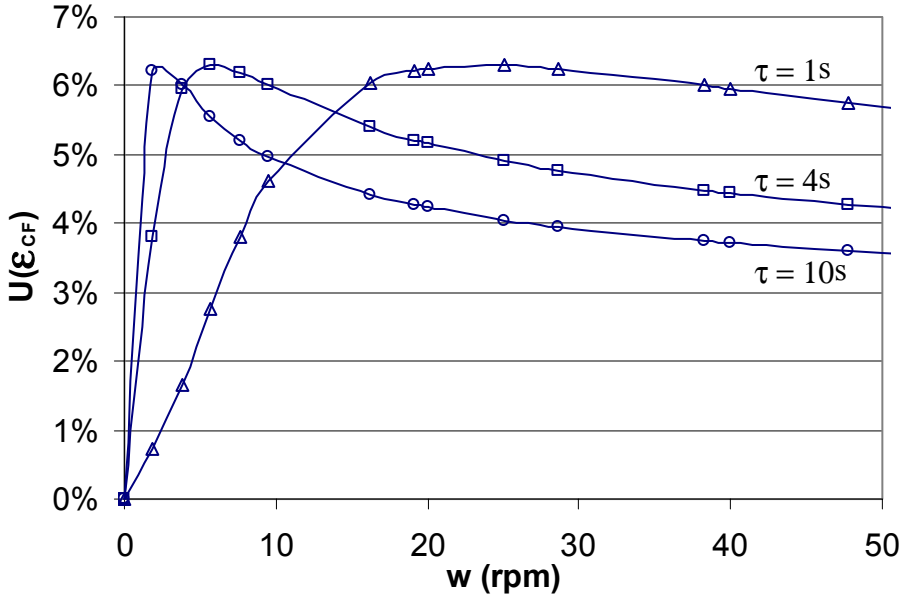

Figure 3.11. *The sensitivity of uncertainty in effectiveness to wheel speed.*

Both the predicted effectiveness and the uncertainty in the predicted effectiveness depend on the wheel speed. To show this effect more clearly, the effectiveness and uncertainty in effectiveness for a wheel with a time constant of 10s having an uncertainty of $U(\tau)/\tau = \pm 10\%$ is shown in Figure 3.12. The figure shows that at a wheel speed of 20 rpm, the effectiveness ε_{CF} = 76% and the uncertainty in effectiveness $U(\varepsilon_{CF}) = \pm 4.2\%$ while at a wheel speed of 40 rpm, the effectiveness ε_{CF} = 79% and the uncertainty in effectiveness is $U(\varepsilon_{CF}) = \pm 3.7\%$. This shows that the effectiveness increases as the wheel speed increases and the uncertainty in effectiveness decreases as the wheel speed increases.

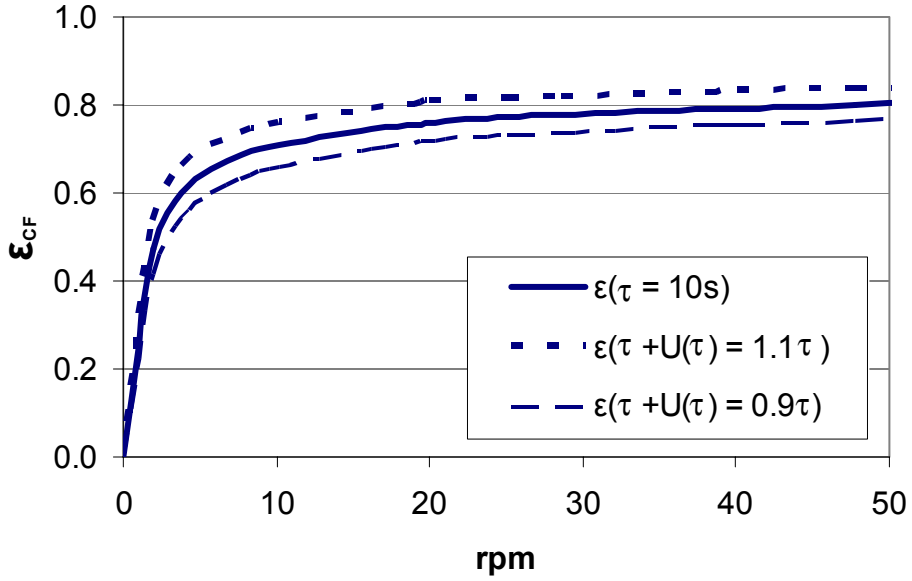

Figure 3.12. *The effect of wheel speed on the predicted effectiveness and uncertainty in effectiveness for* $\tau = 10 \pm 1s$.

3.7 Summary

In this chapter, an analytical model that predicts the effectiveness of a counter flow energy wheel has been developed using first-order linear design theory. Knowing the time constant of the wheel (measured from experiments) and the operating wheel speed, the effectiveness can be predicted. It is found that the effectiveness increases as the time constant and wheel speed increase. In addition, knowing the uncertainty in the measured time constant, the uncertainty in the effectiveness can be predicted. It is also found that as the wheel speed and time constant increase, the uncertainty in the effectiveness decreases.

The next chapter, Chapter 4, will present the time constants of several different wheels determined from transient response experiments. In Chapter 5, these time

constants will be used in the model developed in this chapter to estimate the effectiveness of these wheels and the uncertainty in the effectiveness values.

CHAPTER 4

EXPERIMENTS AND DATA FOR TIME CONSTANTS

In this chapter, transient response experiments are performed on several different wheels with known effectiveness values (i.e. effectiveness determined using the standard testing method of ASHRAE Standard 84-1991 (Shang, 2002)). The experimental test facility described in Chapter 2 is used to measure the transient response characteristics of energy wheels for either a step change in the inlet flow humidity or temperature when humidity sensors and thermocouples are placed upstream and downstream of the wheel. The aim of this chapter is to present measured data for the transient response characteristics (i.e. time constants and weighting factors) of these tested energy wheels alone implying that the transient response characteristics of the humidity and thermocouple sensors must be fully accounted for before the energy wheel response is predicted. The analysis of Wang (2005) presented in Appendix A and partly in this chapter will be used for this purpose. Also, the effect of heat conduction in the wheel matrix outside of the flow tube areas is investigated and the temperature response test data is corrected for this systematic error. Finally, transient characteristics of numerically simulated wheels are also included in this chapter.

Since it is important to quantify the uncertainty in the measured transient characteristics, an uncertainty analysis presented in Appendix B predicts the 95% uncertainty bounds in the measured transient response characteristics.

4.1 Transient response experiments, data and correlation equations

The experimental apparatus shown in Figure 2.1(a) is designed to obtain the latent effectiveness using data from the transient response characteristics of an energy wheel plus humidity sensor or the sensible effectiveness using data from the energy wheel plus thermocouple for a step change in inlet humidity or temperature.

Before the start of each transient test, the test facility, shown in Figure 2.1, is run till steady state conditions are reached for all the properties. Each transient test is started when the inlet conditions of the supply air tubes entering a stationary wheel are interchanged in a step fashion and the outlet sensors (humidity sensors and thermocouples) undergo a decrease or increase in either the humidity or temperature. During this step change in the inlet conditions the stationary wheel matrix gains or loses either moisture or heat until the test is completed. Each test is completed when these outlet sensor readings approach the inlet conditions after about 30 minutes.

Two types of transient experiments (humidity and temperature) are performed on each of three different wheels using the same face velocity used by Shang (2002) so that the steady state and transient effectiveness results can be directly compared. Face velocity is defined as the velocity of the air stream approaching the face of the wheel.

Throughout this thesis, these two tests will be referred to as the wheel plus humidity sensor tests or the wheel plus thermocouple tests. It is necessary to use only the transient response characteristics (i.e., time constants and weighting factors) of an energy wheel alone to predict the effectiveness using the method presented in Chapter 3. To achieve this, the transient response characteristics of the wheel alone are determined knowing the transient response characteristics of the sensors and the transient response characteristics of the wheel plus humidity sensor or wheel plus thermocouples using the method presented by Wang (2005). This analysis is used in this chapter, together with the response characteristics of the humidity sensors and thermocouples determined by Wang (2005).

4.1.1 Energy wheel plus humidity sensor

In this section the measured response characteristics of different wheels plus humidity sensors are presented. The operating conditions under which these experiments are conducted are selected to give a wide range of operating conditions listed in Table 4.1. These are for a range of flow rates and step sizes of inlet air humidities and supply air face velocities.

Table 4.1. Test conditions for energy wheel plus humidity sensor experiments ($\Delta RH \neq 0, \Delta T = 0$).

Test Conditions	Dry inlet	Wet inlet
Temperature	~23°C	~23°C
Relative humidity	~5%	~40%, 50%, 60%
Air flow rate	200 L/min, 100 L/min	200 L/min, 100 L/min
Air face velocity	1.6 m/s, 0.8 m/s	1.6 m/s, 0.8 m/s

Figure 4.1 shows the measured energy wheel plus humidity sensor response data for a typical energy wheel with a step change in inlet humidity from 5%RH to 40%RH with both inlets at the same temperature (~23°C). In this figure, the step change is introduced at a time of 50s as noted in the figure.

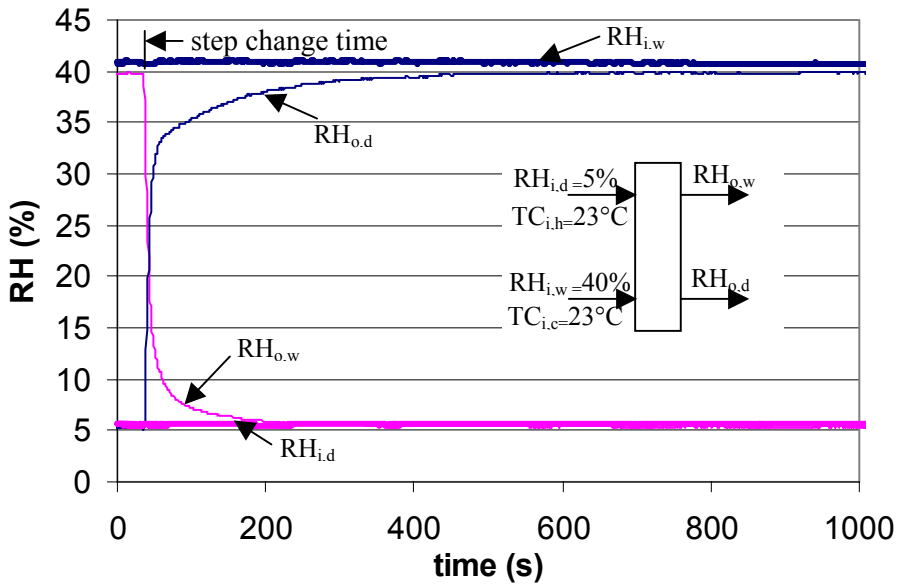

Figure 4.1. *Measured inlet and outlet relative humidities for 100 mm thick energy wheel with a molecular sieve coated wheel matrix exposed to a step change in relative humidity with no change in temperature (ΔRH=35%, ΔT=0).*

Figure 4.1 shows that each outlet humidity sensors ($RH_{o,d}$ and $RH_{o,w}$) appears to indicate data that will correlate with an exponential type of equation with time after the step change. For inlet humidity step change, Wang (2005) found that using only one time constant did not result in good correlations; therefore, two-time constant correlations are used for each outlet humidity increase and decrease. Equations (4.1) and (4.2) are found to result in good correlations when the best values of the empirical

weighting factors (X_1, X_2) and time constants (T_1, T_2) are chosen. The correlation equation describing the adsorption of water vapour into the wheel and sensor is

$$\frac{\Delta\Phi}{\Delta\Phi_o}(t)_{ads} = X_1\left(1-e^{-t/T_1}\right)+X_2\left(1-e^{-t/T_2}\right) \tag{4.1}$$

and for the desorption process,

$$\frac{\Delta\Phi}{\Delta\Phi_o}(t)_{des} = X_1 e^{-t/T_1} + X_2 e^{-t/T_2} \tag{4.2}$$

where the weighting factors X_1 and X_2 satisfy the equation

$$X_1 + X_2 = 1,\ X_1 \geq 0,\ X_2 \geq 0 \tag{4.3}$$

but with different values of X_1 and X_2 for each experiment. Other variables include:

$\Delta\Phi$ = measured change in relative humidity = $\left|\Phi - \Phi_j\right|$, where Φ_j is the initial relative humidity.

$\Delta\Phi_o$ = maximum step change in relative humidity = $\left|\Phi_f - \Phi_j\right|$, where Φ_f is the final relative humidity.

T_1, T_2 = the first and second time constants respectively.

For moisture transfer in the wheel plus humidity sensor, it is found that the first time constant is the most important because the first weighting factor is several times bigger than the second weighting factor. The first time constant is thought to be mostly due to diffusion of water vapour to or from the surface of the wheel matrix and adsorption or desorption on this outer surface of the desiccant particles in the wheel matrix coating. The second time constant, with a correspondingly small weighting factor, was at least an order of magnitude greater than the first time constant. This second time constant is thought to be mostly a consequence of the slow diffusion process of water molecules into the inner regions of the desiccant particles in the

coating of the wheel matrix and the sensor material as the wheel and sensor approach equilibrium.

Tables 4.2 to 4.4 list the characteristic coefficients obtained using a commercial software, Table Curve™ 2D (Jandel Scientific Inc.) using the correlation equations (4.1) and (4.2) for wheel plus humidity sensor tests on three wheels. The data are correlated within a time frame of 0 to 30 minutes for each test on the three wheels and the data acquisition that is used to acquire this data has a sampling rate of 5 samples per second. The r^2 curve fit correlation parameter is defined as the goodness of curve fit; it indicates how well correlation data agrees with the experimental data. For all these tests in Table 4.2 to 4.4, r^2 has a range $0.974 < r^2 < 0.997$ indicating good fits. Note that when X_2 is set equal to zero the resulting r^2 is less than 0.876 indicating a poor correlation. The three energy wheels are labelled according to their thickness and desiccant coating. MS-100 is a 100 mm (4") thick energy wheel coated with molecular sieve desiccant. SG-150 is a 150 mm (6") thick energy wheel coated with silica gel desiccant. MS-200 is a 200 mm (8") thick energy wheel coated with molecular sieve desiccant. These designations are used throughout the thesis. The face velocity used to test each wheel given in Table 4.2 to 4.4 corresponds to the face velocities (V_{air}) used by Shang (2002).

Three different positions on the surface of each wheel are tested resulting in nine step change response tests for each wheel. The results are summarized in Tables 4.2 to 4.4. These results show that the variations in the characteristic coefficients (X_1, X_2, T_1 and T_2) are random. It is also noted that there is no significant change in the

characteristic coefficients (X_1, X_2, T_1 and T_2) with increasing humidity step size for the adsorption process in the wheel matrix. This linear response helps justify the selection of a linear system model in Chapter 3.

Table 4.2. Water vapour adsorption and desorption coefficients (X_1, X_2) and time constants (T_1, T_2) in equations (4.1) and (4.2) for Wheel MS-100 plus humidity sensor with $\Delta RH \neq 0$, $\Delta T = 0$, $V_{air} = 1.6$ m/s for three different humidity step sizes.

Inlet conditions	X_1	T_1(s)	X_2	T_2(s)	r^2
	Adsorption				
dry side: $T_{i,d} \approx 23^oC$, $\Phi_{i,d} \approx 5\%$ wet side: $T_{i,w} \approx 23^oC$, $\Phi_{i,w} \approx 40\%$	0.80	8.3	0.20	133.7	0.983
	0.82	11.2	0.18	146.3	0.992
	0.84	12.1	0.16	152.8	0.979
dry side: $T_{i,d} \approx 23^oC$, $\Phi_{i,d} \approx 5\%$ wet side: $T_{i,w} \approx 23^oC$, $\Phi_{i,w} \approx 50\%$	0.76	7.9	0.24	137.4	0.983
	0.77	10.8	0.23	154.4	0.984
	0.82	6.7	0.18	123.4	0.984
dry side: $T_{i,d} \approx 23^oC$, $\Phi_{i,d} \approx 5\%$ wet side: $T_{i,w} \approx 23^oC$, $\Phi_{i,w} \approx 60\%$	0.79	9.7	0.21	139.1	0.982
	0.81	6.9	0.19	118.4	0.981
	0.78	9.4	0.22	132.4	0.980
	Desorption				
dry side: $T_{i,d} \approx 23^oC$, $\Phi_{i,d} \approx 5\%$ wet side: $T_{i,w} \approx 23^oC$, $\Phi_{i,w} \approx 40\%$	0.84	9.1	0.16	146.9	0.987
	0.85	7.3	0.15	116.8	0.989
	0.82	8.3	0.18	140.4	0.986
dry side: $T_{i,d} \approx 23^oC$, $\Phi_{i,d} \approx 5\%$ wet side: $T_{i,w} \approx 23^oC$, $\Phi_{i,w} \approx 50\%$	0.92	9.5	0.08	188.8	0.986
	0.79	7.2	0.21	131.2	0.986
	0.89	7.2	0.11	93.5	0.993
dry side: $T_{i,d} \approx 23^oC$, $\Phi_{i,d} \approx 5\%$ wet side: $T_{i,w} \approx 23^oC$, $\Phi_{i,w} \approx 60\%$	0.81	6.1	0.19	104.1	0.989
	0.84	7.8	0.16	133.8	0.989
	0.81	6.3	0.19	107.5	0.985

Table 4.3. Water vapour adsorption and desoprtion coefficients (X_1, X_2) and time constants (T_1, T_2) in equations (4.1) and (4.2) for Wheel SG-150 plus humidity sensor with $\Delta RH \neq 0$, $\Delta T = 0$, $V_{air} = 0.8$ m/s for three different humidity step sizes.

Inlet conditions	X_1	T_1(s)	X_2	T_2(s)	r^2
	Adsorption				
dry side: $T_{i,d} \approx 23^oC$, $\Phi_{i,d} \approx 5\%$ wet side: $T_{i,w} \approx 23^oC$, $\Phi_{i,w} \approx 40\%$	0.91	15.2	0.09	201.7	0.981
	0.89	12.2	0.11	172.9	0.983
	0.88	12.3	0.12	203.4	0.946
dry side: $T_{i,d} \approx 23^oC$, $\Phi_{i,d} \approx 5\%$ wet side: $T_{i,w} \approx 23^oC$, $\Phi_{i,w} \approx 50\%$	0.94	12.6	0.06	176.2	0.985
	0.88	12.8	0.12	158.0	0.983
	0.82	14.5	0.18	191.6	0.981
dry side: $T_{i,d} \approx 23^oC$, $\Phi_{i,d} \approx 5\%$ wet side: $T_{i,w} \approx 23^oC$, $\Phi_{i,w} \approx 60\%$	0.85	11.1	0.15	162.7	0.985
	0.88	12.0	0.12	193.1	0.986
	0.88	12.2	0.12	168.1	0.990
	Desorption				
dry side: $T_{i,d} \approx 23^oC$, $\Phi_{i,d} \approx 5\%$ wet side: $T_{i,w} \approx 23^oC$, $\Phi_{i,w} \approx 40\%$	0.95	17.4	0.05	286.2	0.993
	0.94	17.0	0.06	542.0	0.987
	0.95	15.6	0.05	371.2	0.960
dry side: $T_{i,d} \approx 23^oC$, $\Phi_{i,d} \approx 5\%$ wet side: $T_{i,w} \approx 23^oC$, $\Phi_{i,w} \approx 50\%$	0.95	17.9	0.05	326.0	0.995
	0.96	22.0	0.04	404.6	0.987
	0.95	19.5	0.05	325.7	0.994
dry side: $T_{i,d} \approx 23^oC$, $\Phi_{i,d} \approx 5\%$ wet side: $T_{i,w} \approx 23^oC$, $\Phi_{i,w} \approx 60\%$	0.95	22.2	0.05	517.2	0.994
	0.95	24.5	0.05	370.0	0.997
	0.95	23.1	0.05	312.5	0.996

The results in Table 4.3 show that, for the silica gel wheel (SG-150 wheel), the time constants during adsorption are independent of the humidity step size, but the desorption time constant T_1 increases with increasing humidity step size. The molecular sieve coated wheels did not show any significant change in T_1 for desorption as a function of step size.

Table 4.4. Water vapour adsorption and desoprtion coefficients (X_1, X_2) and time constants (T_1, T_2) in equations (4.1) and (4.2) for Wheel MS-200 plus humidity sensor with $\Delta RH \neq 0$, $\Delta T=0$, $V_{air}=1.6$ m/s for three different humidity step sizes.

Inlet conditions	X_1	T_1(s)	X_2	T_2(s)	r^2
	Adsorption				
dry side: $T_{i,d}\approx 23^oC$, $\Phi_{i,d}\approx 5\%$ wet side: $T_{i,w}\approx 23^oC$, $\Phi_{i,w}\approx 40\%$	0.78	16.4	0.22	152.4	0.976
	0.76	16.3	0.24	142.7	0.987
	0.75	17.5	0.25	163.1	0.974
dry side: $T_{i,d}\approx 23^oC$, $\Phi_{i,d}\approx 5\%$ wet side: $T_{i,w}\approx 23^oC$, $\Phi_{i,w}\approx 50\%$	0.77	16.5	0.23	183.5	0.976
	0.76	16.5	0.24	154.6	0.982
	0.75	16.5	0.25	187.0	0.979
dry side: $T_{i,d}\approx 23^oC$, $\Phi_{i,d}\approx 5\%$ wet side: $T_{i,w}\approx 23^oC$, $\Phi_{i,w}\approx 60\%$	0.76	15.3	0.24	152.6	0.975
	0.78	14.3	0.22	192.6	0.971
	0.79	16.4	0.21	161.0	0.978
	Desorption				
dry side: $T_{i,d}\approx 23^oC$, $\Phi_{i,d}\approx 5\%$ wet side: $T_{i,w}\approx 23^oC$, $\Phi_{i,w}\approx 40\%$	0.80	12.3	0.20	103.8	0.993
	0.85	15.2	0.15	145.5	0.988
	0.87	16.2	0.13	163.2	0.988
dry side: $T_{i,d}\approx 23^oC$, $\Phi_{i,d}\approx 5\%$ wet side: $T_{i,w}\approx 23^oC$, $\Phi_{i,w}\approx 50\%$	0.87	14.3	0.13	242.9	0.977
	0.86	14.2	0.14	143.2	0.988
	0.79	12.0	0.21	104.3	0.991
dry side: $T_{i,d}\approx 23^oC$, $\Phi_{i,d}\approx 5\%$ wet side: $T_{i,w}\approx 23^oC$, $\Phi_{i,w}\approx 60\%$	0.87	14.2	0.13	139.1	0.987
	0.83	15.0	0.17	104.4	0.987
	0.80	11.5	0.20	101.5	0.992

Based on the results in Tables 4.2 to 4.4, it can be inferred that the characteristic coefficients of these wheels plus humidity sensor do not depend on the magnitude of the humidity for both adsorption and desorption processes for the MS wheels but depend on the humidity step size for SG wheel during desoprtion process. Since this effect is small for the Wheel SG-150, the coefficients (X_1, X_2, T_1 and T_2) for the wheels plus humidity sensor for both adsorption and desorption processes are statistically averaged or weighted according to the standard deviation of each coefficients, which is given by the curve fit program Table Curve™ 2D**.** The average is calculated such that the results

with the lowest uncertainty are weighted more according to equations (4.4) and (4.5) (Taylor, 1982). Using the data in Tables 4.2 to 4.4, the weighted average time constants ($\overline{T_1}$ and $\overline{T_2}$) and coefficients ($\overline{X}_1$ and $\overline{X}_2$) and their uncertainties are determined using equations (4.4) to (4.7) and the uncertainty analysis presented in Appendix B. Table 4.5 gives the summary of the values.

$$\overline{X_k} = \left\{ \frac{\sum_{j=1}^{n} \left[X_{kj}^2 \left(\frac{1}{R(S_j)} \right)^2 \right]}{\sum_{j=1}^{n} \left[\left(\frac{1}{R(S_j)} \right)^2 \right]} \right\}^{1/2}, \text{ and} \tag{4.4}$$

$$\overline{T_k} = \left\{ \frac{\sum_{j=1}^{n} \left[T_{kj}^2 \left(\frac{1}{R(S_j)} \right)^2 \right]}{\sum_{j=1}^{n} \left[\left(\frac{1}{R(S_j)} \right)^2 \right]} \right\}^{1/2}, \tag{4.5}$$

where

$$R(S_j) = \frac{S_j}{X_{kj}} \text{ or} \tag{4.6}$$

$$R(S_j) = \frac{S_j}{T_{kj}}, \tag{4.7}$$

where S is the standard deviation of the curve fitting for experimental data.

Table 4.5. Average water vapour adsorption and desorption transient coefficients for the three tested wheels plus humidity sensor.

Processes	$\overline{X_1} \pm U(\overline{X_1})$	$\overline{T_1} \pm U(\overline{T_1})$ (s)	$\overline{X_2} \pm U(\overline{X_2})$	$\overline{T_2} \pm U(\overline{T_2})$ (s)
	Wheel MS-100 plus humidity sensor			
Adsorption	0.80±0.02	10±1.4	0.20±0.02	138±12
Desorption	0.84±0.02	8±0.9	0.16±0.02	129±21
	Wheel SG-150 plus humidity sensor			
Adsorption	0.88±0.04	14±1	0.12±0.04	181±20
Desorption	0.95±0.01	20±3	0.05±0.01	384±72
	Wheel MS-200 plus humidity sensor			
Adsorption	0.77±0.02	17±1.6	0.23±0.02	165.5±16
Desorption	0.84±0.02	14±1.1	0.16±0.02	139±25

Comparing values in Table 4.5, it is seen that the coefficients change for each wheel. This change reflects the thickness of each wheel and the type of desiccant. Comparing Wheel MS-100 and Wheel MS-200, which have a molecular sieve desiccant but have different wheel thickness, shows the effect of wheel thickness on the time constants. The thicker wheel has larger time constants. Wheel SG-150 differs from the other two wheels because it has a silica gel desiccant coating.

4.1.2 Energy wheel plus thermocouple

The purpose of this section is to determine the transient response characteristics of the three wheels plus thermocouple sensor. The test conditions used are presented in Table 4.6.

Table 4.6. Test conditions for energy wheel plus thermocouple sensor experiments ($\Delta T \neq 0$, $\Delta RH = 0$).

Test conditions	Cold inlet	Hot inlet
Temperature	~23°C	~50°C, 44°C
Relative humidity	~4%	~4%
Air flow rate	200 L/min, 100 L/min	200 L/min, 100 L/min
Air face velocity	1.6 m/s, 0.8 m/s	1.6 m/s, 0.8 m/s

Transient tests with a step change in the inlet temperatures are performed on same wheels as described in section 4.2.1 with thermocouples located upstream and downstream of the wheel. Figure 4.2 shows the measured temperature data of the MS-100 energy wheel experiencing a step change in inlet temperature from 23°C to 50°C but with no change in humidity conditions. These dry inlet air conditions are chosen (~4%RH) to minimize any effects due to moisture transfer.

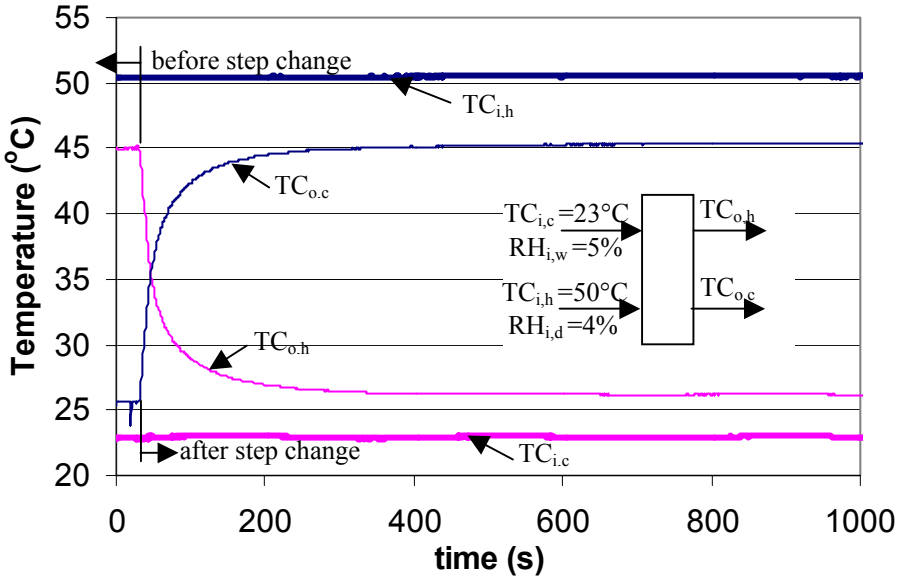

Figure 4.2. *Measured inlet and outlet temperatures for Wheel MS-100 exposed to a step change in temperature with no change in relative humidity* (ΔT=27°C, ΔRH=0).

4.1.3 Conduction effects in the wheel matrix outside the tubes with flow

In the transient response experiments for step changes in temperature shown in Figure 4.2 there appears to be a significant heat conduction effect throughout the wheel matrix because the outlet temperatures do not equal the inlet temperatures at steady state. Conduction effects are evident both before and after the step change in inlet conditions as shown in Figure 4.2. Since the small area of the wheel being tested is not thermally isolated from the surrounding wheel matrix there will be heat transfer between the matrix tubes with air flow and the surrounding tubes of the wheel. Heat conduction will occur in the direction of the negative temperature gradient outside the flow tubes into the wheel matrix surrounding each flow tube as shown in Figure 4.3. The data in Figure 4.2 show that the temperature difference between $TC_{i,h}$ and $TC_{o,h}$ is larger than the difference between $TC_{i,c}$ and $TC_{o,c}$ before the time of the switch. Furthermore, this effect is repeated for temperature difference between $TC_{i,h}$ and $TC_{o,c}$ and between $TC_{i,c}$ and $TC_{o,h}$ after the step change. To experimentally investigate this effect, calibrated thermocouples were arranged in arrays across each flow tube outlet using the facility shown in Figure 2.3. The temperature across each flow tube of the outlet airstream was measured one centimetre from the outlet face of the wheel, as shown in Figure 4.3, before and after typical temperature step changes. The outlet thermocouple array was aligned on a line joining the centers of the two flow tubes.

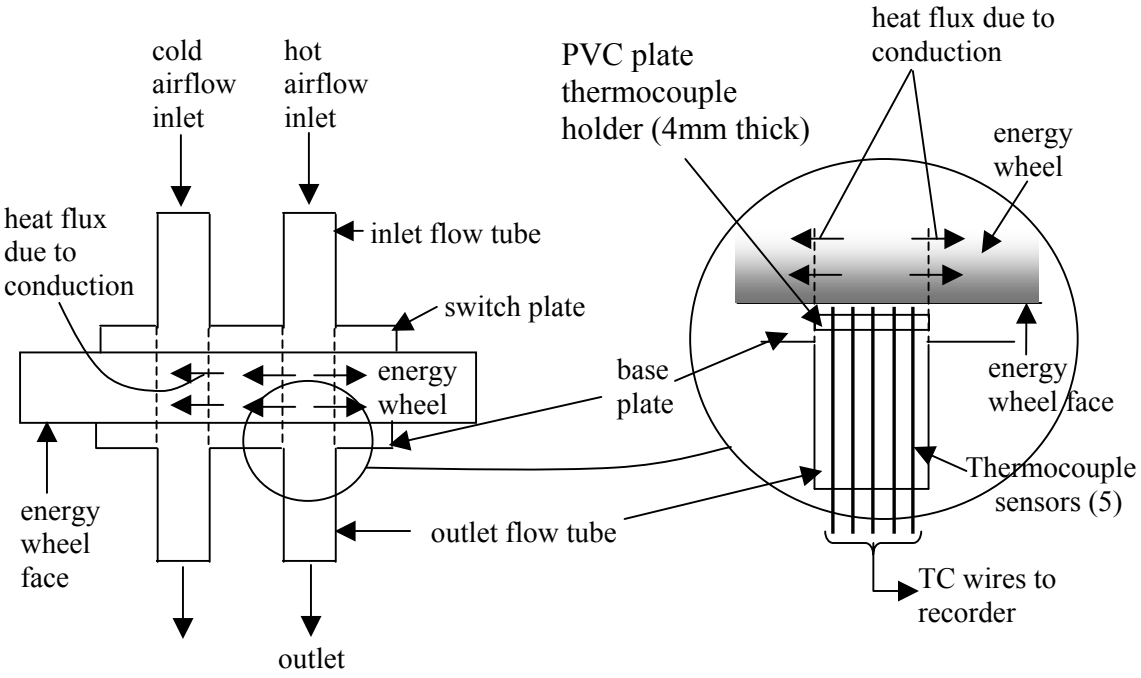

Figure 4.3. *Schematic of an energy wheel being tested with a temperature difference showing conduction heat transfer between the flow tubes and the wheel matrix as well as the position of the thermocouples with respect to the tube in the base plate.*

Typical thermocouple readings of the five outlet and one inlet temperatures are shown in Figures 4.4 for one steady state condition. These data confirm that heat conduction process is going on in the wheel matrix outside of the flow tubes as a result of temperature gradients caused by the inlet air at different temperatures. Figure 4.4(a) shows that for the cold airstream side, the thermocouple TC1, which is positioned closest to the hot airstream side, reads a value higher than the thermocouple TC5 which is positioned farthest away from the hot airstream side. This temperature distribution on the cold side is an indication of the heat conduction process which is not axially symmetrical in the wheel. Figure 4.4(b) shows the corresponding data for the hot side. These nearly uniform outlet temperatures are nearly 7°C cooler than the inlet air temperature indicating a greater heat loss from the hot air side than heat gain on the cold

air side. The nearly uniform air temperature profile across the outlet on the hot side implies a nearly symmetric heat flux into the matrix around the hot air flow tube.

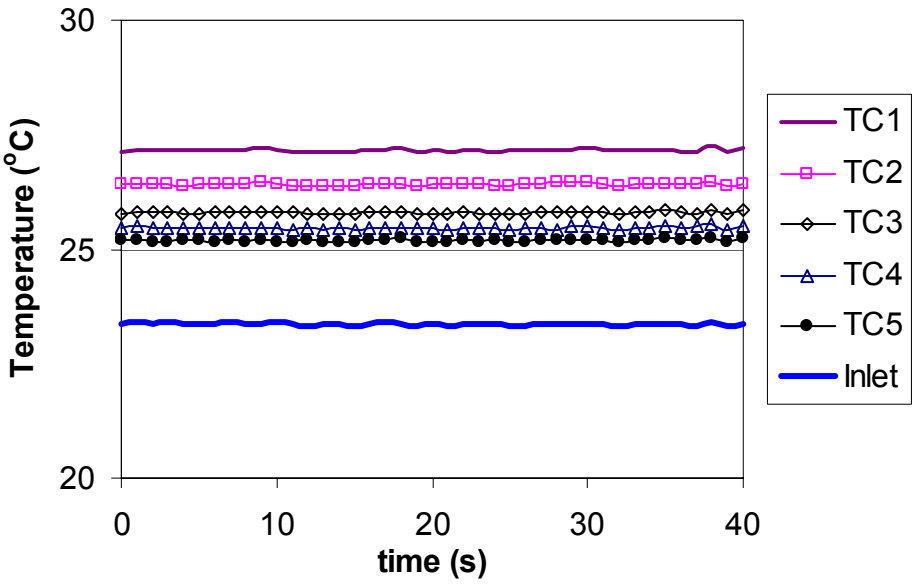

(a)

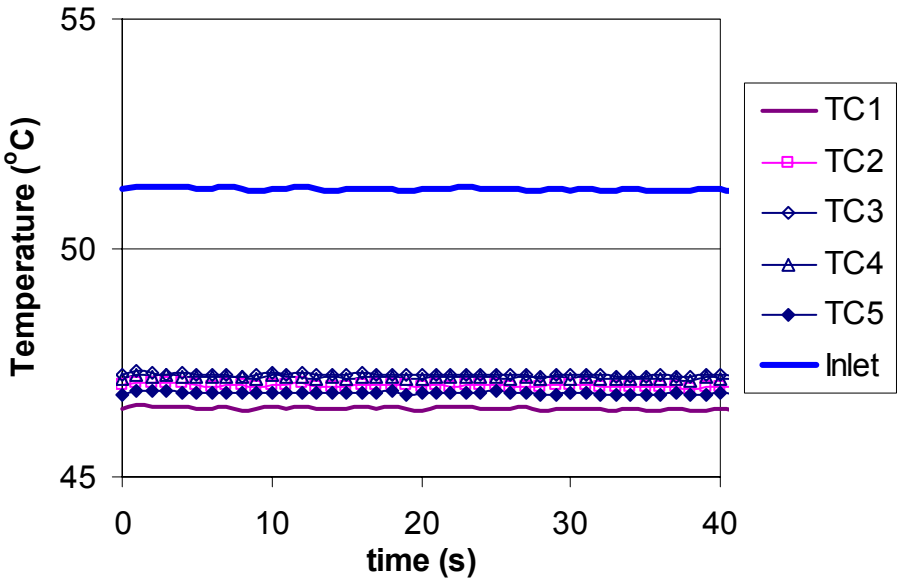

(b)

Figure 4.4. *Steady state inlet and outlet flow tube air temperatures for one typical test (a) Cold side and (b) hot side airflow temperatures of 1 inlet and 5 outlet thermocouples arranged in an array at the outlet face of a wheel* (ΔT=30°C, ΔRH=0).

4.1.4 Effects of conduction on measured time constants

Analytic investigations are carried out to ascertain the effect of heat conduction on the time constants of the wheel. To achieve this, the analytical solution presented by Rizika (1954) is used to predict the thermal response of the air flowing through a tube with an internal matrix similar to the energy wheel but with no external matrix outside the flow tube area. Rizika presented a Laplace transformed analytical solution for the thermal lag of the air leaving the flow tube (Figure 4.5). This is an adiabatic case, where there is no heat loss from the flow tube area to the surrounding wheel matrix.

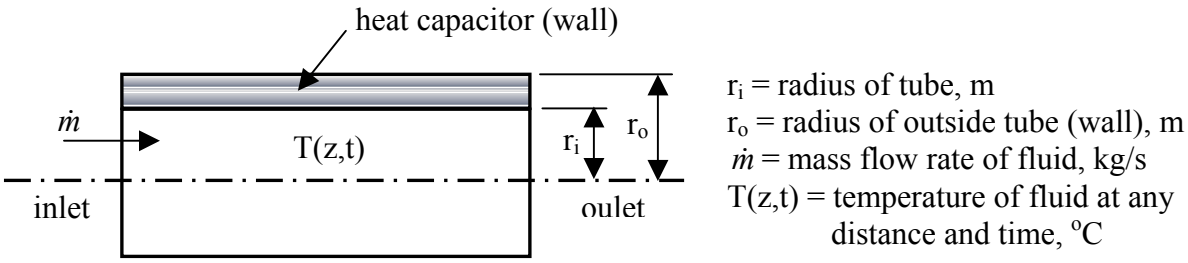

Figure 4.5. *A schematic diagram showing a fluid flowing through a system containing a heat capacitor.*

The thermal response of the airflow through the wheel tube is determined using Rizika's method. The properties of the energy wheel used for this theoretical analysis (adiabatic) are listed in Table 4.7. Some of these properties are taken from the numerical and experimental work of Simonson et al. (2000a and b). The wheel tested was manufactured with 0.025 mm thick aluminium sheet in the wheel matrix that is coated on both sides with 0.075 mm of desiccant. The airflow channels of the energy wheel have a sine wave profile with a wave length of 4 mm and a height of 1.5 mm for Wheel MS-100.

Table 4.7. Properties of the energy wheel used in the analytical solution of the thermal lag of the flow through the wheel tube.

Wheel	L = 0.1 m	D_h = 1.0 mm	porosity = 89%
	ρ_{al} = 2702 kg/m3	Cp_{al} = 903 J/(kg·K)	$\dot{m}$ = 0.0038 kg/s
	Cp_{air} = 1005 J/(kg·K)	h_{air} = 49.4 W/ (m^2·K) (fully developed)	k_{air} = 0.0263 W/ (m·K)
Desiccant	ρ = 350 kg/m3	Cp = 615 J/(kg·K)	porosity = 69%

Results obtained from Rizika's method (exact solution) are compared with the measured data obtained from the transient test in Figure 4.6. This Figure shows that there appears to be agreement between the measured data and the exact solution immediately after the step change; but after 10 or 20 seconds the heat losses or gains are significantly different than Rizika model and this results in very different outlet air temperatures.

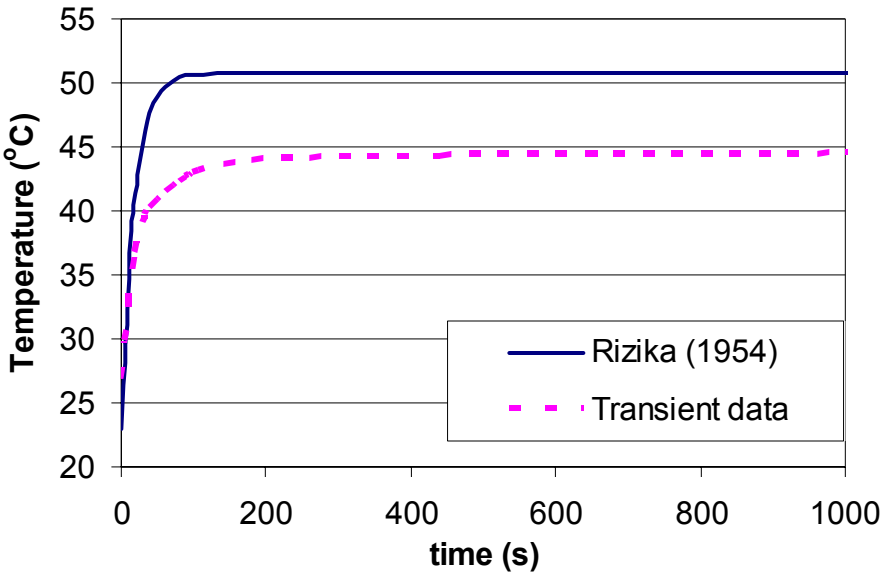

(a)

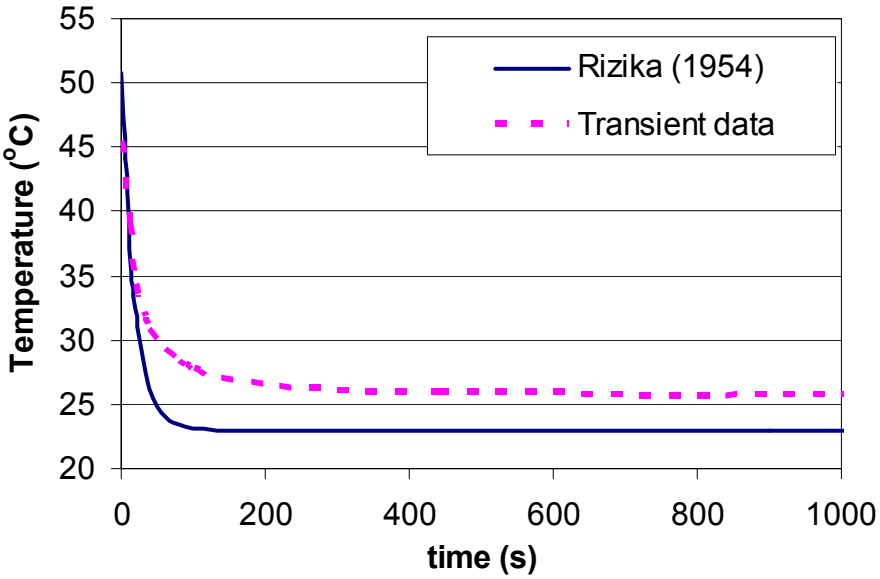

(b)

Figure 4.6. *Experimental data and exact solution for the bulk mean outlet temperatures for (a) temperature increase and (b) temperature decrease of Wheel MS-100 exposed to a step change in temperature with no change in relative humidity* (ΔT=27°C, ΔRH=0).

To determine the time constants of the wheels plus thermocouple, the experimental data are normalized relative to the maximum change obtained in the experimental data. The thermal time constant for a solid subject to a step change in

temperature of the flowing fluid can be expressed as $\tau = \frac{\rho V C_p}{hA}$ when the solid temperature is uniform at all times. The data for the wheel plus thermocouple shows an exponential type increase or decrease in temperature, which is due to the thermal capacity of the solid and heat convection resistance of the air flowing through the wheel matrix. For an inlet temperature step change in the transient experiments, two time constants are observed to give good correlations for both temperature increase and decrease. The first time constant with a corresponding weighting factor of about 0.8 is always the most important and it is thought to be mostly a consequence of heat capacity effect and heat convection resistance in the energy wheel. The time constant of the adiabatic flow tube surroundings obtained from Rizika's solution shown in Figure 4.7 indicates that the time constant obtained from the adiabatic case is reasonably close to the first time constant obtained from the transient experimental data.

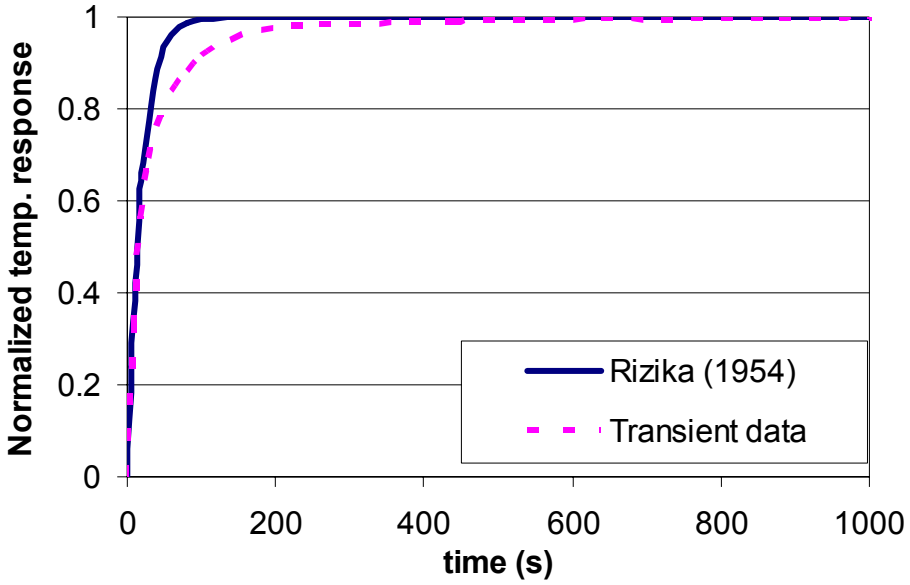

(a)

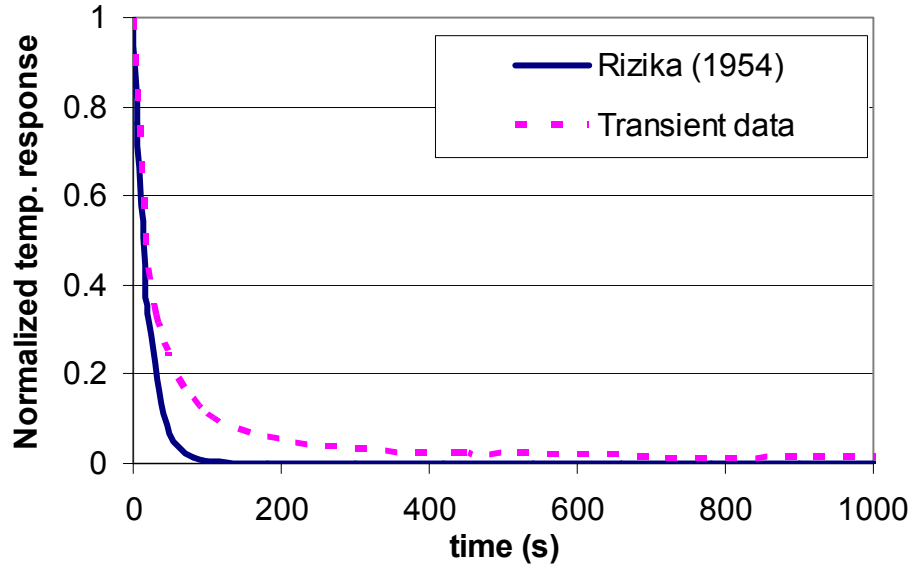

(b)

Figure 4.7. *Normalized temperature response of Wheel MS-100 obtained from the exact solution and the transient experiment for (a) temperature increase and (b) temperature decrease.*

Though there is some heat conduction losses or gains from the flow tube area to the surrounding wheel matrix during the transient experiments, this heat conduction is

seen not to show large effect on the first time constant. It will be seen from the time constant data for the wheels plus thermocouple that the first time constant is dominant because of its larger weighting factor (similarly as was found for the wheel plus humidity sensor in section 4.1.1). This means that the transient response of the wheel plus thermocouple depends mainly on the first time constant and weakly on the second time constant. Hence, this conduction effect will not have much effect on the thermal response of the wheel plus thermocouple and subsequently, on the wheel alone. In Chapter 5, comparisons are made to determine if this normalization of the temperature data adequately represents the response of the wheels plus thermocouple or wheel alone when the sensible effectiveness of the wheel is presented.

Similar to the humidity response in section 4.2.1, the measured data for the transient characteristics of energy wheel plus thermocouple are assumed to follow an exponential correlation equation with two time constants and two weighting factors for both temperature increases and decreases. For the wheel plus thermocouple, the first time constant is most important and the second time constant is at least an order of magnitude greater than the first time constant perhaps because it is mostly a consequence of the slow heat diffusion process into the surrounding wheel matrix.

The correlation equations for the transient response of the wheel plus thermocouple for temperature increase and decrease are presented in equations (4.8) and (4.9) respectively.

$$\frac{\Delta\Theta}{\Delta\Theta_o}(t)_{ads} = Y_1\left(1-e^{-t/T_1}\right)+Y_2\left(1-e^{-t/T_2}\right) \tag{4.8}$$

$$\frac{\Delta\Theta}{\Delta\Theta_o}(t)_{des} = Y_1 e^{-t/T_1} + Y_2 e^{-t/T_2}. \tag{4.9}$$

The weighting factors Y_1 and Y_2 satisfy the equation

$$Y_1 + Y_2 = 1,\ Y_1 \geq 0,\ Y_2 \geq 0 \tag{4.10}$$

with different values of Y_1 and Y_2 for each experiment.

$\Delta\Theta$ = measured change in temperature = $\left|\Theta - \Theta_j\right|$, where Θ_j is the initial temperature.

$\Delta\Theta_o$ = maximum step change in temperature = $\left|\Theta_f - \Theta_j\right|$, where Θ_f is the final temperature.

T_1 , T_2 = the first and second time constants respectively.

The characteristic coefficients representing the transient temperature response of the wheels are listed in Tables 4.8 to 4.10 for both temperature increase and decrease. For the coefficients in Tables 4.8 to 4.10, r^2 has a range $0.990 < r^2 < 0.999$ indicating a good fit. Note that when Y_2 is set equal to zero the resulting r^2 is approximately 0.919.

Table 4.8. Heat transfer heating and cooling coefficients (Y_1, Y_2) and time constants (T_1, T_2) in equations (4.8) and (4.9) for Wheel MS-100 plus thermocouple with $\Delta T \neq 0$, $\Delta RH=0$, $V_{air}=1.6$ m/s.

Inlet conditions	Y_1	T_1(s)	Y_2	T_2(s)	r^2
	Temperature increase				
hot side: $T_{i,d}\approx 23^oC$, $\Phi_{i,d}\approx 4\%$ cold side: $T_{i,w}\approx 53^oC$, $\Phi_{i,w}\approx 4\%$	0.88	27.1	0.12	429.8	0.993
	0.83	20.2	0.17	124.8	0.995
	0.80	20.5	0.20	134.6	0.997
	0.79	22.3	0.16	146.7	0.997
	0.86	23.7	0.14	216.4	0.995
hot side: $T_{i,d}\approx 23^oC$, $\Phi_{i,d}\approx 4\%$ cold side: $T_{i,w}\approx 44^oC$, $\Phi_{i,w}\approx 4\%$	0.85	22.5	0.15	188.6	0.996
	0.79	20.0	0.22	121.8	0.997
	0.79	19.9	0.21	122.6	0.998
	0.84	19.7	0.20	110.9	0.997
	Temperature decrease				
hot side: $T_{i,d}\approx 23^oC$, $\Phi_{i,d}\approx 4\%$ cold side: $T_{i,w}\approx 53^oC$, $\Phi_{i,w}\approx 4\%$	0.84	22.0	0.16	167.0	0.992
	0.83	21.9	0.15	229.4	0.990
	0.79	19.6	0.21	122.2	0.995
	0.81	21.2	0.19	144.0	0.993
	0.82	21.4	0.17	145.3	0.994
hot side: $T_{i,d}\approx 23^oC$, $\Phi_{i,d}\approx 4\%$ cold side: $T_{i,w}\approx 44^oC$, $\Phi_{i,w}\approx 4\%$	0.84	19.1	0.20	132.0	0.995
	0.81	20.2	0.19	127.1	0.993
	0.78	18.2	0.23	113.5	0.994
	0.81	19.2	0.19	111.4	0.994

Table 4.9. Heat transfer heating and cooling coefficients (Y_1, Y_2) and time constants (T_1, T_2) in equations (4.8) and (4.9) for Wheel SG-150 plus thermocouple with $\Delta T \neq 0$, $\Delta RH=0$, $V_{air}=0.8$ m/s.

Inlet conditions	Y_1	T_1(s)	Y_2	T_2(s)	r^2
	Temperature increase				
hot side: $T_{i,d}\approx 23^oC$, $\Phi_{i,d}\approx 4\%$ cold side: $T_{i,w}\approx 53^oC$, $\Phi_{i,w}\approx 4\%$	0.75	47.5	0.25	348.0	0.999
	0.73	42.9	0.27	193.0	0.999
	0.78	45.4	0.22	243.5	0.998
	0.78	49.2	0.22	282.5	0.998
	0.78	52.1	0.22	346.8	0.998
hot side: $T_{i,d}\approx 23^oC$, $\Phi_{i,d}\approx 4\%$ cold side: $T_{i,w}\approx 44^oC$, $\Phi_{i,w}\approx 4\%$	0.79	46.9	0.21	307.6	0.998
	0.72	38.3	0.28	242.8	0.997
	0.75	46.6	0.25	325.3	0.998
	0.77	47.3	0.23	316.0	0.999
	Temperature decrease				
hot side: $T_{i,d}\approx 23^oC$, $\Phi_{i,d}\approx 4\%$ cold side: $T_{i,w}\approx 53^oC$, $\Phi_{i,w}\approx 4\%$	0.79	43.6	0.21	230.9	0.998
	0.70	54.0	0.30	250.9	0.999
	0.79	62.1	0.21	355.3	0.999
	0.75	43.6	0.25	210.9	0.998
	0.78	44.2	0.22	198.9	0.998
hot side: $T_{i,d}\approx 23^oC$, $\Phi_{i,d}\approx 4\%$ cold side: $T_{i,w}\approx 44^oC$, $\Phi_{i,w}\approx 4\%$	0.78	58.7	0.22	287.3	0.999
	0.69	26.2	0.41	126.9	0.998
	0.75	53.3	0.25	283.8	0.999
	0.81	47.1	0.19	285.3	0.997

Table 4.10. Heat transfer heating and cooling coefficients (Y_1, Y_2) and time constants (T_1, T_2) in equations (4.8) and (4.9)) for Wheel MS-200 plus thermocouple with $\Delta T \neq 0$, $\Delta RH=0$, $V_{air}=1.6$ m/s.

Inlet conditions	Y_1	T_1(s)	Y_2	T_2(s)	r^2
	Temperature increase				
hot side: $T_{i,d}\approx 23^oC$, $\Phi_{i,d}\approx 4\%$ cold side: $T_{i,w}\approx 53^oC$, $\Phi_{i,w}\approx 4\%$	0.83	35.9	0.17	243.3	0.998
	0.72	28.8	0.28	162.4	0.998
	0.81	34.0	0.19	183.1	0.998
	0.80	33.5	0.20	177.5	0.998
	0.82	36.7	0.18	239.4	0.998
hot side: $T_{i,d}\approx 23^oC$, $\Phi_{i,d}\approx 4\%$ cold side: $T_{i,w}\approx 44^oC$, $\Phi_{i,w}\approx 4\%$	0.87	42.2	0.13	316.9	0.998
	0.90	38.6	0.10	307.3	0.998
	0.86	37.6	0.14	221.8	0.998
	0.73	32.6	0.27	179.6	0.999
	Temperature decrease				
hot side: $T_{i,d}\approx 23^oC$, $\Phi_{i,d}\approx 4\%$ cold side: $T_{i,w}\approx 53^oC$, $\Phi_{i,w}\approx 4\%$	0.73	27.6	0.27	141.8	0.995
	0.73	26.2	0.27	133.3	0.997
	0.82	32.8	0.18	213.5	0.995
	0.75	27.7	0.25	160.1	0.995
	0.80	32.1	0.20	176.1	0.996
hot side: $T_{i,d}\approx 23^oC$, $\Phi_{i,d}\approx 4\%$ cold side: $T_{i,w}\approx 44^oC$, $\Phi_{i,w}\approx 4\%$	0.76	30.7	0.24	163.7	0.994
	0.87	35.7	0.13	238.6	0.996
	0.81	32.1	0.19	213.0	0.994
	0.85	31.8	0.15	246.8	0.993

The data in Tables 4.8 to 4.10 show that there is no significant change in the characteristic coefficients (Y_1, Y_2, T_1 and T_2) for each wheel as the size of the temperature step change. However, there seems to be some change in Y_1 for Wheel SG-150 compared to Wheels MS-100 and MS-200. This may be due to the fact that Wheel SG-150 has a slightly thicker aluminium sheet in its matrix and a coating of silica gel desiccant. The data also shows that the time constants of Wheel SG-150 are larger than those for Wheels MS-100 and MS-200. It is expected that the time constants of Wheel SG-150 will be larger than that of Wheel MS-100 because of the thickness

(i.e. size) of the wheels. This is confirmed by a comparison of Tables 4.8 and 4.9. However, it is expected that the time constants of Wheel SG-150 will be smaller than those of Wheel MS-200 because of the thickness of these wheels, but the reverse is the case as shown in Tables 4.9 and 4.10. This is because the face velocities at which these coefficients are determined are not the same for both wheels. Coefficients of Wheel SG-150 are determined at a face velocity of 0.8 m/s while the coefficients of Wheel MS-200 are determined at 1.6 m/s. At a lower face velocity, the response of the wheel is slower (i.e., the time constants are larger). This is also confirmed using Rizika's solution.

Similarly as was done in section 4.1.1, the statistically averaged data are used to represent the coefficients of the wheels. These averages of the characteristic coefficients and uncertainties of the wheels plus thermocouple tests are listed in Table 4.11.

Table 4.11. Average characteristic coefficients for the response of the three tested wheels plus thermocouple.

Processes	$\overline{Y_1} \pm U(\overline{Y_1})$	$\overline{T_1} \pm U(\overline{T_1})$ (s)	$\overline{Y_2} \pm U(\overline{Y_2})$	$\overline{T_2} \pm U(\overline{T_2})$ (s)
	Wheel MS-100 plus thermocouple			
Heating	0.83±0.03	22±1.8	0.17±0.03	177±76
Cooling	0.81±0.02	20±1	0.19±0.02	144±3
	Wheel SG-150 plus thermocouple			
Heating	0.76±0.02	46±3	0.24±0.02	290±38
Cooling	0.75±0.05	48±8	0.25±0.05	248±50
	Wheel MS-200 plus thermocouple			
Heating	0.82±0.05	36±3	0.18±0.05	226±43
Cooling	0.79±0.04	31±2	0.21±0.04	187±32

Also, comparing values in Table 4.11, it is seen that these coefficients represent the characteristic properties of each wheel. The coefficients may vary for each wheel depending on the wheel thickness, matrix thickness, face velocity, and the type of desiccant.

4.1.5 Energy wheel response alone

The transient response characteristics and correlation equations discussed in the previous sections are for the combined effects of the wheel plus the humidity sensor and the wheel plus the thermocouple. However, the transient response characteristics of the wheel alone are desired. Wang (2005) presents the analysis and final equations that are required to determine the corrected energy wheel humidity response using correlation equations for both the humidity sensor alone (Appendix A) and the sensor downstream of the wheel (equations (4.1) and (4.2)). Wang also obtained the energy wheel temperature response using correlation equations for both the thermocouple alone (Appendix A) and the thermocouple downstream of the wheel (equations (4.8) and (4.9)).

The equations for the humidity transient response of the wheel alone during adsorption and desorption are stated in equations (4.11) and (4.12) respectively.

$$F(t)_{ads} = X_1\left(1-\frac{T_1-k_1+\frac{k_2}{T_1}}{T_1-k_3}e^{-t/T_1}\right)+X_2\left(1-\frac{k_1-T_2-\frac{k_2}{T_2}}{k_3-T_2}e^{-t/T_2}\right)+$$

$$\left[\frac{k_1}{k_3}-\frac{k_2}{k_3^2}-X_1\left(1+\frac{\frac{T_1k_1}{k_3}-\frac{T_1k_2}{k_3^2}-T_1}{T_1-k_3}\right)-X_2\left(1+\frac{T_2-\frac{T_2k_1}{k_3}+\frac{T_2k_2}{k_3^2}}{k_3-T_2}\right)\right]e^{-t/k_3} \tag{4.11}$$

and

$$F(t)_{des} = X_1\left(\frac{k_1-T_1-\frac{k_2}{T_1}}{T_1-k_3}e^{-t/T_1}\right)+X_2\left(\frac{k_1-T_2-\frac{k_2}{T_2}}{T_2-k_3}e^{-t/T_2}\right)+$$

$$\left(1-\frac{k_1}{k_3}+\frac{k_2}{k_3^2}\right)\left(\frac{X_1T_1}{T_1-k_3}+\frac{X_2T_2}{T_2-k_3}\right)e^{-t/k_3} \tag{4.12}$$

where

$$k_1 = \overline{t_1}+\overline{t_2} \tag{4.13}$$

$$k_2 = \overline{t_1}\,\overline{t_2} \tag{4.14}$$

$$k_3 = \overline{x_1}\,\overline{t_2}+\overline{x_2}\,\overline{t_1} \tag{4.15}$$

t_1 and t_2 are the first and second time constants of the sensors (humidity and thermocouple) while x_1 and x_2 are the corresponding weighting factors of the time constants of the humidity sensor. The coefficients of the humidity sensor alone (t_1, t_2, x_1 and x_2) have been determined by Wang (2005) and are used in the thesis and summarized in Table A.1 in Appendix A.

To obtain the transient response of the wheel alone to a step change in humidity, the corrected energy wheel humidity transient response data obtained from equations

(4.11) and (4.12) are also curve-fitted to have two time constants as shown in equations (4.16) and (4.17). For an adsorption process

$$\frac{\Delta\varphi}{\Delta\varphi_0}(t)_{ads} = \chi_1\left(1-e^{-t/\tau_1}\right)+\chi_2\left(1-e^{-t/\tau_2}\right) \tag{4.16}$$

and for a desorption process

$$\frac{\Delta\varphi}{\Delta\varphi_0}(t)_{des} = \chi_1 e^{-t/\tau_1}+\chi_2 e^{-t/\tau_2} \tag{4.17}$$

where the weighting factors χ_1 and χ_2 satisfy the equation

$$\chi_1+\chi_2=1,\ \chi_1\geq 0,\ \chi_2\geq 0 \tag{4.18}$$

with different values of χ_1 and χ_2 for each experiment.

$\Delta\varphi$ = measured change in relative humidity = $\left|\varphi-\varphi_j\right|$, where φ_j is the initial relative humidity

$\Delta\varphi_0$ = maximum step change in relative humidity = $\left|\varphi_f-\varphi_j\right|$, where φ_f is the final relative humidity

$\tau_1,\ \tau_2$ = the first and second time constants respectively.

The same equations (4.11) and (4.12) are required for the corrected response of energy wheel alone to a step change in temperature, but with the following changes: $x_1=y_1,\ x_2=y_2,\ X_1=Y_1,\ X_2=Y_2$, where y_1 and y_2 are the corresponding weighting factors for the time constants of the thermocouple and Y_1 and Y_2 are the corresponding weighting factors for the time constants of the wheels plus thermocouples. The coefficients of the thermocouple alone ($t_1,\ t_2,\ y_1$ and y_2) have also been determined by Wang (2005) and are summarized in Table A.2 in Appendix A.

Equations (4.19) and (4.20) therefore represent the heating and cooling processes respectively for energy wheel temperature transient response

$$\frac{\Delta\Omega}{\Delta\Omega_0}(t)_{ads} = \beta_1\left(1 - e^{-t/\tau_1}\right) + \beta_2\left(1 - e^{-t/\tau_2}\right) \tag{4.19}$$

$$\frac{\Delta\Omega}{\Delta\Omega_0}(t)_{des} = \beta_1 e^{-t/\tau_1} + \beta_2 e^{-t/\tau_2} \tag{4.20}$$

where the weighting factors β_1 and β_2 satisfy the equation

$$\beta_1 + \beta_2 = 1,\ \beta_1 \geq 0,\ \beta_2 \geq 0 \tag{4.21}$$

but with different values of β_1 and β_2 for each experiment.

$\Delta\Omega$ = measured change in temperature $= \left|\Omega - \Omega_j\right|$, where Ω_j is the initial temperature

$\Delta\Omega_0$ = maximum step change in temperature $= \left|\Omega_f - \Omega_j\right|$, where Ω_f is the final temperature

$\tau_1,\ \tau_2$ = the first and second time constants respectively.

Figure 4.8 shows the transient response of a humidity sensor alone, a wheel plus humidity sensor, and the corrected wheel alone for a step increase or decrease in inlet humidity for Wheel MS-100. In addition, the transient response of a thermocouple alone, a wheel plus thermocouple, and the corrected wheel alone for a step increase or decrease in inlet temperature for Wheel MS-100 are shown in Figure 4.9. The corrected wheel response alone lies between the sensor response and the wheel plus humidity sensor response. A similar result is shown for the thermocouple response and the wheel plus thermocouple response for the case of a step change in inlet temperature. The wheel response alone is very close to the wheel plus humidity sensor response or wheel

plus thermocouple response in both cases. This confirms that the response of the wheel is not significantly altered by the use of a humidity sensor or thermocouple sensor that has a very fast response as reported by Wang (2005).

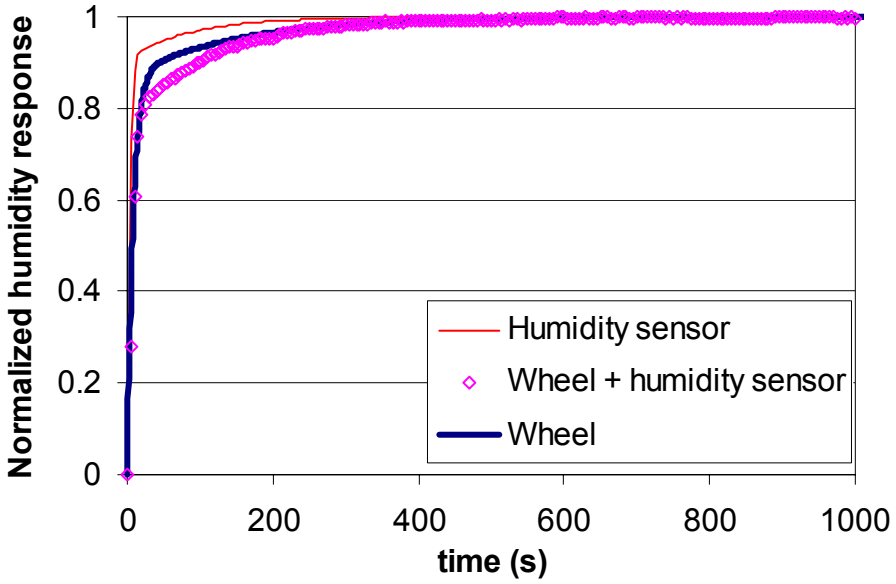

(a)

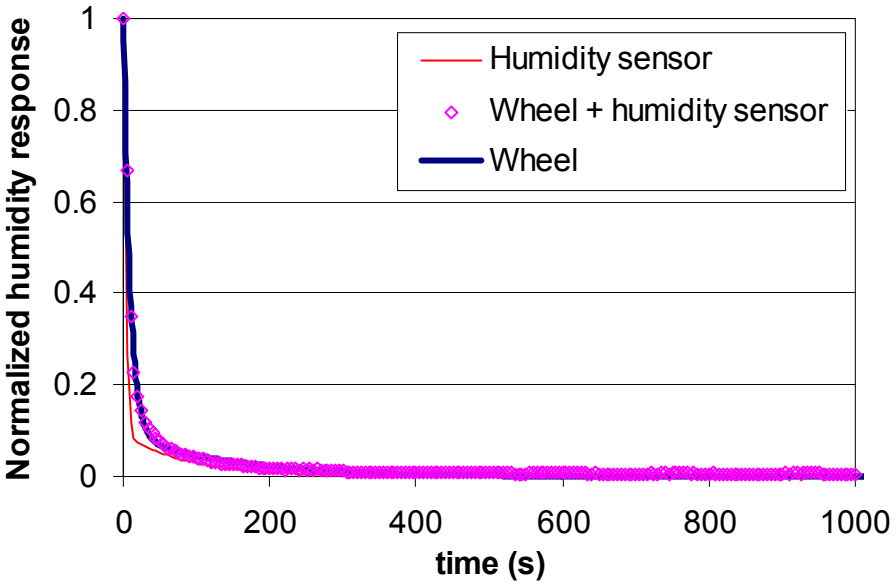

(b)

Figure 4.8. *Normalized humidity transient response of humidity sensor, Wheel MS-100 plus humidity sensor and Wheel MS-100 alone for a (a) step increase in humidity (adsorption) and (b) step decrease in humidity (desorption).*

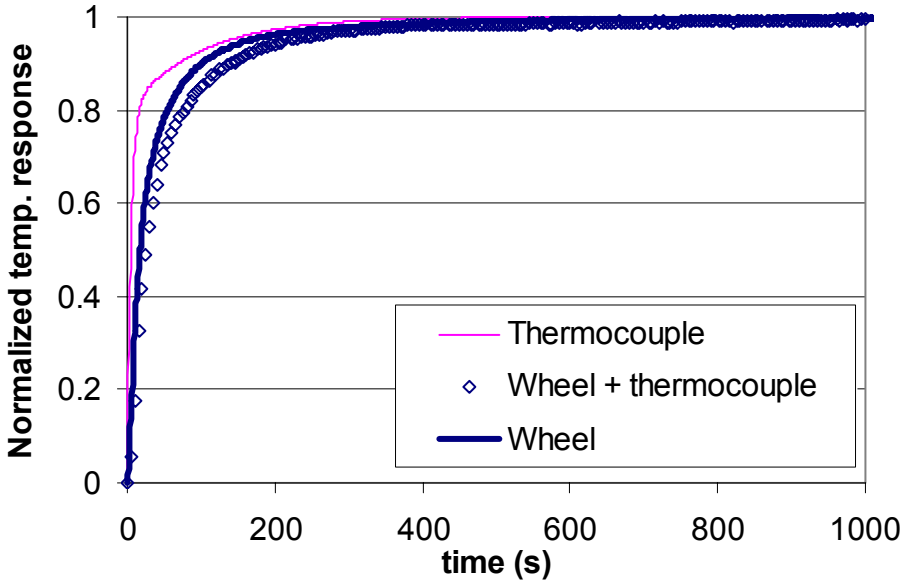

(a)

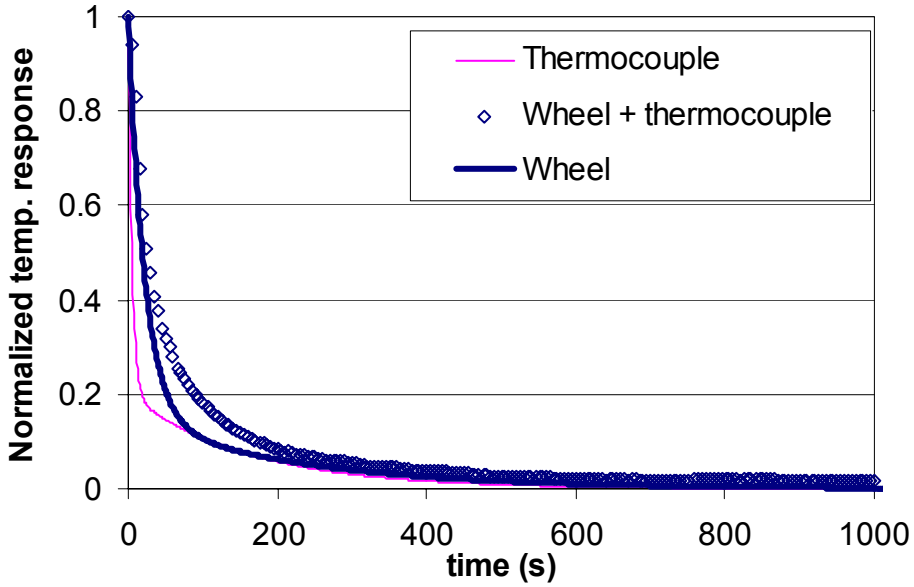

(b)

Figure 4.9. *Normalized temperature transient response of thermocouple, Wheel MS-100 plus thermocouple and Wheel MS-100 alone for a (a) step increase in temperature (heating) and (b) step decrease in temperature (cooling).*

Figure 4.10 compares the response of the wheel alone with the response obtained from analytical solution of Rizika (1954) which does not include any conduction errors. The figure shows that the response of the wheel alone is closer to the

response obtained from the analytical solution of Rizika (1954) than the response of the wheel plus thermocouple. It is therefore expected that the conduction will not have much effect on the thermal response of the wheel alone. Using this normalization, the first time constant obtained from the analytical solution and the transient experimental

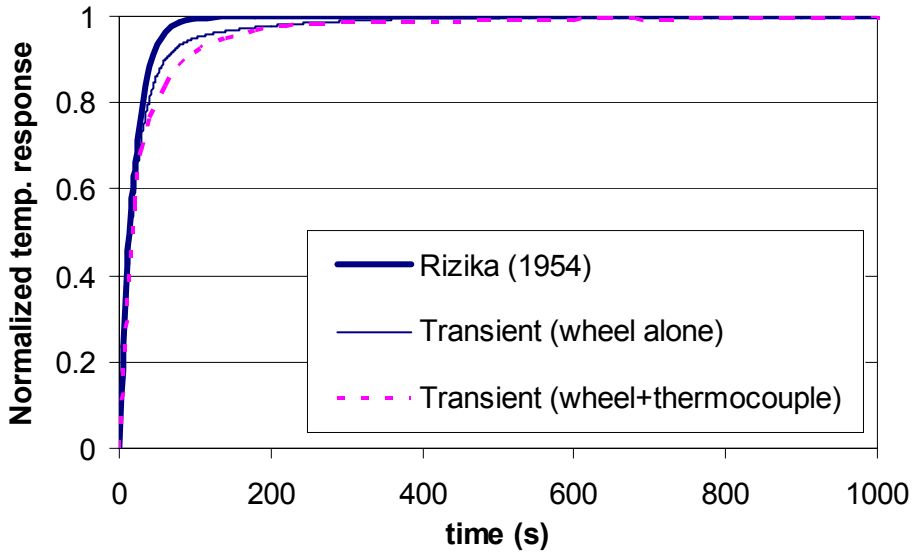

(a)

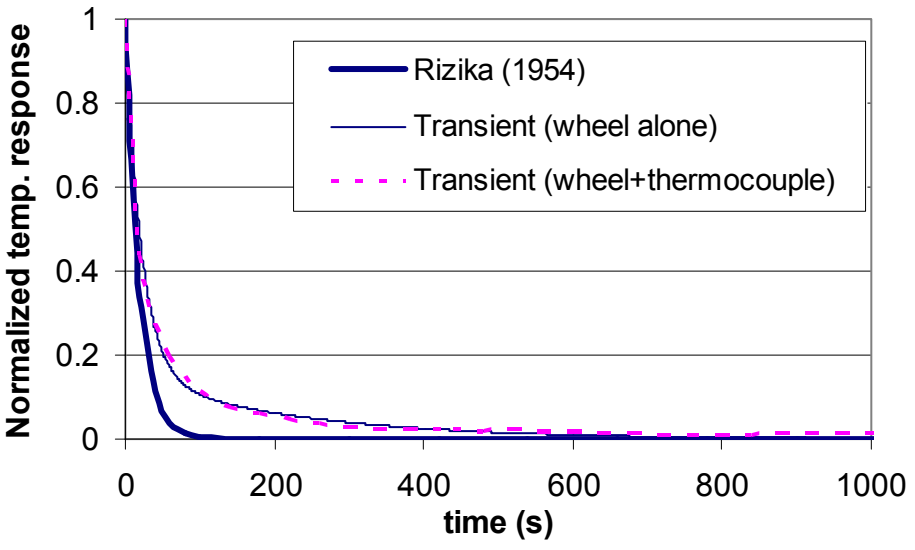

(b)

Figure 4.10. *Comparison of the normalized temperature transient response of Wheel MS-100 alone, Wheel MS-100 plus thermocouple and the analytical solution of Rizika (1954) for a (a) step increase in temperature (heating) and (b) step decrease in temperature (cooling).*

data is found to be close within ±10% uncertainty bounds, assuming a ±10% uncertainty bounds in the properties of the wheel used in Rizika's analytical solution. The difference shown in the response of the wheel alone obtained from the transient data and the analytical solution is due to the inherent conduction effects in the tested wheel and not in the analytical solution.

Tables 4.12 to 4.17 list the characteristic coefficients representing the transient humidity response and transient temperature response of these wheels alone. It can be seen that these coefficients are very close to those coefficients listed in Tables 4.2 to 4.5 and Tables 4.8 to 4.11. As stated previously, this is a confirmation that the sensors (humidity and temperature) respond quite quickly and do not cause a large error in the transient response of the wheel alone. Tables 4.12 to 4.14 list the coefficients obtained from correlation equations (4.16) and (4.17) that represent the humidity transient response of the three tested wheels alone. Tables 4.15 to 4.17 list the coefficients obtained from correlation equations (4.19) and (4.20) that represent the temperature transient response of the three tested wheels alone for the heating and cooling processes. It is also noted as stated previously that these coefficients reflect the properties of the wheels.

Table 4.12. Water vapour adsorption and desorption coefficients (χ_1, χ_2) and time constants (τ_1, τ_2) in equations (4.12) and (4.13) for Wheel MS-100 alone with $\Delta RH \neq 0$, $\Delta T=0$, $V_{air}=1.6$ m/s for three different humidity step sizes.

Inlet conditions	χ_1	τ_1 (s)	χ_2	τ_2 (s)	r^2
	Adsorption				
dry side: $T_{i,d}\approx 23^oC$, $\Phi_{i,d}\approx 5\%$ wet side: $T_{i,w}\approx 23^oC$, $\Phi_{i,w}\approx 40\%$	0.87	8.2	0.13	146.3	0.999
	0.89	11.0	0.11	167.9	0.999
	0.90	11.9	0.10	179.5	0.999
dry side: $T_{i,d}\approx 23^oC$, $\Phi_{i,d}\approx 5\%$ wet side: $T_{i,w}\approx 23^oC$, $\Phi_{i,w}\approx 50\%$	0.82	7.8	0.18	146.0	0.999
	0.83	10.6	0.17	168.7	0.999
	0.90	6.7	0.10	134.9	0.999
dry side: $T_{i,d}\approx 23^oC$, $\Phi_{i,d}\approx 5\%$ wet side: $T_{i,w}\approx 23^oC$, $\Phi_{i,w}\approx 60\%$	0.86	9.6	0.14	152.1	0.999
	0.88	6.9	0.12	125.8	0.999
	0.85	9.3	0.15	141.8	0.999
	Desorption				
dry side: $T_{i,d}\approx 23^oC$, $\Phi_{i,d}\approx 5\%$ wet side: $T_{i,w}\approx 23^oC$, $\Phi_{i,w}\approx 40\%$	0.91	9.1	0.03	141.2	0.999
	0.89	7.3	0.03	112.7	0.999
	0.91	8.3	0.04	135.1	0.999
dry side: $T_{i,d}\approx 23^oC$, $\Phi_{i,d}\approx 5\%$ wet side: $T_{i,w}\approx 23^oC$, $\Phi_{i,w}\approx 50\%$	0.92	9.5	0.03	181.8	0.999
	0.90	7.2	0.03	126.5	0.999
	0.89	7.2	0.03	90.1	0.999
dry side: $T_{i,d}\approx 23^oC$, $\Phi_{i,d}\approx 5\%$ wet side: $T_{i,w}\approx 23^oC$, $\Phi_{i,w}\approx 60\%$	0.90	6.1	0.04	100.5	0.999
	0.92	7.8	0.05	128.7	0.999
	0.90	6.3	0.04	103.8	0.999

Table 4.13. Water vapour adsorption and desorption coefficients (χ_1, χ_2) and time constants (τ_1, τ_2) in equations (4.12) and (4.13) for Wheel SG-150 alone with $\Delta RH \neq 0$, $\Delta T=0$, $V_{air}=0.8$ m/s for three different humidity step sizes.

Inlet conditions	χ_1	τ_1 (s)	χ_2	τ_2 (s)	r^2
	Adsorption				
dry side: $T_{i,d}\approx 23^oC$, $\Phi_{i,d}\approx 5\%$ wet side: $T_{i,w}\approx 23^oC$, $\Phi_{i,w}\approx 40\%$	0.94	14.5	0.06	261.4	0.999
	0.96	11.8	0.04	220.0	0.999
	0.89	11.7	0.11	275.5	0.999
dry side: $T_{i,d}\approx 23^oC$, $\Phi_{i,d}\approx 5\%$ wet side: $T_{i,w}\approx 23^oC$, $\Phi_{i,w}\approx 50\%$	0.95	12.2	0.05	206.3	0.999
	0.94	12.5	0.06	178.3	0.999
	0.90	14.0	0.10	224.4	0.999
dry side: $T_{i,d}\approx 23^oC$, $\Phi_{i,d}\approx 5\%$ wet side: $T_{i,w}\approx 23^oC$, $\Phi_{i,w}\approx 60\%$	0.92	10.9	0.08	176.2	0.999
	0.88	11.6	0.12	213.2	0.999
	0.85	12.0	0.15	180.3	0.999
	Desorption				
dry side: $T_{i,d}\approx 23^oC$, $\Phi_{i,d}\approx 5\%$ wet side: $T_{i,w}\approx 23^oC$, $\Phi_{i,w}\approx 40\%$	0.95	17.4	0.05	250	0.999
	0.94	17.0	0.06	430	0.999
	0.95	15.6	0.05	260	0.999
dry side: $T_{i,d}\approx 23^oC$, $\Phi_{i,d}\approx 5\%$ wet side: $T_{i,w}\approx 23^oC$, $\Phi_{i,w}\approx 50\%$	0.95	17.8	0.05	280	0.999
	0.96	21.0	0.04	190	0.999
	0.95	19.3	0.05	380	0.999
dry side: $T_{i,d}\approx 23^oC$, $\Phi_{i,d}\approx 5\%$ wet side: $T_{i,w}\approx 23^oC$, $\Phi_{i,w}\approx 60\%$	0.95	23.2	0.05	140	0.999
	0.95	24.5	0.05	100	0.999
	0.95	25.1	0.05	180	0.999

Table 4.14. Water vapour adsorption and desorption coefficients (χ_1, χ_2) and time constants (τ_1, τ_2) in equations (4.12) and (4.13) for Wheel MS-200 alone with $\Delta RH \neq 0$, $\Delta T=0$, $V_{air}=1.6$ m/s for three different humidity step sizes.

Inlet conditions	χ_1	τ_1 (s)	χ_2	τ_2 (s)	r^2
	Adsorption				
dry side: $T_{i,d}\approx 23^oC$, $\Phi_{i,d}\approx 5\%$ wet side: $T_{i,w}\approx 23^oC$, $\Phi_{i,w}\approx 40\%$	0.85	16.3	0.15	167.7	0.999
	0.81	16.3	0.19	151.2	0.999
	0.80	17.5	0.20	175.4	0.999
dry side: $T_{i,d}\approx 23^oC$, $\Phi_{i,d}\approx 5\%$ wet side: $T_{i,w}\approx 23^oC$, $\Phi_{i,w}\approx 50\%$	0.80	16.5	0.20	198.8	0.999
	0.76	16.3	0.24	162.1	0.999
	0.78	16.7	0.22	200.6	0.999
dry side: $T_{i,d}\approx 23^oC$, $\Phi_{i,d}\approx 5\%$ wet side: $T_{i,w}\approx 23^oC$, $\Phi_{i,w}\approx 60\%$	0.80	15.3	0.20	163.0	0.999
	0.79	15.4	0.21	198.1	0.999
	0.77	16.4	0.23	170.2	0.999
	Desorption				
dry side: $T_{i,d}\approx 23^oC$, $\Phi_{i,d}\approx 5\%$ wet side: $T_{i,w}\approx 23^oC$, $\Phi_{i,w}\approx 40\%$	0.79	12.3	0.21	99.9	0.999
	0.86	15.2	0.14	139.5	0.999
	0.76	16.1	0.24	157.1	0.999
dry side: $T_{i,d}\approx 23^oC$, $\Phi_{i,d}\approx 5\%$ wet side: $T_{i,w}\approx 23^oC$, $\Phi_{i,w}\approx 50\%$	0.77	14.3	0.23	235.2	0.999
	0.75	14.4	0.25	138.1	0.999
	0.78	12.0	0.22	100.5	0.999
dry side: $T_{i,d}\approx 23^oC$, $\Phi_{i,d}\approx 5\%$ wet side: $T_{i,w}\approx 23^oC$, $\Phi_{i,w}\approx 60\%$	0.76	13.3	0.24	134.1	0.999
	0.82	12.0	0.18	100.4	0.999
	0.82	11.5	0.18	97.8	0.999

Table 4.15. Heat transfer heating and cooling coefficients (β_1, β_2) and time constants (τ_1, τ_2) in equations (4.19) and (4.20) for Wheel MS-100 alone $\Delta RH \neq 0$, $\Delta T = 0$, V_{air}=1.6 m/s.

Inlet conditions	β_1	τ_1 (s)	β_2	τ_2 (s)	r^2
	Temperature increase				
hot side: $T_{i,d} \approx 23^oC$, $\Phi_{i,d} \approx 4\%$ cold side: $T_{i,w} \approx 53^oC$, $\Phi_{i,w} \approx 4\%$	0.91	24.8	0.09	505.7	0.999
	0.91	20.0	0.09	141.3	0.999
	0.88	20.5	0.12	148.7	0.999
	0.91	21.8	0.09	174.3	0.999
	0.91	22.6	0.09	265.4	0.999
hot side: $T_{i,d} \approx 23^oC$, $\Phi_{i,d} \approx 4\%$ cold side: $T_{i,w} \approx 44^oC$, $\Phi_{i,w} \approx 4\%$	0.91	21.6	0.09	229.2	0.999
	0.86	19.9	0.14	128.9	0.999
	0.87	19.8	0.13	131.2	0.999
	0.88	19.6	0.12	115.5	0.999
	Temperature decrease				
hot side: $T_{i,d} \approx 23^oC$, $\Phi_{i,d} \approx 4\%$ cold side: $T_{i,w} \approx 53^oC$, $\Phi_{i,w} \approx 4\%$	0.84	21.9	0.16	159.4	0.999
	0.85	21.9	0.15	221.0	0.999
	0.78	20.5	0.22	116.4	0.999
	0.80	20.1	0.20	137.3	0.999
	0.82	21.3	0.18	138.2	0.999
hot side: $T_{i,d} \approx 23^oC$, $\Phi_{i,d} \approx 4\%$ cold side: $T_{i,w} \approx 44^oC$, $\Phi_{i,w} \approx 4\%$	0.79	19.0	0.21	126.0	0.999
	0.80	20.1	0.20	120.9	0.999
	0.76	19.1	0.24	108.3	0.999
	0.80	21.1	0.20	105.6	0.999

Table 4.16. Heat transfer heating and cooling coefficients (β_1, β_2) and time constants (τ_1, τ_2) in equations (4.19) and (4.20) for Wheel SG-150 alone with $\Delta RH \neq 0$, $\Delta T = 0$, V_{air}=0.8 m/s.

Inlet conditions	β_1	τ_1 (s)	β_2	τ_2 (s)	r^2
	Temperature increase				
hot side: $T_{i,d} \approx 23^oC$, $\Phi_{i,d} \approx 4\%$ cold side: $T_{i,w} \approx 53^oC$, $\Phi_{i,w} \approx 4\%$	0.78	45.8	0.22	341.8	0.999
	0.79	41.3	0.21	205.1	0.999
	0.82	43.0	0.18	261.8	0.999
	0.81	46.2	0.19	300.3	0.999
	0.80	48.6	0.20	364.3	0.999
hot side: $T_{i,d} \approx 23^oC$, $\Phi_{i,d} \approx 4\%$ cold side: $T_{i,w} \approx 44^oC$, $\Phi_{i,w} \approx 4\%$	0.82	43.9	0.18	328.1	0.999
	0.76	36.4	0.24	256.9	0.999
	0.78	43.6	0.22	341.7	0.999
	0.80	44.2	0.20	334.0	0.999
	Temperature decrease				
hot side: $T_{i,d} \approx 23^oC$, $\Phi_{i,d} \approx 4\%$ cold side: $T_{i,w} \approx 53^oC$, $\Phi_{i,w} \approx 4\%$	0.84	43.5	0.16	159.4	0.999
	0.85	53.8	0.15	221.0	0.999
	0.78	62.2	0.22	116.4	0.999
	0.80	43.4	0.20	137.3	0.999
	0.82	44.0	0.18	138.2	0.999
hot side: $T_{i,d} \approx 23^oC$, $\Phi_{i,d} \approx 4\%$ cold side: $T_{i,w} \approx 44^oC$, $\Phi_{i,w} \approx 4\%$	0.79	58.7	0.21	126.0	0.999
	0.80	23.3	0.20	120.9	0.999
	0.76	53.3	0.24	108.3	0.999
	0.80	47.1	0.20	105.6	0.999

Table 4.17. Heat transfer heating and cooling coefficients (β_1, β_2) and time constants (τ_1, τ_2) in equations (4.19) and (4.20) for Wheel MS-200 alone with $\Delta RH \neq 0$, $\Delta T=0$, V_{air}=1.6 m/s for three different humidity step sizes.

Inlet conditions	β_1	τ_1 (s)	β_2	τ_2 (s)	r^2
	Temperature increase				
hot side: $T_{i,d}\approx 23^oC$, $\Phi_{i,d}\approx 4\%$ cold side: $T_{i,w}\approx 53^oC$, $\Phi_{i,w}\approx 4\%$	0.87	16.1	0.13	275.2	0.999
	0.79	16.1	0.21	172.6	0.999
	0.87	17.2	0.13	206.8	0.999
	0.86	16.1	0.14	198.7	0.999
	0.86	15.0	0.14	268.1	0.999
hot side: $T_{i,d}\approx 23^oC$, $\Phi_{i,d}\approx 4\%$ cold side: $T_{i,w}\approx 44^oC$, $\Phi_{i,w}\approx 4\%$	0.90	16.1	0.10	361.0	0.999
	0.93	13.8	0.07	374.6	0.999
	0.91	11.9	0.09	261.8	0.999
	0.79	13.8	0.21	192.1	0.999
	Temperature decrease				
hot side: $T_{i,d}\approx 23^oC$, $\Phi_{i,d}\approx 4\%$ cold side: $T_{i,w}\approx 53^oC$, $\Phi_{i,w}\approx 4\%$	0.72	27.3	0.28	134.7	0.999
	0.72	25.9	0.28	126.5	0.999
	0.82	32.7	0.16	204.4	0.999
	0.74	27.3	0.26	152.0	0.999
	0.79	31.9	0.21	167.3	0.999
hot side: $T_{i,d}\approx 23^oC$, $\Phi_{i,d}\approx 4\%$ cold side: $T_{i,w}\approx 44^oC$, $\Phi_{i,w}\approx 4\%$	0.75	30.5	0.25	155.7	0.999
	0.87	35.7	0.13	228.7	0.999
	0.81	32.0	0.19	204.1	0.999
	0.85	31.8	0.15	237.5	0.999

Table 4.18 lists the averaged (adsorption and desorption) characteristic properties (coefficients) of Wheels MS-100, SG-150 and MS-200 while Table 4.19 lists the averaged (heating and cooling) characteristic properties of the wheels. In addition, an uncertainty analysis was performed according to ASME Standard PTC 19.1-1998 using the 95% uncertainty limits (analysis is included in Appendix B of this thesis). The uncertainties in the characteristic coefficients are thus included in the data presented in Tables 4.18 and 4.19.

Table 4.18. Humidity transient characteristic properties of Wheels MS-100, SG-150 and MS-200.

Humidity response				
Wheel	$\overline{\chi_1} + U(\overline{\chi_1})$	$\overline{\tau_1} + U(\overline{\tau_1})$ (s)	$\overline{\chi_2} + U(\overline{\chi_2})$	$\overline{\tau_2} + U(\overline{\tau_2})$ (s)
MS-100 (V_{air} = 1.6 m/s)	0.89±0.02	8.4±0.9	0.11±0.02	138±17
SG-150 (V_{air} = 0.8 m/s)	0.91±0.02	16.2±2.4	0.09±0.02	296±49
MS-200 (V_{air} = 1.6 m/s)	0.79±0.02	15.1±1.8	0.13±0.02	151±26

Table 4.19. Temperature transient characteristic properties of Wheels MS-100, SG-150 and MS-200.

Temperature response				
Wheel	$\overline{\beta_1} + U(\overline{\beta_1})$	$\overline{\tau_1} + U(\overline{\tau_1})$ (s)	$\overline{\beta_2} + U(\overline{\beta_2})$	$\overline{\tau_2} + U(\overline{\tau_2})$ (s)
MS-100 (V_{air} = 1.6 m/s)	0.87±0.02	20.7±1.2	0.13±0.02	171±59
SG-150 (V_{air} = 0.8 m/s)	0.80±0.02	45.7±5.6	0.20±0.02	220±32
MS-200 (V_{air} = 1.6 m/s)	0.83±0.04	32.2±2.4	0.17±0.04	218±43

The characteristic properties of the wheels presented in Tables 4.18 and 4.19 will be used later in Chapter 5 to determine the effectiveness of these wheels.

4.2 Numerical simulations

Simonson and Besant (1997a and b) developed a numerical model to predict the latent and sensible effectivenesses of rotary energy exchangers for different wheel designs and operating conditions. They validated their numerical results by comparing with experimental data and agreement was obtained. In this section, the numerical model of Simonson and Besant (1997a and b) is used to generate transient response data for energy wheels subjected to a step change in humidity (20% - 80% RH) at a constant temperature of 22°C and a step change in temperature (20°C - 40°C) at a constant relative humidity of 5% RH. These responses are determined at three different air face

velocities of 1.6, 0.8 and 0.3 m/s. Table 4.20 summarizes the properties of the wheel simulated.

Table 4.20. Properties of the simulated energy wheel

Desiccant	zeolite
Mass of desiccant (g/m^2)	30
Mass fraction of desiccant kg_{des}/kg_{matrix}	0.2
Wheel depth or thickness (mm)	100
Face velocity, V_{air} (m/s)	1.6, 0.8, 0.3
Wheel speed (rpm)	20
$D_{outside}$ (mm)	914
D_{inside} (mm)	288
Flute size – height (mm) – width (mm)	1.5 4.1

The same wheel (Table 4.20) with different amount of desiccants are used. For simplicity and clear reference, these wheels will be referred to as Wheels 5%D, 10%D and 20%D for the wheel with 0.05 mass fraction of desiccant on the wheel matrix, 0.1 mass fraction of desiccant and 0.2 mass fraction of desiccant respectively. This numerical investigation represents a test for quality control of the amount of desiccant on the wheel quoted by an energy wheel manufacturer. Energy wheel typically contains about 20% desiccant by mass, but this may vary between wheels and batches of manufactured wheels. A wheel that has less desiccant is expected to show a lower performance when compared with a wheel that has a full desiccant. In the same manner, the new transient model could be used to determine if different batches of energy wheels manufactured have the quoted amount of desiccant.

To determine the time constants of these simulated wheels, the simulated data are normalized relative to the maximum change obtained in the simulated data. The simulated transient responses are found to result in good correlations with one time constant using correlation equations (4.16), (4.17), (4.19) and (4.20), which means χ_1 or $\beta_1 = 1$ and χ_2 or $\beta_2 = 0$. Tables 4.21, 4.22 and 4.23 present the average (desorption and adsorption, and heating and cooling) wheels' response characteristics and their uncertainties for the wheels. The uncertainties are determined from the standard deviation of the curve fitting of the simulated response data using Table Curve™ 2D curve fit program and correlation equations (4.16), (4.17), (4.19) and (4.20). It is found that Wheel 20%D with the largest amount of desiccant has the highest time constants at all face velocities. This is expected because the greater the amount of desiccant on each wheel, the greater the moisture storage capacity and thus the slower the wheel will respond to changes in the inlet conditions. It is also observed that, as the face velocity decreases, the time constants increase for all the wheels. This is because a decrease in face velocity also results in a slower response of the wheel. A decrease in the air face velocity reduces the rate of advection heat and moisture transfer of water vapour in the air entering the wheel matrix and so the wheel will respond slowly to the inlet air. Note that the characteristic properties listed in Table 4.21 to 4.23 will also be used later in Chapter 5 to determine the latent and sensible effectiveness of these wheels.

Table 4.21. Humidity and temperature transient characteristic properties (time constants) of Wheel 5%D at face velocities 1.6, 0.8 and 0.3 m/s.

Face velocity (m/s)	Humidity response	Temperature response
	$\bar{\tau} \pm U(\bar{\tau})$ (s)	$\bar{\tau} \pm U(\bar{\tau})$ (s)
1.6	2±0.2	10±0.9
0.8	5±0.4	19±1.6
0.3	14±1.1	86±10
Note: Wheel 5%D is an energy wheel that has 0.05 mass fraction of desiccant		

Table 4.22. Humidity and temperature transient characteristic properties (time constants) of Wheel 10%D at face velocities 1.6, 0.8 and 0.3 m/s.

Face velocity (m/s)	Humidity response	Temperature response
	$\bar{\tau} \pm U(\bar{\tau})$ (s)	$\bar{\tau} \pm U(\bar{\tau})$ (s)
1.6	6±0.5	10±0.9
0.8	22±2.1	19±2
0.3	36±3.8	86±10
Note: Wheel 10%D is an energy wheel that has 0.1 mass fraction of desiccant		

Table 4.23. Humidity and temperature transient characteristic properties (time constants) of Wheel 20%D at face velocities 1.6, 0.8 and 0.3 m/s.

Face velocity (m/s)	Humidity response	Temperature response
	$\bar{\tau} \pm U(\bar{\tau})$ (s)	$\bar{\tau} \pm U(\bar{\tau})$ (s)
1.6	14±1.2	11±0.9
0.8	30±2.8	20±1.9
0.3	80±10	88±10
Note: Wheel 20%D is an energy wheel that has 0.2 mass fraction of desiccant		

4.3 Summary

The time constants and weighting factors of several different wheels determined from step response experiments have been presented in this chapter. It has been seen that these characteristic coefficients reflect the properties of the wheels. At the same face velocity, the larger the wheel, the larger the time constant. In the next chapter, Chapter 5, these characteristic properties will be used to predict the effectiveness and uncertainty in effectiveness of the wheels using the model presented in Chapter 3.

CHAPTER 5

COMPARISON OF TRANSIENT AND STEADY STATE EFFECTIVENESSES

The effectiveness and uncertainty results for Wheels MS-100, SG-150, MS-200, 5%D, 10%D and 20%D are presented in this chapter. As earlier stated, Wheels MS-100, SG-150 and MS-200 had previously been tested using the proposed revised standard of ASHRAE Standard 84-1991 using the ARI Standard 1060-2003 test conditions. Wheels 5%D, 10%D and 20%D are wheels whose effectiveness values have been determined using a validated numerical model. During the transient tests presented in Chapter 4, these wheels are subjected to step changes in humidity or temperature to determine their humidity or temperature responses. The time constants and weighting factors obtained from these tests are then used in the new theoretical model to predict the latent and sensible effectiveness of each wheel. The results obtained from this new effectiveness model are compared with the measured steady state data for Wheels MS-100, SG-150 and MS-200 and with the simulated results for Wheels 5%D, 10%D and 20%D.

5.1 Comparison with steady state experiments

5.1.1 Latent effectiveness

Figure 5.1 compares the latent effectiveness and its uncertainty obtained from the new transient time-constant derived effectiveness model with the results obtained from the steady state experiments for Wheels MS-100, SG-150 and MS-200. For steady state standard tests, the uncertainty in the latent effectiveness should not exceed ±7% (Ciepliski et al., 1998) while for the transient experiment, the uncertainty in latent effectiveness is found to be about ±5%. This comparison shows that the results obtained from the new transient experimental method agrees within the uncertainty bounds of the results obtained from the steady state experimental method.

As discussed in Chapter 4, the time constants of Wheel MS-100 are the shortest of all the three wheels because it has the lowest moisture transfer area for the 100 mm thick wheel matrix with a molecular sieve coating; thus the effectiveness is the lowest. Wheel SG-150 has a longer time constant because of its higher moisture transfer area (i.e., 150 mm thick wheel) and silica gel coating. Wheel MS-200, with a thickness of 200 mm, has the largest moisture transfer area with a molecular sieve coating. It has a slightly higher effectiveness than Wheel SG-150.

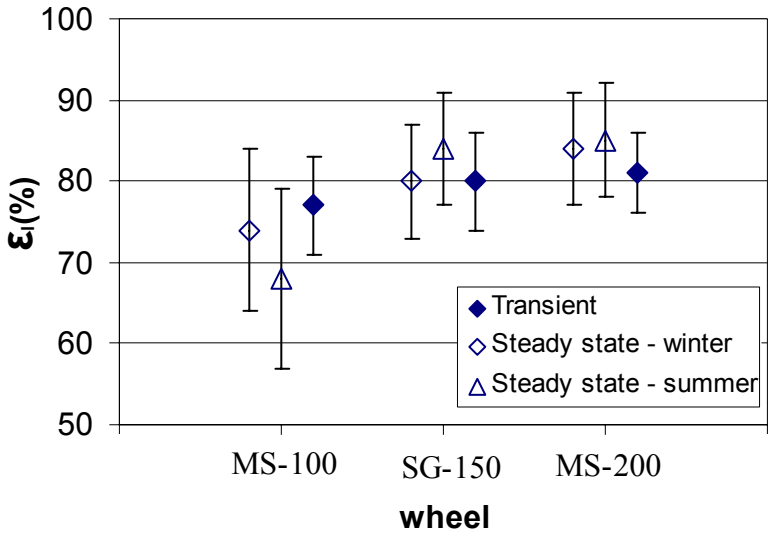

Figure 5.1. *Comparison of the latent effectiveness and uncertainty obtained from the new effectiveness model (transient) and the steady state standard tests for Wheels MS-100 (V_{air}=1.6 m/s), SG-150 (V_{air} =0.8 m/s), and MS-200 (V_{air} =1.6 m/s) under ARI winter and summer test conditions.*

A new effectiveness can be determined based on the weighted average of the two effectivenesses (i.e., transient and steady state) shown in Figure 5.1. This average is calculated such that the effectiveness with the lowest uncertainty is weighted more according to equations (5.1) to (5.3) (Taylor, 1982). Using these equations, the calculated weighted effectiveness is presented in Table 5.1 for the latent effectiveness and Table 5.2 for the sensible effectiveness.

$$\bar{\varepsilon} = \frac{\sum_{j=1}^{n} \sigma_j \varepsilon_j}{\sum_{j=1}^{n} \sigma_j} \tag{5.1}$$

where the weights σ_j are the inverse squares of the corresponding uncertainties, i.e.

$$\sigma_j = \frac{1}{[U(\varepsilon)]^2} \quad \text{for } j = 1, 2, \ldots n, \tag{5.2}$$

and n is the number of separate measurements of ε (which is 2 for this case). The uncertainty in the weighted effectiveness $U(\bar{\varepsilon})$ is calculated as:

$$U(\bar{\varepsilon}) = \left(\sum_{j=1}^{n} \sigma_j \right)^{-1/2} \tag{5.3}$$

Table 5.1. Weighted averages of the latent effectiveness calculated from steady state and transient tests

Wheels	**Weighted latent effectiveness (transient and steady state tests)**	
	(ARI winter)	(ARI summer)
MS-100	76±5%	75±5%
SG-150	80±5%	82±5%
MS-200	82±4%	82±4%

Although it is not likely that manufacturers would want to pay for both tests, the results in Table 5.1 imply that it is possible to reduce the uncertainty in the effectiveness when the two independently measured effectiveness values shown in Figure 5.1 are appropriately combined.

In Figure 5.2, Wheels MS-100 and MS-200 are compared at different face velocities. The reason why these two wheels are compared is because they are identical in coating and matrix geometry except for the wheel thickness. Wheel MS-100 is a 100 mm thick wheel that has molecular sieve desiccant coating. Wheel MS-200 has the same desiccant coating but the wheel has a thickness of 200 mm. Using experimental data and extrapolation from the transient model, the latent effectiveness of these two wheels are compared as a function of face velocity in Figure 5.2. It is expected that Wheel MS-200 will perform better than Wheel MS-100 because of its greater thickness

or greater surface area which results in $NTU_{MS\text{-}200} = 2NTU_{MS\text{-}100}$ for the same face velocity. For clarity, uncertainty bounds are only shown at face velocities of 0.2, 1.6, 2.8 and 5.0 m/s. The overlapping uncertainty bounds for these two wheels implies that a user could not be guaranteed that the MS-200 wheel will have a higher effectiveness than the MS-100 wheel even though is more likely. In practical applications of energy wheels, face velocities from 1.5 to 4.0 m/s are typical but under part load conditions the face velocity or wheel speed may be reduced.

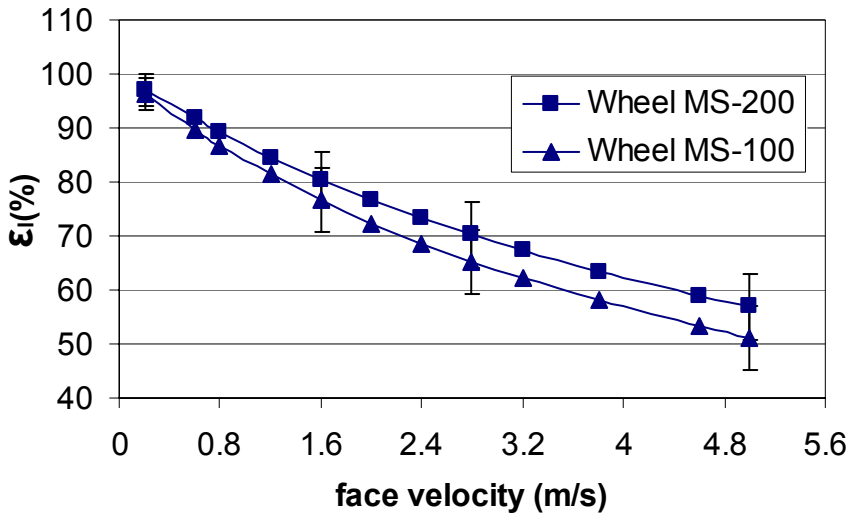

Figure 5.2. *Predicted latent effectiveness (using the transient model) of Wheels MS-100 and MS-200 versus face velocity.*

5.1.2 Sensible effectiveness

The sensible effectiveness and the uncertainty using the new effectiveness model are compared with the steady state experiments for Wheels MS-100, SG-150 and MS-200 in Figure 5.3. Typical uncertainty in the sensible effectiveness for the steady state standard tests should not exceed ±5% (Ciepliski et al., 1998). For the transient tests, the uncertainty is found to be about ±4%. It can also be inferred from Figure 5.3

that the effect of heat conduction studied in section 4.1.4 is trivial on the predicted effectiveness at the face velocities used. The weighted averages of the two effectiveness shown in Figure 5.3 are presented in Table 5.2.

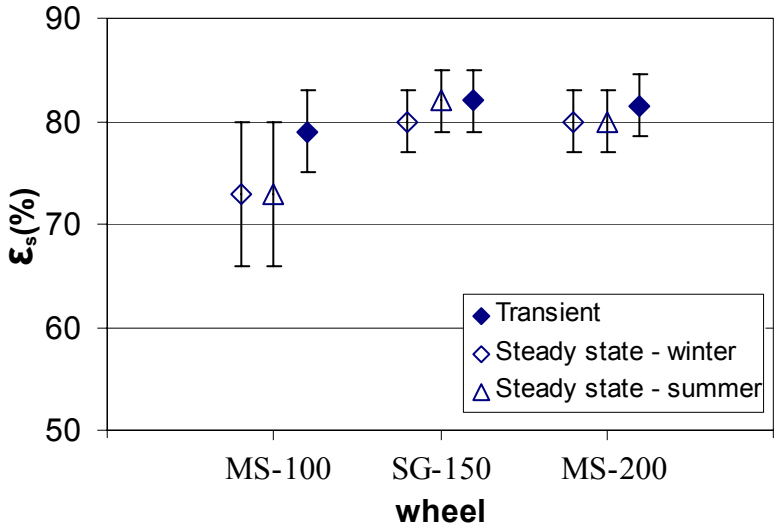

Figure 5.3. Comparison of the sensible effectiveness and uncertainty obtained from the new effectiveness model and the steady state standard tests for Wheels MS-100 (V_{air}=1.6 m/s), SG-150 (V_{air} =0.8 m/s), and MS-200 (V_{air} =1.6 m/s) under ARI winter and summer test conditions.

Table 5.2. Weighted averages of the sensible effectiveness calculated from steady state and transient tests.

Wheels	**Weighted sensible effectiveness (transient and steady state tests)**	
	ARI winter	ARI summer
MS-100	77±3%	78±3%
SG-150	81±2%	82±2%
MS-200	81±2%	81±2%

Figure 5.4 shows the sensible effectiveness of Wheels MS-100 and MS-200 at various face velocities. Again, Wheel MS-200 shows a better performance at the same face velocity because its surface area is double that of Wheel MS-100.

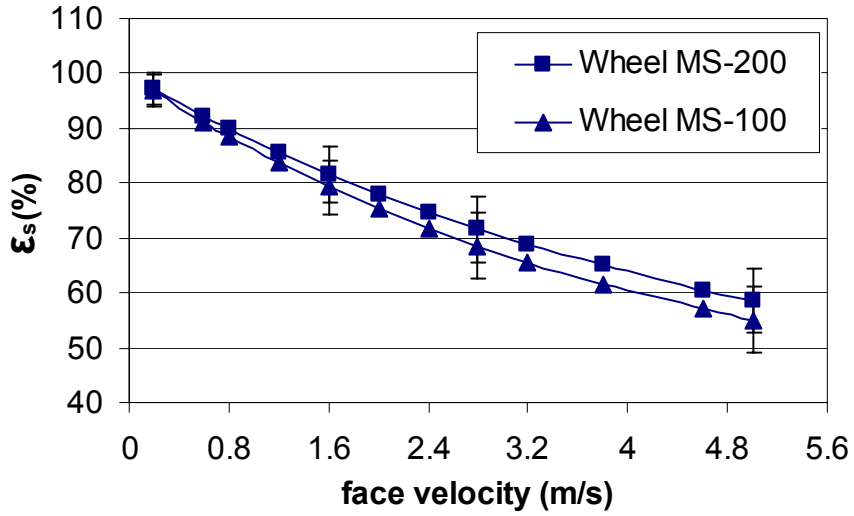

Figure 5.4. *Predicted sensible effectiveness (using the transient model) of Wheels MS-100 and MS-200 versus face velocity.*

5.2 Comparison with steady state numerical simulations

5.2.1 Latent effectiveness

Figure 5.5 shows the comparison of the latent effectiveness obtained from the new effectiveness model (transient) with the results obtained from the numerical simulations for 100 mm thick MS-100 Wheels 5%D, 10%D and 20%D. The simulations were carried out at face velocities of 1.6, 0.8 and 0.3 m/s.

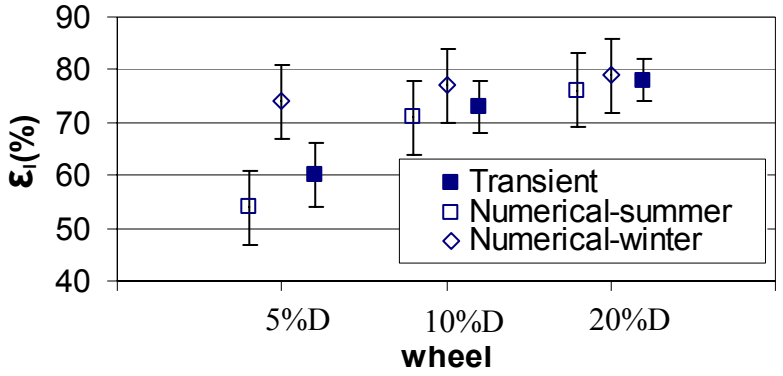

(a)

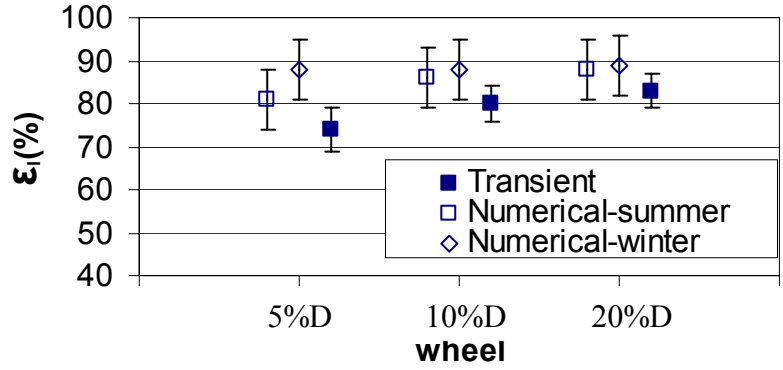

(b)

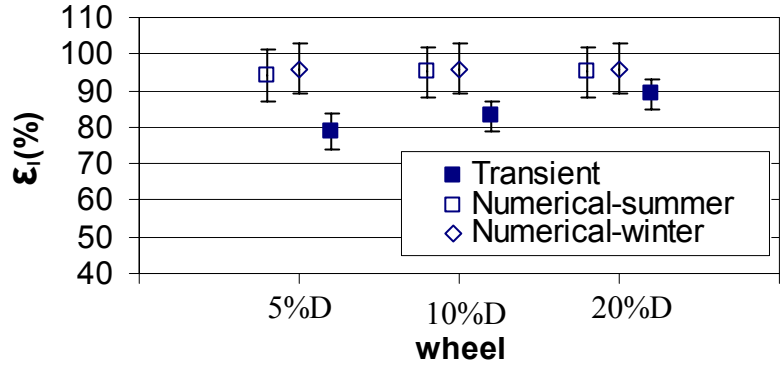

(c)

Figure 5.5. Comparison of the latent effectiveness and uncertainty using the new (transient) effectiveness model and numerical simulations at ARI summer and winter conditions for Wheels 5%D, 10%D and 20%D at (a) V_{air}*=1.6 m/s, (b)* V_{air} *=0.8 m/s and (c)* V_{air} *=0.3 m/s.*

These results in Figure 5.5 show that as the face velocity decreases, the effectiveness increases. These results can be explained because the *NTU* is inversely proportional to the flow rate; so that as the face velocity reduces, *NTU* increases (equation (3.4)). Thus, the effectiveness in equation (3.46) which depends directly on the *NTU* is seen to increase as the face velocity decreases as shown in Figure 5.5. Agreement between the new effectiveness model and the simulation within uncertainty bounds are obtained for all wheels with face velocities of 1.6 and 0.8 m/s. There is, however, a lack of agreement for Wheels 5%D and 10%D for a face velocity of 0.3 m/s as shown in Figure 5.5*(c)*. It must be noted that at this small face velocity of 0.3 m/s, the numerical simulation results obtained for Wheels 5%D and 10%D could not be verified experimentally because there is no practical way the desiccant on the wheel could be removed to result in a desiccant coating mass fraction of a quarter or half of the typical value of 20% by mass. This investigation was meant to be a sensitivity study, which, if practical, could be used as test for quality control for the amount of desiccant on the wheel quoted by an energy wheel manufacturer. Wheels 5%D and 10%D, which have a matrix desiccant mass fractions of quarter and half respectively, have less desiccant to enhance moisture transfer in the wheel compared to Wheel 20%D with a full desiccant mass fraction. Despite, the poorer agreement between steady state and transient methods shown in Figures 5.5*(c)*, both methods show a decrease in effectiveness as the mass fraction of desiccant decreases. This indicates that the transient method could be used to compare different batches of energy wheels from the same manufacturer to ensure that the amount of desiccant has not changed.

5.2.2 Sensible effectiveness

Figure 5.6 shows a comparison of the sensible effectiveness obtained from the new effectiveness model and the numerical simulations for Wheels 5%D, 10%D and 20%D. There is agreement between the new model and the numerical simulation within uncertainty limits for all the wheels at the face velocities of 1.6 and 0.8 m/s. In Figure 5.6*(c)* (V_{air}= 0.3 m/s), the effectiveness obtained from the numerical simulation is lower than that obtained from the transient model. This simulation result, which includes corrections for axial conduction in the matrix, is contrary to a previous statement in section 5.2.1 where the effectiveness was shown to be inversely related to the flow rate. In Figure 5.5, the simulation shows that as the face velocity is reduced to a low value (e.g. 0.3 m/s), the latent effectiveness increases but Figure 5.6 shows that the sensible effectiveness reduces. This reduction in sensible effectiveness is likely due to the coupled heat and moisture transfer that occurs at ARI test conditions. At these test conditions, the moisture transfer will cause the sensible effectiveness to decrease from the value that would exist with no moisture transfer (Simonson and Besant, 1999b). This difference between sensible and latent effectiveness is not accounted for in the new (transient) effectiveness model which depends only on the humidity and temperature time constants which are measured independently, and the speed of the wheel alone. In addition, at very low wheel speeds and face velocities, the axial conduction is dominant and tends to have some effects on the sensible effectiveness of the wheel. However, axial conduction is not of great importance at the face velocities typically used in HVAC systems (1.5 to 4 m/s). The effect of axial conduction is likely different for parallel flow and counter flow heat exchangers and the model does not consider this.

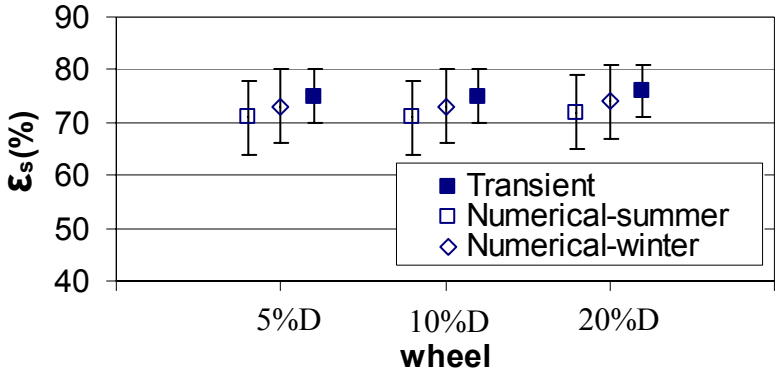

(a)

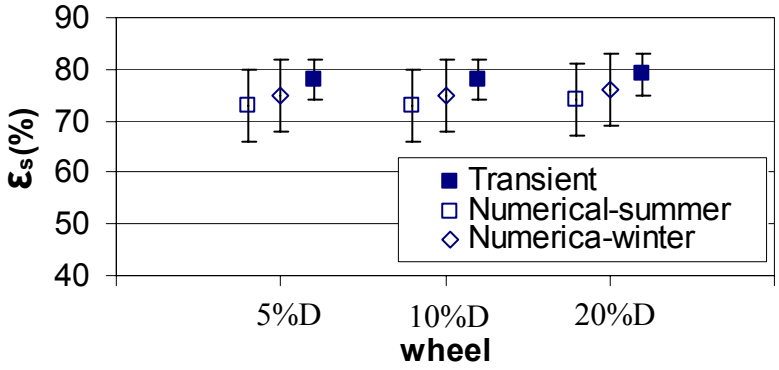

(b)

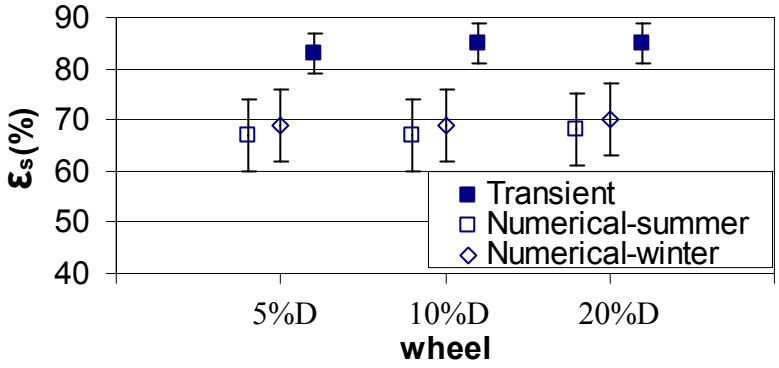

(c)

Figure 5.6. Comparison of the sensible effectiveness and uncertainty using the new (transient) effectiveness model and numerical simulations at ARI summer and winter conditions for Wheels 5%D, 10%D and 20%D at (a) V_{air}*=1.6 m/s, (b)* V_{air} *=0.8 m/s and (c)* V_{air} *=0.3 m/s.*

5.3 Summary

In this chapter, latent and sensible effectiveness predicted from the new transient effectiveness model have been shown to agree within uncertainty bounds with the results obtained from steady state standard tests and with few exceptions, with the numerical simulations.

CHAPTER 6

RESEARCH SUMMARY, CONCLUSIONS AND FUTURE WORK

6.1 Research summary

The general objective of this research is to predict the effectiveness of an energy wheel using only data obtained during a single step response, i.e. the response of the wheel when the wheel is exposed to a step change in inlet humidity or temperature conditions. To achieve this objective, the first challenge is the development of a mathematical model from a first-order linear design theory since the simplified governing equations which relate the properties of the air and matrix of an energy wheel are coupled, linear first-order differential equations. This model establishes a relationship between the step response and the periodic response of an energy wheel. In other words, the relationship relates the response of an energy wheel exposed to a step input to the response when the input is steady and periodic.

An effectiveness correlation is then developed from the mathematical model to predict the performance of the wheel using the data obtained from the step response (i.e. time constants and weighting factors of the wheel). In addition, knowing the uncertainty in the measured time constants, the uncertainty bounds in the predicted effectiveness are also determined. These uncertainty bounds show the confidence in the predicted results.

6.2 Conclusions

The conclusions of this thesis are summarized below:

1. In this research, a mathematical model that predicts a relationship between the transient response of an energy wheel and the steady state periodic response is developed using first-order linear design theory.
2. Using the mathematical model developed, an equation that predicts the latent and sensible effectiveness of energy wheels from the measured time constants and weighting factors and the operating wheel speed is defined. The effectiveness increases as the measured time constants increase. For example, for a time constant of 4s, the effectiveness ε_{CF} = 69% while for a time constant of 10s, effectiveness ε_{CF} = 76%. The effectiveness also increases as the wheel speed increases. For example, for a time constant of 10s, the effectiveness ε_{CF} = 76% at a wheel speed of 20 rpm whereas at a wheel speed of 40 rpm, the effectiveness ε_{CF} = 79%. Furthermore, it is seen that knowing the uncertainty in the measured time constant, the uncertainty in the predicted effectiveness can be determined. As the uncertainty in time constant increases, the uncertainty in effectiveness increases. For example, at a wheel speed of 20 rpm, a time constant of 4s having an uncertainty of $\pm 10\%$ results in an uncertainty in effectiveness of $U(\varepsilon_{CF}) = \pm 5.2\%$, while for a time constant of 4s having an uncertainty of $\pm 15\%$, the uncertainty in effectiveness is $U(\varepsilon_{CF}) = \pm 7.7\%$. In addition, as the wheel speed and time constant increase, the uncertainty in

effectiveness decreases. For example, at a wheel speed of 20 rpm and assuming an uncertainty of $\pm 10\%$ in the measured time constant, the uncertainty in effectiveness is $U(\varepsilon_{CF}) = \pm 5.2\%$ for a time constant of 4s and $U(\varepsilon_{CF}) = \pm 4.2\%$ for a time constant of 10s; whereas, at a wheel speed of 40 rpm, the uncertainty in effectiveness is $U(\varepsilon_{CF}) = \pm 4.4\%$ for a time constant of 4s and $U(\varepsilon_{CF}) = \pm 3.7\%$ for a time constant of 10s.

3. The time constants measured using the test facility developed by Wang (2005) reflect the properties of different wheels. At the same mass face velocity, the thicker the wheel (or the larger the heat transfer area), the larger the time constant.
4. The effectiveness values calculated using the new analytical model and the measured time constants show good agreement, within uncertainty bounds, with the effectiveness values obtained from steady state experiments and with few exceptions, with the numerical simulations. For example, for a 100 mm thick (4") wheel coated with molecular sieve desiccant, the latent effectiveness result obtained from the new transient model is $77 \pm 5\%$, while the latent effectiveness obtained from a standard steady state tests is $74 \pm 7\%$. Also, the sensible effectiveness obtained from the new model for a 100 mm thick (4") wheel coated with molecular sieve desiccant is $79 \pm 4\%$, while the sensible effectiveness obtained from the steady state tests is $73 \pm 7\%$.
5. The latent effectiveness calculated with the new effectiveness model can be predicted within about ±5% whereas for the steady state standard tests, latent effectiveness can be predicted within ±7%. Also the sensible effectiveness

calculated with the new effectiveness model can be predicted within about ±4% whereas for the steady state standard tests, sensible effectiveness can be predicted within ±5%.

6.3 Future work

In this thesis, it is seen that using the test facility developed by Wang (2005) to measure the time constants of energy wheels, the latent and sensible effectiveness can be predicted. Therefore, the test facility and testing method can be developed as a new testing standard for testing and rating the performance of energy wheels using transient measurements.

REFERENCES

Abdelghani-Idrissi, M.A., Bagui, L., Estel, L., 2003, Analytical and experimental response time to flow rate step along a counter-flow double pipe heat exchanger *International Journal of Heat and Mass Transfer*, **44** (19) 3721-3730.

ARI Standard 1060-2003, 2003, Rating Air-to-Air Energy Recovery Equipment *Air-Conditioning and Refrigeration Institute*, Arlington, VA.

Arpaci, V.S and Clark, J.A., 1958, Dynamic response of heat exchangers having internal heat sources – part II , *Transactions of the ASME*, **80**, 625 -634.

ASHRAE, 1996, HVAC systems and equipment handbook, *American Society of Heating, Refrigerating and Air Conditioning Engineers Inc*., Atlanta.

ASHRAE Standard 84-1991, 1991, Method of testing air-to-air heat exchangers, *American Society of Heating, Refrigerating and Air Conditioning Engineers Inc*., Atlanta.

Asiedu, Y., Besant, R.W. and Simonson, C.J., 2004, Wheel selection for heat and energy recovery in simple HVAC ventilation design problems, *ASHRAE Transactions* **110**(1), 381-398.

Asiedu, Y., Besant, R.W. and Simonson, C.J., 2005, Cost-effective design of dual heat and energy recovery exchangers for 100% ventilation air in HVAC cabinet units, *ASHRAE Transactions* **111**(1), 857-872.

ASME PTC 19.1-1998, Test uncertainty, *The American society of Mechanical Engineers*, New York.

Besant, R.W. and Simonson, C.J., 2000, Air-to-air energy recovery, ASHRAE Journal, **42** (5), 31-42.

Ciepliski, D.L., Simonson, C.J. and Besant, R.W., 1998, Some recommendations for improvements to ASHRAE Standard 84-1991, *ASHRAE Transactions* **104**(1B), 1651-1965.

Carriere, M.L., 1996, A new method for optimal thermal design and retrofit of large commercial buildings, Department of Mechanical Engineering, University of Saskatchewan, Saskatoon.

Clark, J.A., Arpaci, V.S. and Treadwell, K.M., 1958, Dynamic response of heat exchangers having internal heat sources – part I , *Transactions of the ASME*, **80**, 612 -624.

Cochin, I. and Plass, H.D.(Jr.), 1990, Analysis and design of dynamic systems, *HarperCollins*, New York.

Coppage, J.E. and London, A.L., 1953, The periodic-flow regenerator – a summary of design theory, *Transactions of the ASME*, **75**, 779.

Dhital, P., Besant, R.W., and Schoenau, G.J., 1995, Integrating run around heat exchanger systems into the design of large office buildings, *ASHRAE Transactions* **101**, 978-990.

Gawley, H.N. and Fisher, D.R., 1975, The effectiveness and rating of air-to-air heat exchangers, *ASHRAE Transactions* **81**(2), 401-409.

Han Y.I., Kim, D. and Kim, S.J., 2005, Study on the transient characteristics of the sensor tube of a thermal mass flow meter, *International Journal of Heat and Mass Transfer*, **48**, 2583-2592.

Hausen, H., 1983, Heat transfer in counter flow, parallel flow and cross flow, *McGraw-Hill*, New York.

Incropera, F.P. and Dewitt, D.P., 2002, Fundamentals of heat and mass transfer, *Wiley*, New York.

Lachi, M., Wakil, N. El, and Padet J., 1997, The time constant of double pipe and one pass shell-and-tube heat exchangers in the case of varying flow rates, *International Journal of Heat and Mass Transfer* **40**(9), 2067-2079.

Kaplan, W., 1981, Advanced mathematics for engineers, *Addison-Wesley*, Ontario.

Kays, W.M., and London, A.L., 1984, Compact heat exchangers, *McGraw-Hill*, New York.

Klein, H., Klein, S.A. and Mitchell, J.W., 1990, Analysis of regenerative enthalpy exchangers, *International Journal of Heat and Mass Transfer*, **33**, 735-744.

Kuse, T. and Takahashi, S., 2000, Transient behaviour of tin oxide semiconductor under a step-like humidity change, *Sensors and Actuators B,* **67**, 36-42.

Kreyszig, E., 1999, Advanced engineering mathematics, *Wiley*, New York.

Rizika, J.W., 1954, Thermal lags in flowing system containing heat capacitors, *Transactions of the ASME*, **76**, 411-420.

Romie, F.E., 1984, Transient response of the counterflow heat exchanger, *Journal of Heat Transfer*, **106**(3), 620-626.

Romie, F.E., 1985, Transient response of the parallel flow heat exchanger, *Journal of Heat Transfer*, **107**(3), 727-730.

Romie, F.E., 1992, A solution for the parallel flow regenerator, *Journal of Heat Transfer*, **114**, 278-280.

Romie, F.E., 1999, Response of counterflow heat exchangers to step changes of flow rates, *Journal of Heat Transfer*, **121**(3), 746-748.

Roetzel, W. and Xuan, Y., 1992, Transient response of parallel and counterflow heat exchangers, *Journal of Heat Transfer*, **114**(2), 510-512.

Shah, R.K., 1981, Thermal design theory for regenerators, in: *Heat exchangers: Thermal-hydraulic fundamentals and design*, (edited by S. Kakaç, Bergles, A.E. and Mayinger, F.), Hemishere, New York.

Shang, W., 2002, *Evaluation of energy wheel performance*, Ph.D. thesis in mechanical engineering, University of Saskatchewan, Saskatoon.

Simonson, C.J. and Besant, R.W., 1997a, Heat and moisture transfer in desiccant coated rotary energy exchangers: part I – numerical model, *International Journal of HVAC&R Research* **3**(4), 325-350.

Simonson, C.J. and Besant, R.W., 1997b, Heat and moisture transfer in desiccant coated rotary energy exchangers: part II – validation and sensitivity studies, *International Journal of HVAC&R Research* **3**(4), 351-368.

Simonson, C.J. and Besant, R.W., 1999a, Energy wheel effectiveness: part I – development of dimensionless groups, *International Journal of Heat and Mass Transfer* **42**, 2161-2170.

Simonson, C.J. and R.W. Besant, 1999b, Energy wheel effectiveness: part II – correlations, *International Journal of Heat and Mass Transfer* **42**, 2171-2185.

Simonson, C.J., Ciepliski, D.L. and Besant, R.W., 1999a, Determining the performance of energy wheels: part I - experimental and numerical methods, *ASHRAE Transactions* **105**(1), 188-205.

Simonson, C.J., Ciepliski, D.L. and Besant, R.W., 1999b, Determining the performance of energy wheels: part II - experimental data and numerical validation, *ASHRAE Transactions* **105**(1), 177-187.

Tan, K.S. and Spinner, I.H., 1991, Approximate solutions for transient response of a shell and tube heat exchanger, *Ind. Eng. Chem. Res*. **30**(7), 1639-1646.

Taylor, J.R., 1982, An introduction to error analysis – the study of uncertainties in physical measurements, *University Science Books*, California.

Vaisala, 1998, HMP230 Series Transmitter operating manual, Helsinki.

Wang, Y.H., 2005, Transient characteristics of humidity sensors and their application to energy wheels, M.Sc. thesis in mechanical engineering, University of Saskatchewan, Saskatoon.

Wang, Y.H., Simonson, C.J., Besant, R.W., and Shang, W., 2005, Transient humidity measurements and characteristics for humidity sensors and energy wheels, *Accepted for publication in ASHRAE Transactions*, **111**(2).

Wylie, C.R.,1975, Advanced engineering mathematics, *McGraw-Hill*, New York.

Yin, J. and Jensen, M.K., 2003, Analytical model for transient heat exchanger response, *International Journal of Heat and Mass Transfer*, **46**, 3255-3264.

APPENDIX A: HUMIDITY SENSOR AND THERMOCOUPLE RESPONSE

The transient response correlations and characteristics of the humidity sensor and thermocouple used in the correction of the transient responses of wheel plus humidity sensor and wheels plus thermocouple for wheel alone are presented in this appendix. This work was performed by Wang (2005).

Humidity sensor transient response

The humidity sensor transient response experiments are performed under isothermal conditions listed in Table 4.1. The measured data for the transient response of the humidity sensor were found to follow exponential correlation equations (A.1) and (A.2) with two time constants, t_1 and t_2, each with a corresponding weighting factor, x_1 and x_2. Equation (A.1) shows the response with a step increase in relative humidity (i.e. the sensor undergoes an adsorption process).

$$\frac{\Delta\phi}{\Delta\phi_0}(t)_{ads} = x_1\left(1-e^{-t/t_1}\right)+x_2\left(1-e^{-t/t_2}\right) \tag{A.1}$$

and for a step decrease in relative humidity (i.e. desorption)

$$\frac{\Delta\phi}{\Delta\phi_0}(t)_{des} = x_1 e^{-t/t_1}+x_2 e^{-t/t_2} \tag{A.2}$$

where the step fraction coefficients or weighting factors x_1 and x_2 satisfy the equation (A.3) for both adsorption and desorption.

$$x_1 + x_2 = 1,\quad x_1 \geq 0,\quad x_2 \geq 0 \tag{A.3}$$

but with different values of x_1 and x_2 for each case.

$\Delta\phi$ = measured change in relative humidity = $\left|\phi - \phi_j\right|$, where ϕ_j is the initial relative humidity.

$\Delta\phi_0$ = maximum step change in relative humidity = $\left|\phi_f - \phi_j\right|$, where ϕ_f is the final relative humidity.

t_1, t_2 = the first and second time constants respectively.

Table A.1 lists the weighted averages of the transient characteristic properties and uncertainties for the transient response of the humidity sensor alone (equations (A.1) and (A.2)) obtained from the data from 9 tests.

Table A.1. Average coefficients and uncertainties for the transient response of the humidity sensor.

Test conditions	Coefficients	Adsorption	Desorption
$\Delta RH \neq 0$	$\overline{x_1} \pm U(\overline{x_1})$	0.91±0.03	0.97±0.01
$\Delta T = 0$	$\overline{t_1} \pm U(\overline{t_1})$ (s)	3.1±0.4	2.6±0.3
V_{air} = 1.6m/s	$\overline{x_2} \pm U(\overline{x_2})$	0.09±0.03	0.03±0.01
Flow rate = 200 L/min	$\overline{t_2} \pm U(\overline{t_2})$ (s)	90±10	290±90
$\Delta RH \neq 0$	$\overline{x_1} \pm U(\overline{x_1})$	0.95±0.01	0.97±0.01
$\Delta T = 0$	$\overline{t_1} \pm U(\overline{t_1})$ (s)	3.6±0.6	3.1±0.4
V_{air} = 0.8m/s	$\overline{x_2} \pm U(\overline{x_2})$	0.05±0.01	0.03±0.01
Flow rate = 100 L/min	$\overline{t_2} \pm U(\overline{t_2})$ (s)	140±60	310±110

It can be seen from Table A.1, that humidity sensor response to a step change in humidity alone for the adsorption process is approximately 3 seconds for the first time constant for about 90% of the step change in humidity recorded by the sensor. The second time constant is about 100 seconds for adsorption process for about 10% of the step change in humidity recorded by the sensor. As shown in Table A.1, the coefficients

of the humidity sensor response was found not to be sensitive to the size of step change in humidity or to changes in flow rates or face velocities (Wang et al., 2005).

Thermocouple transient response

The temperature transient response experiments for the thermocouple are performed under dry test conditions shown in Table 4.2 where there is negligible moisture transfer.

The measured data for the transient response of thermocouple follows exponential correlation equations (A.4) and (A.5) with two time constants t_1 and t_2, each with a corresponding weighting factor y_1 and y_2. For a step increase in temperature

$$\frac{\Delta\gamma}{\Delta\gamma_0}(t)_{ads} = y_1\left(1-e^{-t/t_1}\right)+y_2\left(1-e^{-t/t_2}\right) \tag{A.4}$$

and for a step decrease in temperature

$$\frac{\Delta\gamma}{\Delta\gamma_0}(t)_{des} = y_1 e^{-t/t_1}+y_2 e^{-t/t_2} \tag{A.5}$$

where the step fraction coefficients or weighting factors y_1 and y_2 satisfy the equation

$$y_1 + y_2 = 1,\ y_1 \geq 0,\ y_2 \geq 0 \tag{A.6}$$

but with different values of y_1 and y_2 for each experiment.

$\Delta\gamma$ = measured change in temperature = $\left|\gamma-\gamma_j\right|$, where γ_j is the initial temperature.

$\Delta\gamma_0$ = maximum step change in temperature = $\left|\gamma_f-\gamma_j\right|$, where γ_f is the final temperature.

$t_1,\ t_2$ = the first and second time constants respectively.

Table A.2 shows the weighted average characteristics describing the transient temperature response of the thermocouple (equations (A.4) and (A.5)).

Table A.2. Average coefficients and uncertainties for the transient response of the thermocouple sensor.

Test conditions	Coefficients	Temperature increase	Temperature decrease
$\Delta RH = 0$	$\overline{y_1} \pm U(\overline{y_1})$	0.76±0.07	0.80±0.08
$\Delta T \neq 0$	$\overline{t_1} \pm U(\overline{t_1})$ (s)	5.1±1.5	5.1±0.8
V_{air} = 1.6m/s	$\overline{y_2} \pm U(\overline{y_2})$	0.24±0.07	0.2±0.08
Flow rate = 200 L/min	$\overline{t_2} \pm U(\overline{t_2})$ (s)	130±20	160±110

It can be inferred from Table A.2 that, for a step change in temperature alone, the thermocouple response has the first time constant of about 5 seconds while the second time constant is about 150 seconds. It is therefore obvious from Tables A.1 and A.2 that the response of these sensors (humidity sensor and thermocouple) is very fast and is expected not to affect or cause a consequential delay in the response of the wheel alone. The transient characteristics of the humidity sensor (x_1, x_2, t_1 and t_2) and thermocouple (y_1, y_2, t_1 and t_2) are the properties necessary to predict the transient response of an energy wheel when the same sensor or thermocouple placed downstream of the energy wheel are subjected to either a step change in humidity or temperature. These results are discussed in detail in section 4.1 of this thesis.

APPENDIX B: UNCERTAINTY ANALYSIS

Appendix B lists the uncertainty analysis used to determine the uncertainty in the transient response characteristics of the wheels alone using 95% confidence limits. This uncertainty analysis is also used to determine the uncertainty in the predicted effectiveness of the wheels.

Uncertainty analysis is used to quantify the uncertainty associated with each measured data and calculated results using a quantitative standard method. This procedure allows one to know the level of confidence that should be put in data and computed results. According to *ASME PTC 19.1-1998*, precision and bias errors or uncertainties are the main components of uncertainty analysis and these are calculated independently. This standard defines the uncertainty as the root–sum–square uncertainty in any calculated dependent variable $r(\eta_k)$ and the independent variables η_k. This uncertainty is expressed as

$$U = \sqrt{U_P^2 + U_B^2} \tag{B.1}$$

where the confidence level of the uncertainty is 95%. U_P is the precision uncertainty and U_B is the bias uncertainty. For example, the uncertainty in the calculation of the dependent variable $r(\eta_k)$ can be approximated by equation

$$U_r = \left[\sum_{k=1}^{n} (\theta_k U_k)^2 \right]^{1/2}, \tag{B.2}$$

where θ_k is defined as the sensitivity coefficient of the dependent variable, *r*, to the changes in the k[th] variable η_k by

$$\theta_k = \frac{\partial r}{\partial \eta_k}. \tag{B.3}$$

Equation (B.2) is a general equation for calculating the precision index as a measure of the uncertainty U_P for $r(\eta_k)$ and the results from measurements of several statistically independent properties η_k. For example, for a property ε representing the effectiveness defined as

$$\varepsilon = 0.5 - \sum_{n=1}^{\infty} \frac{4a^2}{(\pi n)^2\left(a^2 + (nw)^2\right)}, \text{ where} \tag{B.4}$$

the values of a are obtained from measurements of several statistically independent properties while *n* and *w* are constants. The uncertainty in ε is estimated as

$$U(\varepsilon) = \left(U_{P(a)}^2 + U_{B(a)}^2\right)^2. \tag{B.5}$$

The precision unceratinty $U_{P(a)}$ in a is estimated as

$$U_{P(a)}^2 = \left(\left(\frac{\partial \varepsilon}{\partial a}\right)(tS_a)\right)^2, \tag{B.6}$$

where *t* is the *student t* for the 95% confidence level and *S,* the precision index is calculated as the sample standard deviation for n samples of data a

$$S_k^2 = \frac{\sum_{j=1}^{n}\left(a_{kj} - \overline{a}_k\right)^2}{n-1}, \tag{B.7}$$

where a_{kj} is the parameter which is measured and

$$\bar{a}_k = \frac{1}{n}\sum_{j=1}^{n} a_{kj} \tag{B.8}$$

is the average value of measured a.

The bias error $U_{B(a)}$ in a is calculated in similar way as

$$U_{B(a)}^2 = \left(\left(\frac{\partial \varepsilon}{\partial a}\right)(B_a)\right)^2, \text{ where} \tag{B.9}$$

B is the fixed or bias error associated with a.

The standard deviation is calculated based on the measured data so as to determine the repeatability of the experiments. Therefore in calculating the absolute uncertainty in the measured characteristic data, the precision uncertainty was calculated using the standard deviation while the bias error estimated by Wang (2005) to be 0.2s for the sensor, wheel plus sensor and wheel alone was used. The precision uncertainty is a result of random error caused by the data spread about the mean as shown in equation (B.7). This error will change based on the repeatability and accuracy of the measurements. The bias error is a fixed or steady error which remains constants for all the measurements a. Bias errors are often more difficult to quantify because they come from various sources like: calibration errors, scale reading errors, data acquisition, etc.